

**The use of idealised experiments in testing a new
convective parameterization: Performance of CoMorph-A**

Journal:	<i>QJRMS</i>
Manuscript ID	QJ-23-0169.R2
Wiley - Manuscript type:	Research Article
Date Submitted by the Author:	21-Dec-2023
Complete List of Authors:	Lavender, Sally; University of Southern Queensland, Centre for Applied Climate Sciences; Met Office, Stirling, Alison; Met Office, Whitall, Michael; Met Office, Atmospheric Parameterisations and Processes Stratton, Rachel; Met Office, Daleu, Chimene Laure; University of Reading, Meteorology Plant, Robert; University of Reading, Meteorology Lock, Adrian; Met Office, Gu, Jian-Feng; University of Reading Department of Meteorology,
Keywords:	convection parameterization, idealised modelling, climate models, cloud resolving models, diurnal cycle
Country Keywords:	AAA - No country

1
2
3
4
5
6
7

1 **The use of idealised experiments in testing a new convective**
2 **parameterization: Performance of CoMorph-A**

8 Sally L. Lavender^{1,2}, Alison J. Stirling², Michael Whitall², Rachel Stratton², Chimene L.
9 Daleu³, Robert S. Plant³, Adrian Lock², Jian-Feng Gu^{3,4}

10
11
12 ¹ *Centre for Applied Climate Sciences, University of Southern Queensland, Toowoomba, Australia*

13
14 ² *Met Office, Fitzroy Road, Exeter, UK*

15
16 ³ *Department of Meteorology, University of Reading, Reading, UK*

17
18 ⁴ *Key Laboratory of Mesoscale Severe Weather, Ministry of Education, and School of Atmospheric Sciences,*
19 *Nanjing University, Nanjing, China*

20
21
22
23
24
25
26
27 ¹² *Corresponding author: Sally Lavender, Sally.lavender@usq.edu.au*

For Peer Review

28
29
30
31
32
33
34
35
36
37
38
39
40
41
42
43
44
45
46
47
48
49
50
51
52
53
54
55
56
57
58
59
60

13 ABSTRACT

14 CoMorph is a new mass-flux convection parameterization under development at the Met
15 Office designed for use within the Unified Model and its successor model, LFRic. Use of a
16 three-dimensional idealised model enables controlled tests of the performance of the scheme
17 across different regimes. This includes the interaction between the physical parametrizations
18 and the resolved dynamics, allowing study of the emergent organisation of convection on the
19 resolved scale. A selection of well-known cases is revisited here, with the purpose of
20 documenting the extent to which CoMorph captures a range of important, but challenging
21 behaviour such as the diurnal cycle and sensitivity to tropospheric moisture. Simulations
22 using CoMorph-A, a new physics package, that has been demonstrated to perform well at
23 NWP and climate scales, are compared against the current global atmosphere configuration
24 and high-resolution results. In addition to an entirely new convection scheme, the package of
25 changes includes significant changes to the cloud, microphysics, and boundary layer
26 parametrizations. Recognising that CoMorph-A is the first version of a scheme that will
27 continue to be substantially developed and to obtain good performance, compromises in
28 tuning have had to be made. These idealised tests therefore show what works well in this
29 configuration, and what areas will require further work. As such, it is quite a demanding
30 testbed and could be viewed as some of the equipment required for a 'convective
31 playground'.

32 KEYWORDS: convection parameterization, idealised modelling, cloud resolving models,
33 climate models, diurnal cycle

35 1. Introduction

36 Convective clouds act to transport heat, moisture and mass upwards, fuelled by the latent heat
37 release of condensing water from rising air parcels. Since this motion cannot accurately be
38 represented on the resolved model grid, a convection parameterization needs to represent the
39 effects of this dynamical process by estimating its influence on the temperature, moisture and
40 horizontal winds of the atmosphere, in addition to predicting the precipitation generated. The
41 subsequent adjustment of the temperature profile by the resolved scale has an influence on
42 the wider circulation patterns. As such, whether the convection scheme in a model adequately
43 represents the spatial and temporal distribution of convective precipitation and diabatic

1
2
3 44 heating has implications not only for local precipitation accumulations but also for global
4
5 45 circulation patterns through convective-dynamical coupling.
6

7
8 46 The Met Office Unified Model (UM; Brown et al. 2012) is used extensively across the world
9
10 47 with partnership institutions including the Australian Bureau of Meteorology, the National
11 48 Centre for Medium Range Weather Forecasting (NCMRWF) in India and the Meteorological
12
13 49 Service Singapore. For over 30 years, the Met Office convection scheme has been based on
14
15 50 the mass-flux approach of Arakawa and Schubert (1974), in which the role of the convection
16
17 51 scheme is to stabilise atmospheric profiles via the removal of CAPE (convectively available
18
19 52 potential energy) through subsidence within a grid column. The existing scheme, based on
20
21 53 Gregory and Rowntree (1990), lacks much of the structural flexibility required to address
22
23 54 systematic biases generated by convection in the UM (e.g. Walters et al. 2019). To address
24
25 55 this, a new convection scheme, CoMorph, has been developed (see Whitall et al. 2022 for full
26
27 56 details). Whilst still a bulk mass-flux scheme, CoMorph removes previously hardwired
28
29 57 structural assumptions such as initiation from a pre-determined cloud-base height and the use
30
31 58 of separate schemes for shallow, deep and mid-level convection which must be pre-
32
33 59 diagnosed. CoMorph has been written in a way that allows the inclusion of additional
34
35 60 physics and couples more fully and consistently to other physics components of the model
36
37 61 (see Section 2.2). A package of changes called CoMorph-A has been released and
38
39 62 simulations in a full global circulation model (GCM) have shown the positive impact of
40
41 63 including this package in the GCM (A. Lock, submitted work). These benefits include a
42
43 64 reduction in radiative flux biases across the tropics, improvements in tropical and
44
45 65 extratropical cyclone statistics, strengthening of the Madden Julian oscillation (MJO) and
46
47 66 other tropical waves as well as improvements in overall scores in numerical weather
48
49 67 prediction trials.
50

51
52 68 It is common to use single column models (SCMs) alongside convection resolving models
53
54 69 (CRM) or large-eddy simulation (LES) together with field observations whilst developing
55
56 70 and testing parameterizations (e.g. Lenderink et al., 2004; Grabrowski et al. 2006; Couvreux
57
58 71 et al., 2015). However, SCMs are unable to capture feedbacks between subgrid- and grid-
59
60 72 scale processes which can lead to different behaviour than the full GCM. For example, SCM
61
62 73 cases have been successfully used to develop improvements to convective parametrizations to
63
64 74 represent the diurnal cycle of convection over land (e.g. Rio et al., 2009) but additional
65
66 75 modifications may be needed to perform well in the GCM due to interactions not originally
67
68

1
2
3 76 exposed by the SCM (e.g. Rio et al., 2013). In a recent study, Hwong et al. (2022) found that
4 77 as convection becomes more organised, there are larger differences in results between one-
5 78 and three-dimension (3D) simulations. Although the UM SCM has been used extensively
6 79 during development of CoMorph, this study uses the 3D idealised UM. While still being
7 80 substantially cheaper to run than the full GCM, this enables controlled tests of the interaction
8 81 between the physical parametrisations and the resolved dynamics, enabling more
9 82 comprehensive testing of the scheme, including the emergent organisation of convection on
10 83 the resolved scale.

11 84 A selection of well-known cases is revisited here, with the purpose of documenting the extent
12 85 to which CoMorph-A captures a range of important, but challenging behaviour. These
13 86 idealised cases have the advantage that they can be accompanied by high-resolution
14 87 analogues, where the convection is well captured by the resolved grid. Many of these cases
15 88 were originally designed for use in a SCM for testing parameterizations over a grid box of
16 89 order 100—200 km² however the UM, along with many other GCMs, is now routinely run at
17 90 much higher resolutions of order of 10—50 km. Using the idealised UM configured to use
18 91 the same physics as in the full GCM allows some exploration of how the model will behave
19 92 at these higher resolutions. Results from a coarser resolution (10 km and lower) model setup
20 93 with parameterized convection (with and without CoMorph-A) are presented alongside high-
21 94 resolution (250 m or higher) CRM results. CoMorph has around 30 tuneable parameters, so
22 95 many different versions have been tested in the development of a package that performs well
23 96 operationally. Recognising that CoMorph-A is the first version of a scheme that will continue
24 97 to be substantially developed, compromises in tuning have had to be made in order to obtain
25 98 good performance. These idealised tests evaluate where this configuration performs well and
26 99 identifies any deficiencies that require further work. This testbed is designed to serve as a
27 100 reference for others to replicate, and could be viewed as some of the equipment required for a
28 101 ‘convective playground’; a platform to enable testing of convection parametrizations with
29 102 differing levels of complexity, from simple idealized tests through to comparisons with field
30 103 campaigns.

31 104 The following section describes the idealised UM and details of the CoMorph-A package of
32 105 changes. Section 3 gives an overview of multiple experiments and documents the
33 106 performance of CoMorph-A. The results are summarised in Section 4.

34 107 2. Model experiments

108 2.1. Model overview

109 The atmospheric model used is version 12.1 of the UM. In the idealised configuration the
110 model has bicyclic boundary conditions over a limited area domain on a flat, cartesian grid.

111 The full science setup with parameterized convection is based on the current operational
112 global atmosphere and land configuration, GAL8. This configuration is based on that
113 described by Walters et al. (2019) with updates to some of the physics. These include the
114 addition of a drag package, changes to the boundary layer scheme to improve representation
115 of shear-driven boundary layers as well as the numerical stability of stable boundary layers,
116 and a new riming parameterization in the large-scale precipitation scheme. For the control
117 run (CTRL) using GAL8 as officially defined i.e., with the current UM convection scheme,
118 there have been significant changes to the existing convection scheme including the use of a
119 prognostic entrainment rate to allow some memory of recent convection (Willett & Whittall,
120 2017). The additional changes in replacing the convection scheme with CoMorph-A are
121 detailed in Section 2.2.

122 For the CRM with only explicit convection, the tropical regional atmosphere configuration,
123 RAL2-T, is used as described in detail by Bush et al. (2023) but using the Smith (1990) cloud
124 parameterization scheme and the same higher order interpolation scheme for dry potential
125 temperature and moisture. Tests have shown benefits of using the Smith (1990) diagnostic
126 cloud parameterization scheme, as in the RAL2-M configuration (Bush et al., 2023) instead
127 of the PC2 scheme (Wilson et al., 2008) when running at sub-km resolutions. Additionally,
128 the Fountain Buster scheme is used which modifies the semi-lagrangian advection scheme to
129 address local conservation errors caused by unrealistically intense updrafts. Unless specified
130 in the text, updraught mass fluxes from the CRM are calculated over buoyant cloudy
131 updrafts whereby sub-grid velocity is upwards relative to the layer mean ($w' > 0$ m/s),
132 cloudy points are defined by a cloud condensate mixing ratio greater than 1×10^{-5} (kg kg⁻¹)
133 and are positively buoyant relative to the layer mean ($\theta'_v > 0$).

134 A selection of idealised experiments has been used to develop and test the performance of
135 CoMorph-A. Rather than provide details of all the idealised experiments here, these are
136 described in Table 1 and the relevant results section where they are first mentioned. The
137 reader is directed to the original papers for full details but any divergence from the original

1
2
3 138 experiments is outlined. Where available, the results are compared against the CRM and
4
5 139 previously documented results and observations.
6

7 140 2.2. The CoMorph-A physics package

8
9
10 141 The CoMorph convection scheme is detailed in Whitall et al (2022). Here we briefly
11
12 142 describe some of the fundamental components of the scheme and detail differences from the
13
14 143 existing scheme.
15

- 16 144 • In the previous scheme, updrafts are prescribed from a predetermined cloud-base
17 145 height with a CAPE closure assumption to calculate the mass flux at cloud base. In
18 146 CoMorph, mass-flux is allowed to initiate independently from all heights where there
19 147 is local vertical instability (dry-statically unstable layers such as near a heated surface,
20 148 or moist stratiform cloud layers which become moist-unstable layers such as from
21 149 large-scale cloud). When convection triggers from non-cloudy model-levels, the
22 150 cloud-base height emerges from the scheme when the modelled bulk plume rises high
23 151 enough to reach saturation. The amount of mass initiated is set to depend on the
24 152 vertical instability, and this is effectively the “closure” for the scheme. The cloud-base
25 153 mass -flux then becomes determined by the balance of entrainment versus
26 154 detrainment in the layer below cloud-base.
- 27 155 • Entrainment rate scales with the inverse “parcel radius”, which is based on a
28 156 boundary-layer turbulence length-scale in the parcel’s source-layer. The parcel radius
29 157 in CoMorph-A is also scaled by an ad-hoc function of the previous time step
30 158 precipitation rate allowing a crude representation of increased organisation of
31 159 convection by precipitation-driven cold pools.
- 32 160 • The detrainment rate is based on a power-law probability distribution function of in-
33 161 plume buoyancy and other properties, with the core (lower entrainment rate) and
34 162 mean properties of the plume treated separately. The ascent terminates at the level at
35 163 which the parcel core is negatively buoyant. This detrainment calculation also uses an
36 164 implicit method to ensure it evolves smoothly over successive timesteps.
- 37 165 • CoMorph includes a microphysics parameterization allowing formation of different
38 166 hydrometeors within the parcel and allows the parcel and detrained air to remain
39 167 supersaturated with respect to ice. All convectively generated precipitation is passed
40 168 on the model-level where it falls out of the parcel to the “large-scale” microphysics
41 169 scheme, which then simulates the fall to the surface, evaporation, melting etc. To aid

170 coupling between CoMorph and the large-scale microphysics at coarse resolution,
 171 both schemes update a prognostic precipitation fraction, so that convection can
 172 modify rain mass and area fraction consistently.

- 173 • CoMorph represents convective momentum transport (CMT) by transporting the
 174 zonal and meridional wind components within the bulk plume and allowing the
 175 exchange of momentum between the plume and environment with a parameterisation
 176 of the horizontal pressure gradient force based on a quadratic drag law.

177 Compared to the previous UM convection scheme, CoMorph is much more closely coupled
 178 to the model's boundary layer, large-scale microphysics and prognostic cloud schemes and
 179 modifications to all four schemes have been required to ensure they operate consistently
 180 together. The improved coupling between CoMorph and the resolved dynamics enables
 181 organised convective structures to develop over a range of scales.

182 3. Focussed testing of CoMorph-A

183 In this section we focus on the performance of CoMorph-A in a range of different
 184 experiments targeting different model behaviours. An overview of all the test cases is given
 185 in Table 1 along with a summary of the rationale for selection of these cases. Since many of
 186 these cases are based on field campaigns, where the large-scale forcings have been
 187 observed/evaluated for specific areas, the domain sizes are chosen to be the same as those
 188 original cases. Where the original domain was smaller than $100 \times 100 \text{ km}^2$ this has been
 189 increased to allow large-scale circulations to form in the parametrized cases. In cases where
 190 the domain size is $100 - 200 \text{ km}^2$, the runs have been repeated to check for any domain
 191 dependence. In all cases a discussion of the CRM results compared to other high-resolution
 192 results will be discussed and, where appropriate, plots are shown in a form that can be
 193 directly compared with earlier papers describing the case.

Section	Case title	Original reference	Domain (& resolution)	Interactive radiation?	Additional details	Scientific rationale
3.1. Mean State	RCE	Wing et al. (2018)	GA: $200 \times 200 \text{ km}^2$, $6000 \times 400 \text{ km}^2$ (10 km) CRM: $200 \times 200 \text{ km}^2$ (200m)	Yes	SST= 300K.	Analysis of the mean-state and organisation of convection under radiative-convective equilibrium (RCE)

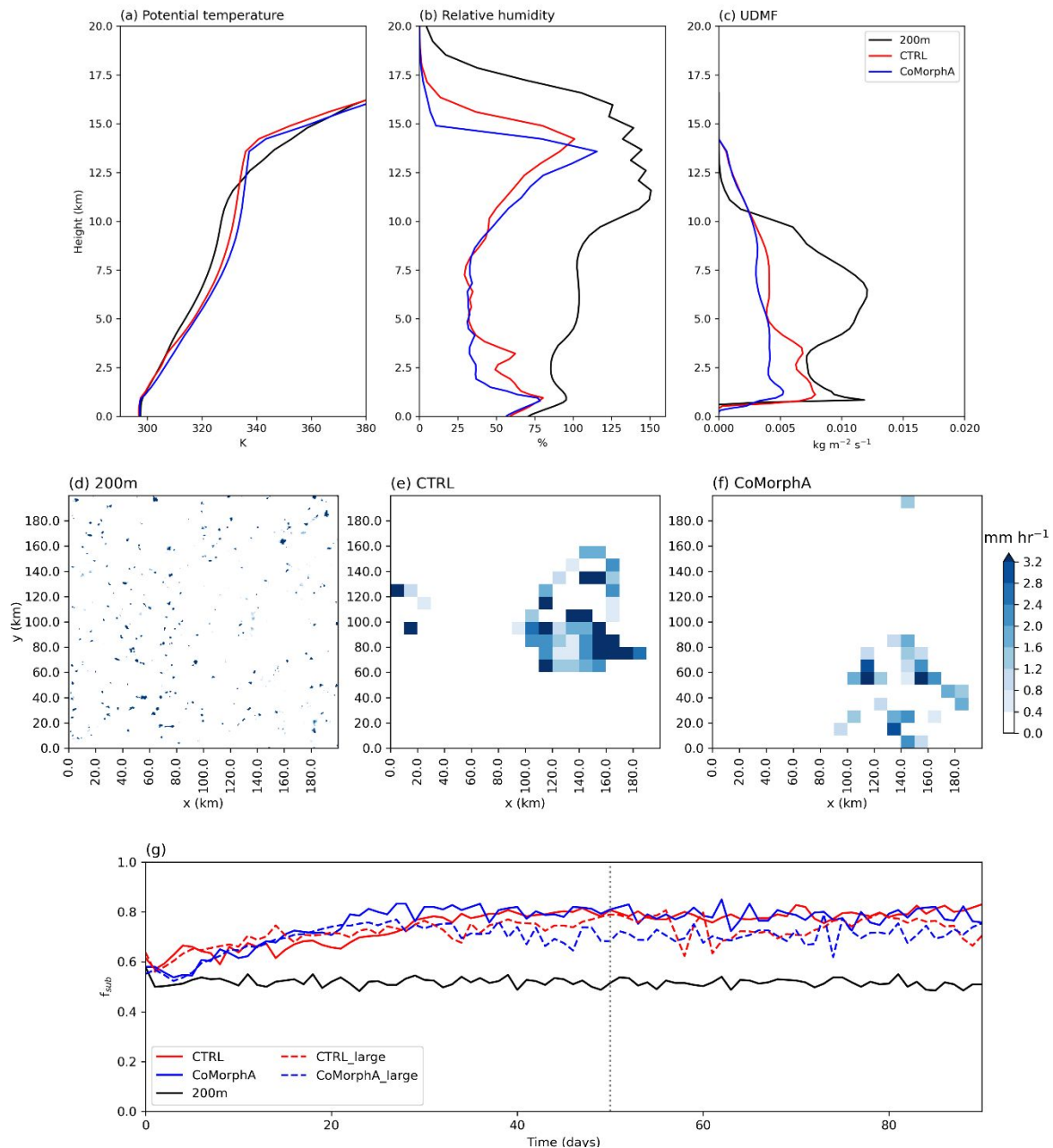
3.2 Sensitivity to tropospheric humidity	EUROCS	Derbyshire et al. (2004)	Multiple - see text.	No	Relax (1 hour timescale) to theta, wind and relative humidity profiles. 4 different humidity profiles.	Examining the moisture-convection relationship, shown to be important for simulating the MJO.
3.3 Diurnal cycle	Shallow ARM	Brown et al. (2002), Lenderink et al. (2004)	GA: 160×160 km ² (10 km) CRM: 160×160 km ² (100m)	No	Prescribed surface fluxes, geostrophic wind of (u,v)=(10,0) m s ⁻¹ .	Development of shallow cumulus over land with no transition to deep convection.
	AMMA	Couvreur et al. (2012, 2015)	GA: 100×100 km ² (10 km) CRM: 100×100 km ² (100m)	No	Prescribed surface fluxes and temperature, moisture and vertical velocity tendencies.	Large amplitude diurnal cycle with deep, dry boundary layer. Transition from shallow to deep convection.
	Deep ARM	Guichard et al. (2004)	GA: 100×100 km ² (10 km) CRM: 100×100 km ² (200 m)	No	Prescribed surface fluxes and temperature tendencies. Relax to zero wind.	Idealised diurnal cycle case representing transition from dry to shallow to deep convection. Forced with the same cycle over 10 days.
3.4 Memory in diurnal cycle	As above (Deep ARM)	Daleu et al. (2020)	As above.		As above.	Quantifying the memory of the system in terms of the development of convection being influenced by previous convection
3.5 Multi-day tropical case	TWP-ICE	Fridlind et al. (2012)	GA: 200×200 km ² (10 km), CRM: 200×200 km ² (100 m)	Yes	SST = 302.15, nudging of horizontal winds, moisture and temperature.	Performance when simulating convective systems over multiple days. A well-documented case with interactive radiation.
3.6 Inland propagation and nocturnal convection	Island case	N/A	GA: 1200 × 300 km ² , CRM: 1200 × 300 km ² (250 m.)	Yes	Island 300 km in x-dimension, real, flat, sandy land surface with plenty of moisture initially. u=0 m s ⁻¹ and u=5 m s ⁻¹ .	A newly developed case based on an island in the maritime continent to examine the initiation of convection by sea-breeze circulation and propagation of convection.
3.7 Convective momentum transport	Cold-air outbreak	Kershaw & Gregory (1997)	GA: 200×200 km ² (10 km), CRM: 200×200 km ² (100 m)	No	Prescribed, constant surface fluxes. u=0 m s ⁻¹ and v linearly varies from 0 m s ⁻¹ at the surface to 10 m s ⁻¹ at 6 km.	Sensitivity to different parameterizations of convective momentum transport

Table 1: Summary of the experiments used in this paper to evaluate the performance of CoMorph-A.

3.1. Modelled mean state

To give an idea of the mean state, radiative-convective equilibrium (RCE) experiments were performed based on the RCEMIP setup (Wing et al. 2018) with a sea surface temperature of 300 K. The simulations are run for 100 days, reaching equilibrium after 20 days. The original RCEMIP CRM simulations show a large range of results. Figure 1a-c shows profiles of potential temperature, relative humidity and updraught mass flux averaged over the final 70 days of the simulation. The parameterized runs have a warmer troposphere and

203 higher altitude inversion than the CRM, leading to a higher termination of the updraft mass
 204 flux. CoMorph-A has a slightly warmer mid to upper-troposphere than CTRL and both
 205 parameterizations have a sharper inversion at cloud top than the CRM, with CoMorph-A
 206 slightly sharper than CTRL, possibly due to the current lack of representation of overshoots
 207 that would smooth out the inversion.



208

209 **Fig 1.RCE. Profiles of (a) potential temperature [K], (b) relative humidity [%], with respect to**
 210 **water (ice) above (below) 0 °C, and (c) updraught mass flux, averaged over the final 70 days of**
 211 **simulation. Snapshot of surface precipitation rate [mm hr⁻¹] on day 50 of the simulations from**
 212 **(d) 200m CRM (native resolution), (e) CTRL and (f) CoMorph-A, both 10 km resolution, (g)**

1
2
3 213 **time series of f_{sub} , calculated as in the text, for the CRM, CTRL and CoMorph-A. The dashed**
4 **lines are the CTRL and CoMorph-A results over the large $6000 \times 400 \text{ km}^2$ domain. The**
5 **vertical grey dotted line in f shows the timing of the snapshots in a-d.**
6
7

8
9 216 Consistent with other model results in Wing et al. (2020), the mid-tropospheric humidity in
10 217 the parameterized runs is much lower than in the CRM where it remains above 75% in both
11 218 simulations and becomes supersaturated with respect to ice above 8 km. This may suggest
12 219 not enough detrainment in the plume formulation in both parameterizations. The CRM has a
13 220 higher mass flux near cloud base and in the mid-troposphere but terminates at a lower altitude
14 221 than both CTRL and CoMorph-A. CoMorph-A is drier than CTRL in the low to mid-
15 222 troposphere with a resulting smaller mass flux.

16
17
18
19
20
21
22 223 A snapshot of the surface precipitation from day 50 of the 200 m CRM, CTRL and
23 224 CoMorph-A simulations are shown in Fig 1d-f. Both parameterized runs show some
24 225 aggregation of convection that isn't so evident in the CRM simulation. The degree of
25 226 aggregation in each simulation is quantified by calculating the subsidence fraction (f_{sub}), the
26 227 fraction of the domain where there is subsidence, as in Wing et al. (2020) using daily 500 hPa
27 228 vertical velocity averaged over $10 \times 10 \text{ km}^2$ blocks. The parameterized simulations were
28 229 repeated using a domain of $6000 \times 400 \text{ km}^2$ to check how the spatial organisation compares
29 230 with the smaller domain. Using the large domain, the dependence of f_{sub} on the size of the
30 231 blocks ($10 \times 10 \text{ km}^2$ compared to $100 \times 100 \text{ km}^2$ as used in the original study) was investigated
31 232 and the values of f_{sub} were found to be similar. The values of f_{sub} in the CRM range from
32 233 0.5—0.6 compared to 0.7—0.8 in the parameterized runs, suggesting that there is greater
33 234 organisation in the parameterized runs which may be excessive. However, these higher
34 235 values of f_{sub} are within the same range as other CRM models analysed in RCEMIP (Fig 12
35 236 in Wing et al. 2020).

36
37
38
39
40
41
42
43
44
45
46
47 237 This section has shown the mean profiles under RCE and how convection self-aggregates
48 238 using CoMorph-A, with similar performance to CTRL. The following section will examine
49 239 how convection is related to mid-tropospheric humidity and the organisation of convection in
50 240 the different simulations will be revisited.

51 241 3.2. Sensitivity to tropospheric humidity

52
53
54
55
56
57
58 242 For models to adequately represent convective clouds, they must capture the interaction
59 243 between convection and mid-tropospheric humidity. This moisture-convection relationship

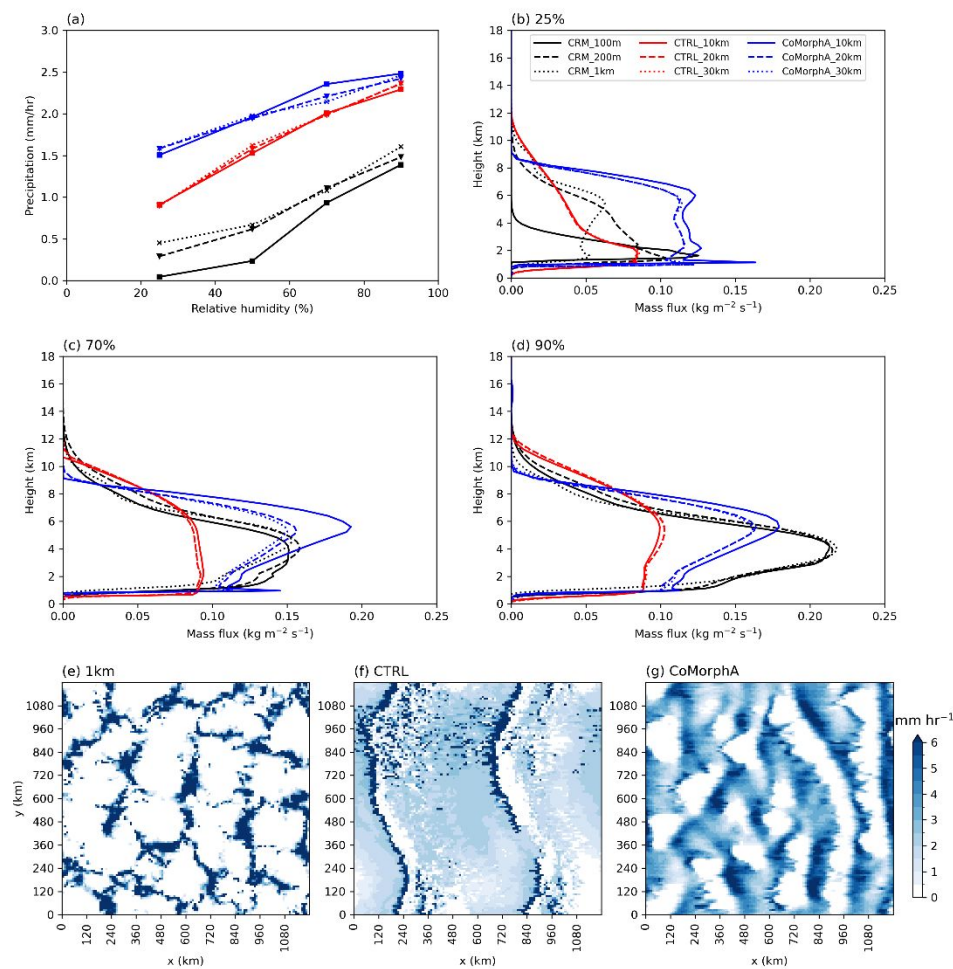
1
2
3 244 has been found to be important for simulating the MJO (e.g. Kim et al. 2014, Hirons et al.
4 245 2013), but is poorly simulated in the UM, in terms of amplitude and propagation across the
5 246 maritime continent (Ahn et al. 2020, Williams et al. 2017).
6
7
8

9 247 The experimental setup has been kept as similar to Derbyshire et al. (2004) as possible,
10 248 although accounting for a higher model top in more recent versions of the model. The model
11 249 is initialised and above 1 km is relaxed back to fixed profiles of potential temperature, zonal
12 250 wind and relative humidity (RH) with a relaxation timescale of 1 hour. Between 2 km and 16
13 251 km there are 4 different experiments with reference values of RH of 25%, 50% 70% and
14 252 90%. The simulation is run for 5 days with the initial day discarded from the analysis. The
15 253 3D idealised setup of this case has been useful for investigating propagating convective bands
16 254 that have been seen in earlier versions of the UM (e.g. Roberts 2001; Tomassini et al. 2017).
17 255 In addition to the results shown here for $50 \times 50 \text{ km}^2$ (CRM) and $1200 \times 1200 \text{ km}^2$ domains, the
18 256 CRM has been run at 100 m, 200 m, 500 m and 1 km resolution over $25 \times 25 \text{ km}^2$, $50 \times 50 \text{ km}^2$
19 257 and $100 \times 100 \text{ km}^2$ domains and CTRL and CoMorph-A at 10 km, 20 km, 30 km and 60 km
20 258 resolutions over $100 \times 100 \text{ km}^2$ (10 km resolution only), $600 \times 600 \text{ km}^2$ and $1200 \times 1200 \text{ km}^2$
21 259 domain sizes.
22
23
24
25
26
27
28
29
30
31
32

33 260 The original paper showed the sensitivity to humidity was highly variable depending on the
34 261 single-column model analysed. While the CRM results show a similar overall increase in
35 262 precipitation rate from 25% to 90% humidity as documented in Derbyshire et al. (2004), there
36 263 is clear variation with resolution: The highest resolution (100 m; solid line) tending to have
37 264 the lowest precipitation values whilst the coarsest resolution (1km; dotted line) has the largest
38 265 values, with large differences in the mass flux profiles for the 25% experiment (Fig 2b),
39 266 consistent with the results of the original study (Fig 4 in Derbyshire et al. 2004).
40
41
42
43
44
45

46 267 Using this experimental setup, CoMorph-A rapidly responds to the unstable profile and has
47 268 too high precipitation amounts for all humidity cases (Fig 2a). This is a similar result to the
48 269 SCMs examined in the original study (see Fig 15 in Derbyshire et al. 2004). The moisture
49 270 sensitivity is lower in CoMorph-A than CTRL with an increase of 1.0 mm hr^{-1} between the
50 271 25% and 90% cases compared to 1.4 mm hr^{-1} in CTRL. CoMorph-A shows more resolution
51 272 sensitivity than CTRL particularly at the higher humidities but is relatively insensitive to
52 273 domain size (not shown). The updraught mass flux profiles from the 70% and 90%
53 274 experiments (Fig 2c, d) show both parameterized runs peaking at too high altitude relative to
54 275 the CRM with CoMorph-A also terminating too low. The peak values of mass flux are more
55
56
57
58
59
60

276 similar to the CRM in CoMorph-A than CTRL, but this is associated with much higher
 277 precipitation rates in CoMorph-A. The CRM has additionally been run over the same
 278 $1200 \times 1200 \text{ km}^2$ domain as CTRL and CoMorph-A but at 1 km resolution. A snapshot of
 279 precipitation rate over this large domain after 4 days is shown in Fig 2e-g with the CRM
 280 regridded to the same 10 km grid as CTRL and CoMorph-A. Both parameterized runs have
 281 too much background precipitation and a less cellular structure than is evident in the CRM
 282 although this is arguably improved in CoMorph-A relative to CTRL. Developments to allow
 283 a greater sensitivity to relative humidity in future versions of CoMorph will be discussed in
 284 Section 4.



285

286 **Fig 2. EUROCS. (a) Precipitation [mm hr⁻¹] against relative humidity and (b-d) Updraught**
 287 **mass flux [kg m⁻² s⁻¹] for the 25%, 70% and 90% cases. Results for multiple resolutions**
 288 **from the $50 \times 50 \text{ km}^2$ domain CRM (black), large (1200 km^2 domain) CTRL (red) and**
 289 **CoMorph-A (blue). Snapshot of surface precipitation rate [mm hr⁻¹] on day 4 of the 90%**
 290 **case, $1200 \times 1200 \text{ km}^2$ domain simulations from the (e) 1km CRM; regridded to same 10 km**
 291 **grid (f) CTRL and (g) CoMorph-A.**

1
2
3 292 This is a highly idealised case which relaxes back to the same profiles and, like the RCE,
4 293 generates a steady state enabling the analysis of mean profiles and precipitation rates as well
5 294 as the emergent spatial structures. In the following section the model uses time-varying
6 295 forcings to represent the initiation and development of convection during the day.
7
8
9

10 296 3.3. Diurnal cycle

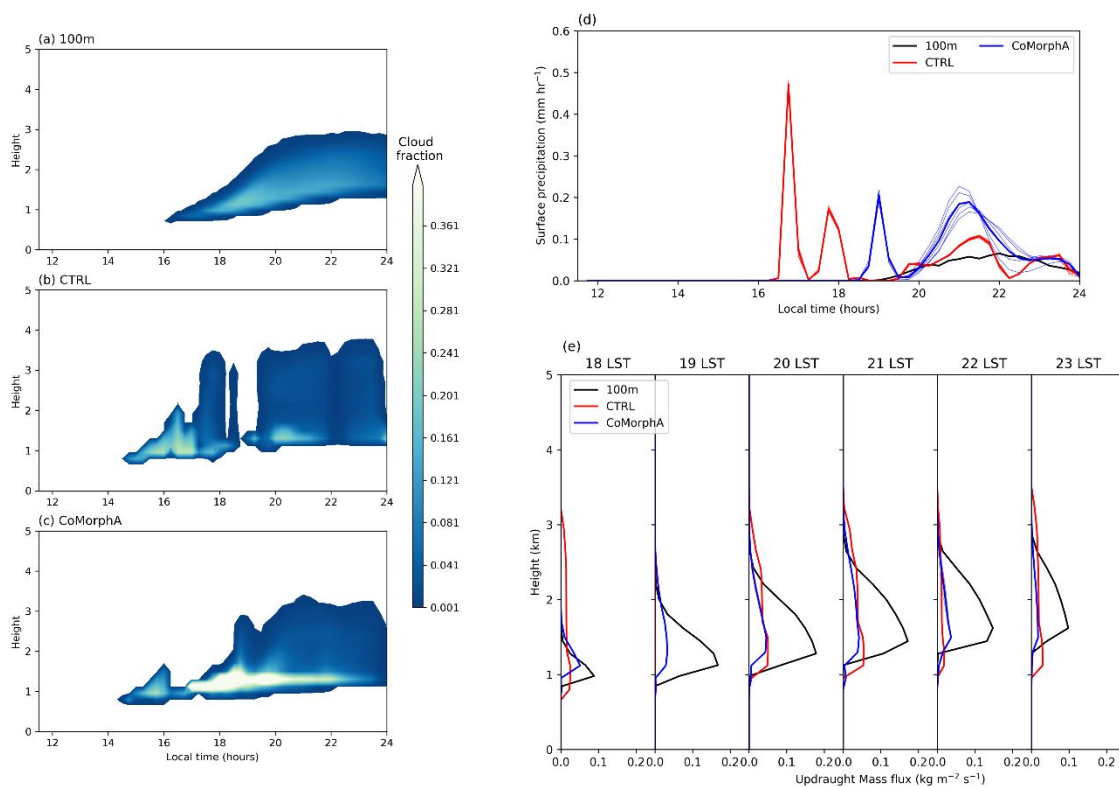
11
12
13
14 297 The failure of models with parameterized convection to fully represent the diurnal cycle is
15 298 well known, with convection often occurring too early in the day, particularly over land (e.g.
16 299 Yang and Slingo 2001). This has been an issue in earlier versions of the UM (e.g.
17 300 Christopoulos and Schneider 2021). Here we examine the performance of CoMorph-A at
18 301 simulating the diurnal cycle using three well-documented experiments examining different
19 302 aspects of the development of convection; a shallow convection case, transition to deep
20 303 convection in a semi-arid environment and a mid-latitude, deep convection case. All three
21 304 cases have interactive radiation turned off. To help understand the sensitivity of the
22 305 parameterized simulations in the single day cases (ARM and AMMA), an ensemble of six
23 306 simulations is performed by perturbing the initial random noise.
24
25
26
27
28
29
30

31 307 3.3.1. Shallow ARM case

32
33
34
35 308 The first diurnal case is based on observations made at the mid-latitude Southern Great Plains
36 309 (SGP) site of the Atmospheric Radiation Measurement (ARM) Program on 21 June 1997
37 310 (Brown et al. 2002, Lenderink et al. 2004), commonly referred to as the ARM case. This
38 311 tests the development of shallow cumulus over land with no development to deep convection.
39 312 The original paper had a very small domain ($6.4 \times 6.4 \text{ km}^2$) domain with a low model top
40 313 depth (4.4 km) and 40 m vertical resolution. Here, the same operational global and regional
41 314 stretched grid vertical levels (Bush et al. 2023) are used with a 40 km model top and
42 315 consequently the vertical resolution above the near-surface layer is lower.
43
44
45
46
47
48
49

50 316 Figs 3a-c show the evolution of the cloud in the three simulations. In the high-resolution run
51 317 this is similar to previous studies (Fig 2b in Lenderink et al. 2004; Fig 5 in Brown et al. 2002,
52 318 Fig 2a in McIntyre et al. 2022). Both CTRL and CoMorph-A overestimate the cloud fraction
53 319 relative to the high resolution, consistent with early SCM results (Lenderink et al. 2004). The
54 320 cloud fraction near cloud base is significantly higher in CoMorph-A than both the CRM and
55 321 CTRL. The evolution of the height of cloud base is well simulated by both parametrized runs
56 322 and both remain shallow although the cloud-top height differs between the runs, with
57
58
59
60

323 CoMorph-A increasing more gradually than CTRL. All runs generate precipitation (Fig 3d)
 324 unlike the original simulations where microphysical parameterizations were switched off.
 325 CTRL has a small cloud fraction at 19Z, after precipitating, before increasing again in both
 326 amplitude and altitude. Both parameterized runs also have a rapid reduction in cloud top
 327 height at the end of the simulation once they stop precipitating. Although the cloud fractions
 328 have larger maxima in CTRL and CoMorph-A, the values of updraught mass flux remain
 329 lower than the CRM (Fig 3e) and remain almost identical for the different ensemble
 330 members.



331

332 **Fig 3.ARM. Time evolution of cloud fraction in (a) 100 m CRM, (b) CTRL and (c) CoMorph-A**
 333 **simulations of the shallow ARM case. (d) Timeseries of precipitation [mm hr⁻¹] from the three**
 334 **simulations. (e) Updraught mass flux [kg m⁻² s⁻¹] profiles between 1800 and 2300 local time. (d)**
 335 **and (e) are shown for each ensemble member (thin lines) and the ensemble mean (thick line).**

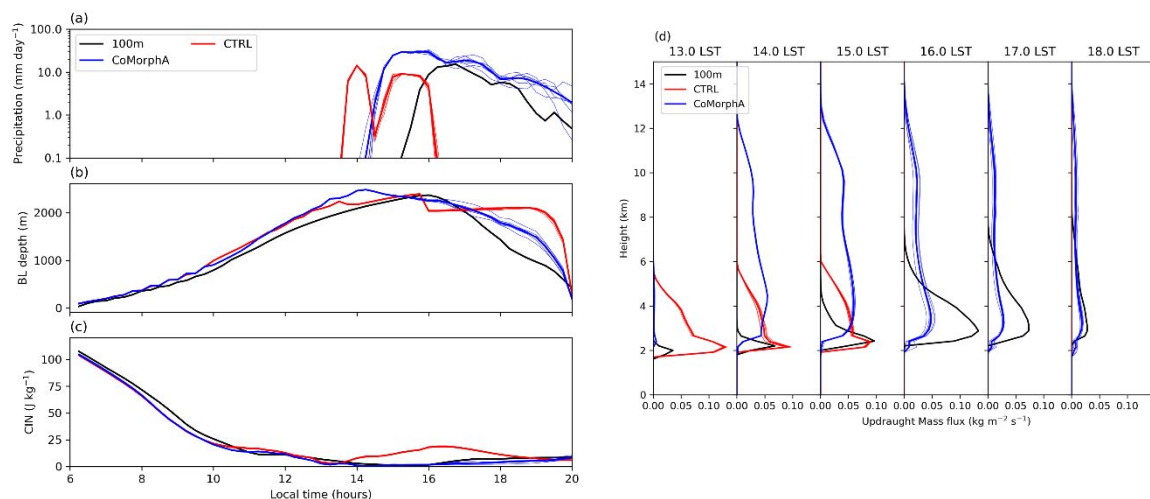
336 3.3.2 AMMA case

337 The second diurnal case is based on observations from the African Monsoon
 338 Multidisciplinary Analysis (AMMA) showing the development of daytime convection in a
 339 semi-arid region with a much larger amplitude diurnal cycle (Couvreur et al. 2012).
 340 Comparison of Fig 4a with Fig 2 in Couvreur et al. (2015) shows that the CRM differs

341 somewhat from the original LES results, with the onset of precipitation and its subsequent
 342 peak occurring approximately 2 hours earlier. CTRL initiates precipitation almost 2 hours
 343 too early relative to the CRM and only persists for 3 hours before abruptly stopping.
 344 CoMorph-A initiates an hour earlier than the CRM and has almost double the precipitation
 345 rate, which is maintained into the evening.

346 Observations from the AMMA case-study (Fig 3 in Couvreux et al. 2012) showed the
 347 boundary layer grows throughout the morning reaching 2.5 km in the mid-afternoon
 348 consistent with the present CRM results (Fig 4b). This was associated with a decrease in
 349 convective inhibition (CIN; Fig 4c) during the morning. The CRM shows a decrease in
 350 boundary layer height and slight increase in CIN into the evening. Both CTRL and CoMorph-
 351 A capture the growth of boundary layer height and evolution of CIN although these evolve
 352 too quickly, consistent with the earlier development of precipitation. The positive values of
 353 mass flux (Fig 4d) are confined to lower altitudes in the CRM than CoMorph-A. The CTRL
 354 convective mass flux is zero for 1600 LST with only large-scale precipitation contributing to
 355 the total surface precipitation rate.

356



357

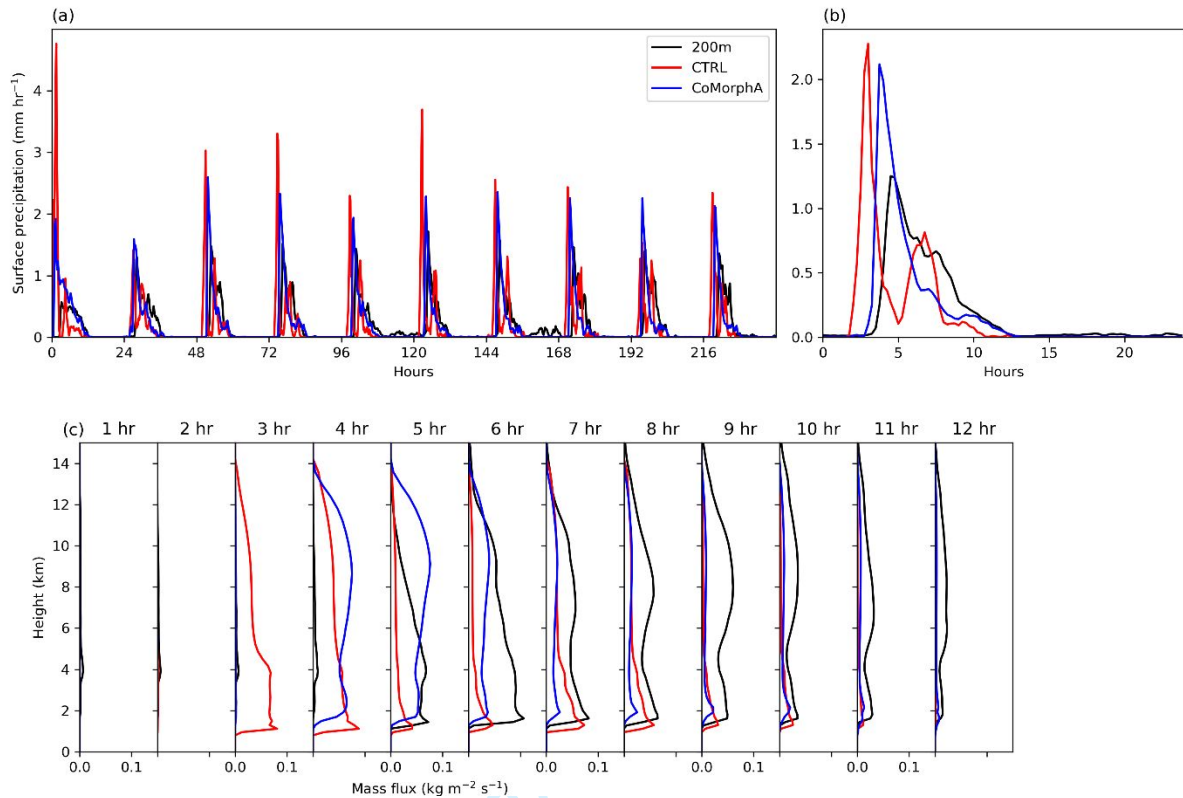
358 **Fig 4.AMMA. Timeseries of (a) surface precipitation [mm day⁻¹], (b) boundary layer depth [m]**
 359 **and (c) CIN [J Kg⁻¹] from the 100m CRM (black), CTRL (red) and CoMorph-A (blue) ensemble**
 360 **members (thin lines) and ensemble mean (thick line) simulations of the AMMA case. (d) Hourly**
 361 **mass flux [kg m⁻² s⁻¹] profiles from 1300 to 1800 local time.**

60

362 3.3.3 Deep ARM case

363 The final diurnal case is based on the same field campaign as 3.3.1 but for a different day
364 (27th June 1997; Guichard et al. 2004) using the experimental setup of Daleu et al. (2020).
365 The model is forced with surface sensible and latent heat fluxes which vary sinusoidally
366 throughout the day (0-12 hours), reaching a peak at 6 hours and set to zero overnight (12-24
367 hours) with a prescribed radiative cooling applied to the potential temperature (Daleu et al.
368 2020). The original papers (Guichard et al. 2004 and Chaboureau et al. 2004) applied the
369 same fluxes but with an earlier start time of 6 hours which is accounted for when comparing
370 the results. This forcing is repeated over 10 days to get the mean diurnal cycle, with the initial
371 day excluded from the diurnal means.

372 The timeseries of precipitation is shown along with the mean diurnal cycle (Fig 5a,b). All
373 simulations reach peak precipitation rate prior to the peak in surface fluxes (6 hours into run);
374 3—4 hours earlier than in the original papers (Figure 3, Guichard et al. 2004 and Figure 2a
375 Chaboureau et al. 2004). As with the previous cases, CTRL initiates convection earlier than
376 CoMorph-A and the CRM which is also evident in the updraught mass flux profiles (Fig 5c).
377 CoMorph-A initiates slightly earlier than the CRM and the peak precipitation rate in both
378 parameterized runs is greater than in the high-resolution run. CTRL peaks at hour 3,
379 decreases until hour 5 before peaking again at hour 8. CoMorph-A precipitation rate reaches
380 an initial peak after 4 hours and then declines rapidly over the next 3 hours before decreasing
381 more gradually until 12 hours. The CRM has a higher rate than CoMorph-A between hours 6
382 and 9, consistent with the higher values of mass flux at these times. but after this the rate
383 remains similar to CoMorph-A.



384

385 **Fig 5. Deep ARM. (a) Timeseries of precipitation [mm hr⁻¹] over 10 days of the**
 386 **simulation of the deep ARM case, (b) mean diurnal cycle of precipitation [mm hr⁻¹] and**
 387 **(c) mean updraught mass flux [kg m⁻² s⁻¹] profiles shown for the first 12 hours. Means**
 388 **are calculated over the final 9 days of the simulation.**

389 This section has highlighted an improvement in the timing of the diurnal cycle using
 390 CoMorph-A. The following section extends this diurnal cycle analysis by examining how the
 391 development of convection is influenced by previous convection.

392 3.4. Memory in the diurnal cycle

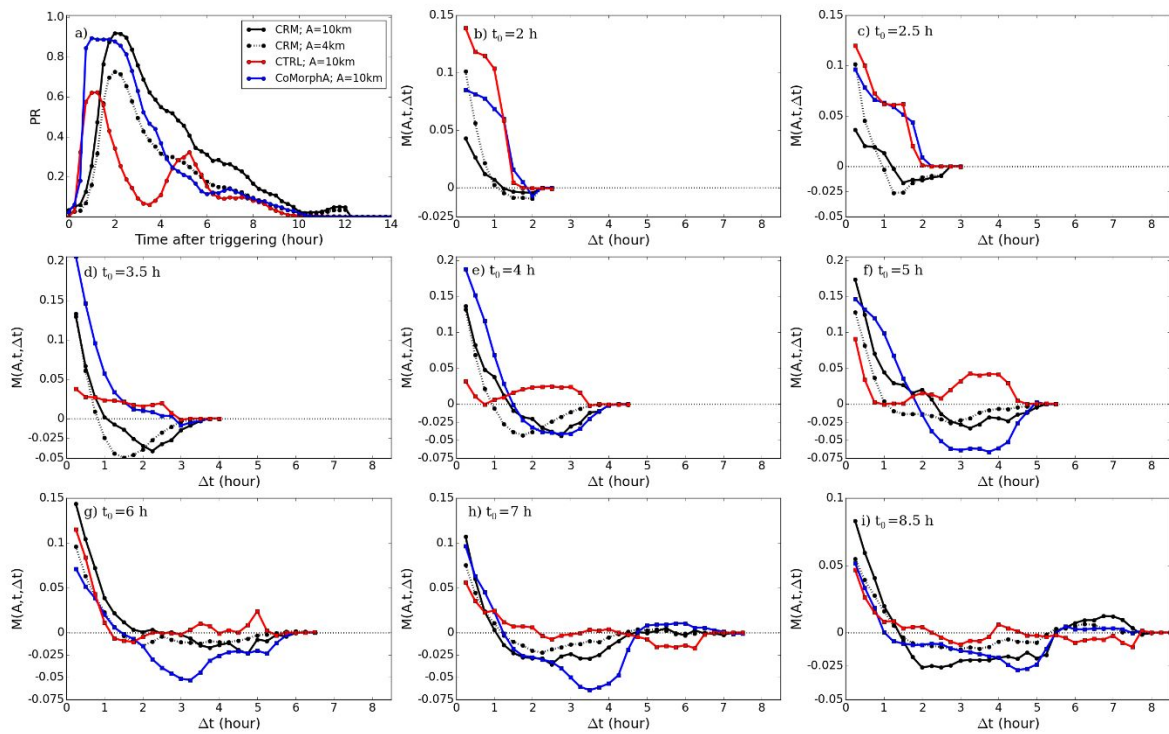
393 Using the setup from section 3.3.3 (Guichard et al., 2004), Daleu et al. (2020) introduced a
 394 memory function which could be separated into three phases; the first representing the
 395 persistence of convection, the second representing the suppression of convection in areas
 396 which had precipitation in the previous few hours and the third representing a secondary
 397 enhancement of precipitation. This is calculated for each of the final 9 days of the simulation
 398 as with the mean diurnal precipitation rate shown in Fig 5b.

399 The memory function, M , is defined in Daleu et al. (2020), and is based on the probability of
 400 finding rain (mean precipitation greater than 0.1 mm hr⁻¹) at both time, t_0 , and at an earlier

time, $t_0 - \Delta t$, over a given area, A , compared to the expected probability assuming that these two events occur independently of each other ($P^2[R(A, t_0, \Delta t)] = P[R(A, t_0)] \times P[R(A, t_0 - \Delta t)]$):

$$M(A, t_0, \Delta t) = P[R(A, t_0) \cap R(A, t_0 - \Delta t)] - P^2[R(A, t_0, \Delta t)]. \quad (1)$$

A value of zero indicates that there is no memory in the system, while positive values indicate an increased chance of raining at the later time, t_0 if it rained at the earlier time, $t_0 - \Delta t$, and a negative value suggests that there is suppression of rainfall linked to the earlier rainfall event. The threshold for Figure 6 shows the probability of finding rain ($P[R(A, t_0)]$) and the memory function for a box of size $A = 10 \times 10 \text{ km}^2$ and $t_0 = 2, 2.5, 3.5, 4, 5, 6, 7$, and 8.5 hours after the initial precipitation (triggering). The memory function is set to zero beyond time lags (i.e., prior to triggering).



412
413 **Figure 6: Memory case. (a) Probability of finding rain ($P[R(A, t_0)]$) for $A = 10 \times 10 \text{ km}^2$ in the deep**
414 **ARM case. The time axis is shifted relative to triggering time such that time 0 corresponds to**
415 **the time of triggering in all three simulations. Memory function ($M(A, t_0, \Delta t)$) for $A = 10 \times 10 \text{ km}^2$**
416 **and $t_0 =$ (b) 2, (c) 2.5, (d) 3.5, (e) 4, (f) 5, (g) 6, (h) 7, (i) 8.5 hours after triggering. Results are the**
417 **ensemble mean obtained in the 200m CRM (black, solid), CTRL (red) and CoMorph-A (blue)**
418 **simulations. Results for $A = 4 \times 4 \text{ km}^2$ are also shown for the CRM (black, dotted).**

1
2
3 419 The results using the UM CRM differ slightly from those in Daleu et al. (2020) which used
4 420 the Met Office NERC cloud model (MONC; Brown et al., 2015). The results using $A=4\times 4$
5 421 km^2 are shown for comparison with Figure 6 in the original paper. The UM CRM triggers
6 422 slightly later than MONC and the increase is more gradual over the initial 30 mins, but
7 423 rainfall remains higher for a longer time. The initial persistence of convection and subsequent
8 424 suppression (phase 2) is weaker in the CRM than MONC. The secondary enhancement
9 425 (phase 3) can only be seen after 5 hours for convection produced 8 hours after triggering and
10 426 is weaker than MONC. The difference between using different values of A ($A=4\times 4$ and
11 427 $A=10\times 10 \text{ km}^2$) are consistent with results using MONC (Fig 5c in Daleu et al. 2020). Results
12 428 using $A=10\times 10 \text{ km}^2$ for CRM, CTRL and CoMorph-A will now be compared to assess the
13 429 performance of CoMorph-A.

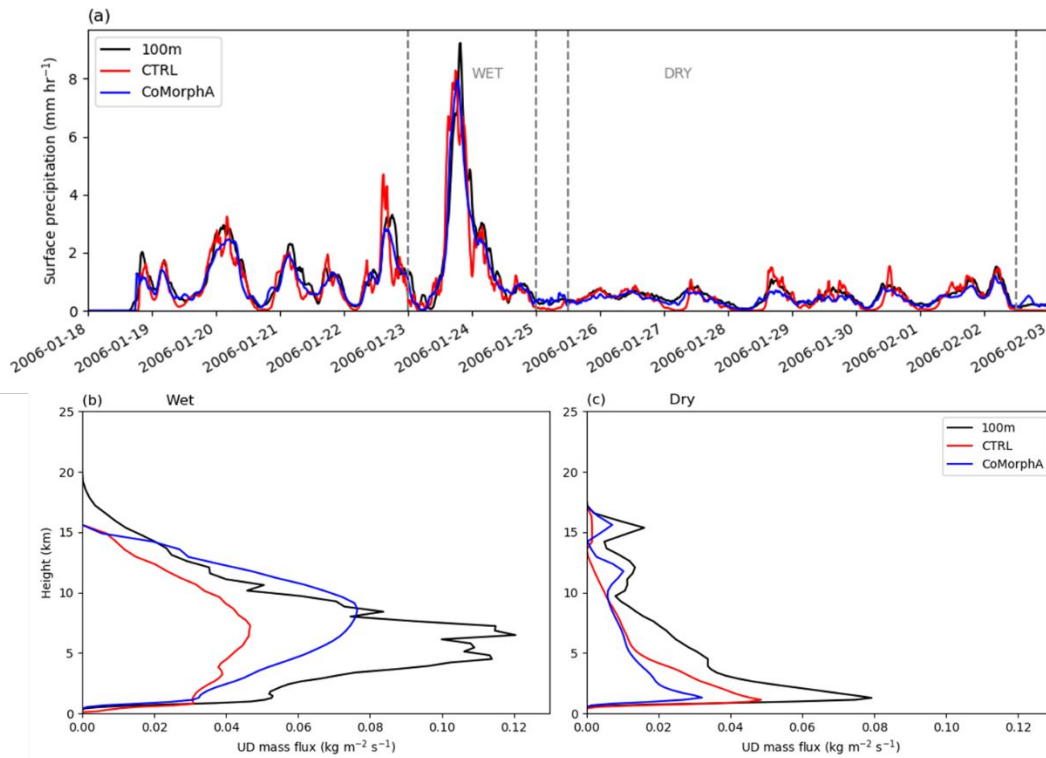
20
21
22
23 430 In the previous section we noted that CTRL triggers over an hour earlier than CoMorph-A
24 431 and the CRM. There are bigger differences in the probability of finding rain (Fig 6a) in the
25 432 two parameterized simulations than we saw in the rainfall rate in Fig 5 due to differences in
26 433 the number and spatial size of the events. Both CTRL and CoMorph-A show a higher
27 434 probability of finding rain over the first hour than the CRM, remaining lower for subsequent
28 435 times (Fig 6a). The probability of rain in CTRL decreases after the first 2 hours, reaching a
29 436 minimum 3—4 hours after triggering before increasing again. Neither CoMorph-A or the
30 437 CRM show this secondary peak. Over the first 2 hours after triggering (first phase) CTRL and
31 438 CoMorph-A have comparable memory with persistence of convection maintained for longer
32 439 than the CRM (Fig 6b). The suppression of convection (second phase) in the CRM starts
33 440 within 1.5 hours for convection produced 2.5 hours after triggering (Fig 6c). For CoMorph,
34 441 there is an indication of suppression for convection produced before $t_0=3.5 \text{ h}$ (Fig 6d) but this
35 442 is weak, and only lasts 15 minutes. For convection produced from $t_0=4 \text{ h}$ (Fig 6e), the initial
36 443 persistence of convection is followed by a suppression for a further 2.5 h in both CoMorph-A
37 444 and CRM with a maximum suppression of 4 h (for convection produced from $t_0=7 \text{ h}$; Fig 6h).
38 445 This suppression of convection happens much later in CTRL and is only evident after 5 hours
39 446 for convection produced over 7 hours after triggering (Figs 6ghi). The secondary
40 447 enhancement of convection (third phase) is weak but evident in the CRM for convection
41 448 produced over 8.5 hours after triggering (Figs 6i). This weak secondary enhancement can
42 449 also be seen in CoMorph-A for convection produced at $t=7 \text{ h}$ (Fig 6h) but is not captured by
43 450 CTRL. It is found that this secondary enhancement can be enhanced using CoMorph-A but
44 451 with a fixed low entrainment rate (not shown).

1
2
3 452 These results show that CoMorph-A has a more realistic relationship between earlier
4 453 precipitation than CTRL and although it is able to capture the secondary enhancement form
5 454 of memory, the timings and strength vary from the CRM. This was a multi-day case but
6 455 applying the same forcing each day to build up an ensemble. The next section evaluates a
7 456 multi-day case using time-varying forcing based on observations to show the performance of
8 457 CoMorph-A in simulating convective systems over a longer time period.

14 458 3.5. Multi-day tropical case

17 459 The multi-day analysis uses a well-documented case based on observations from the Tropical
18 460 Warm Pool–International Cloud Experiment (TWP-ICE; May et al. 2008) using a set-up
19 461 based on Fridlind et al. (2012). This involves a 16-day period during the Australian monsoon
20 462 featuring an active monsoon period followed by suppressed conditions and a monsoon break
21 463 (May et al. 2008). This case has interactive radiation, so provides evaluation of the influence
22 464 of cloud-radiative feedback on CoMorph but is highly constrained by the nudging to
23 465 observational data.

26 466 The CRM results compare well with other models (Petch et al. 2014). The peak precipitation
27 467 values differ slightly from observed as they did in the original comparison (Fridlind et al.
28 468 2012; Petch et al. 2014), particularly when there is only very light precipitation in the later
29 469 part of the period. CTRL shows more high-frequency variability than CoMorph-A.



470

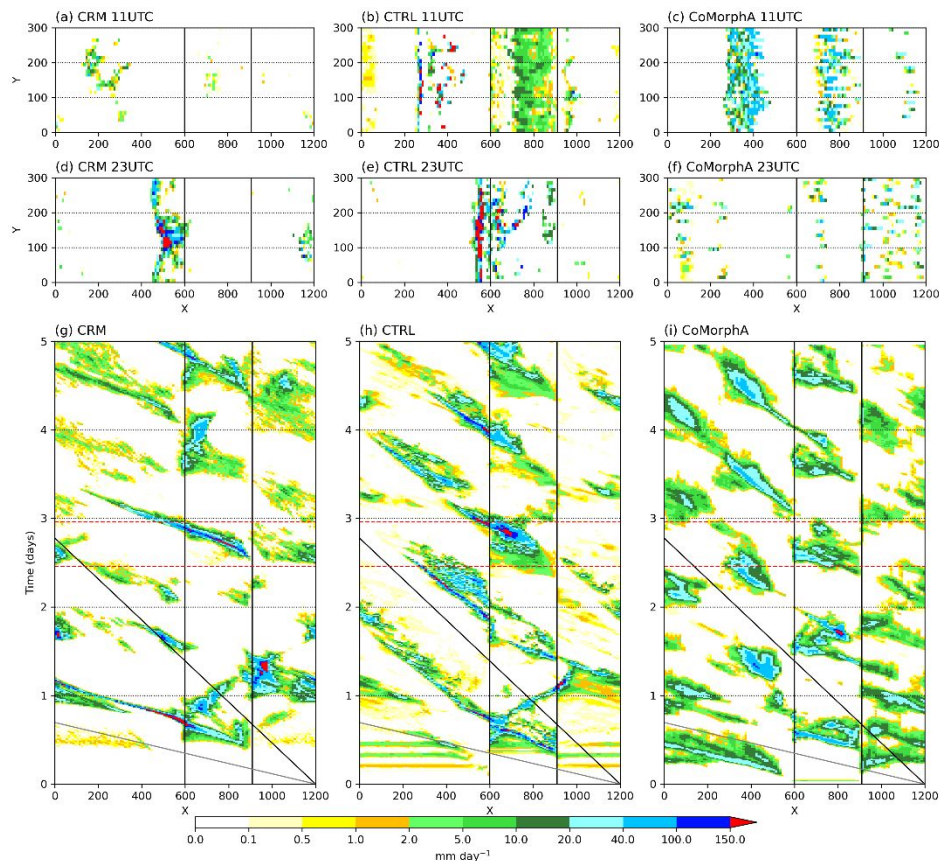
471 **Fig 7. TWP-ICE. (a) Timeseries of 15-minute precipitation rates [mm hr⁻¹] and mean updraught**
 472 **mass flux [kg m⁻² s⁻¹] during the (b) wet and (c) dry period of TWP-ICE from the 100 m CRM**
 473 **(black), CTRL (red) and CoMorph-A (blue) simulations. The wet and dry periods are shown**
 474 **by the grey dashed lines on (a).**

475 The mass flux profiles from the wet and dry periods are shown in Figure 7. The mass flux
 476 profiles from the wet period are very similar to those from the 90% EUROCS case (Fig 2d)
 477 with the parametrized runs peaking at higher altitude than the CRM. Like that case,
 478 CoMorph-A has a higher mass flux than CTRL while both are lower than the CRM peak.
 479 Although, in this case both parameterised runs terminate 4 km lower than the CRM, again
 480 suggesting a need for the representation of overshoots in the parameterization. For the dry
 481 period all mass flux profiles show the expected bottom-heavy profile and terminate at the
 482 same altitude. The CRM has a higher mass flux throughout the profile than both
 483 parameterized runs. Compared to CTRL, CoMorph-A has a lower mass flux in the lower
 484 troposphere but higher in the upper troposphere. The CoMorph-A results from the dry period
 485 are very different from the 25% humidity case shown in Section 3.2 (Fig 2b) suggesting that
 486 under a different experimental setup CoMorph-A could be more sensitive to humidity than
 487 the earlier results implied.

60

488 All cases so far have assumed a homogenous surface. The following section details a new
 489 idealised case for evaluating the behaviour of convection when there is a strip of land (an
 490 island) in the domain and how this affects the propagation of convection under different wind
 491 regimes.

492 3.6. Inland propagation and nocturnal convection



493

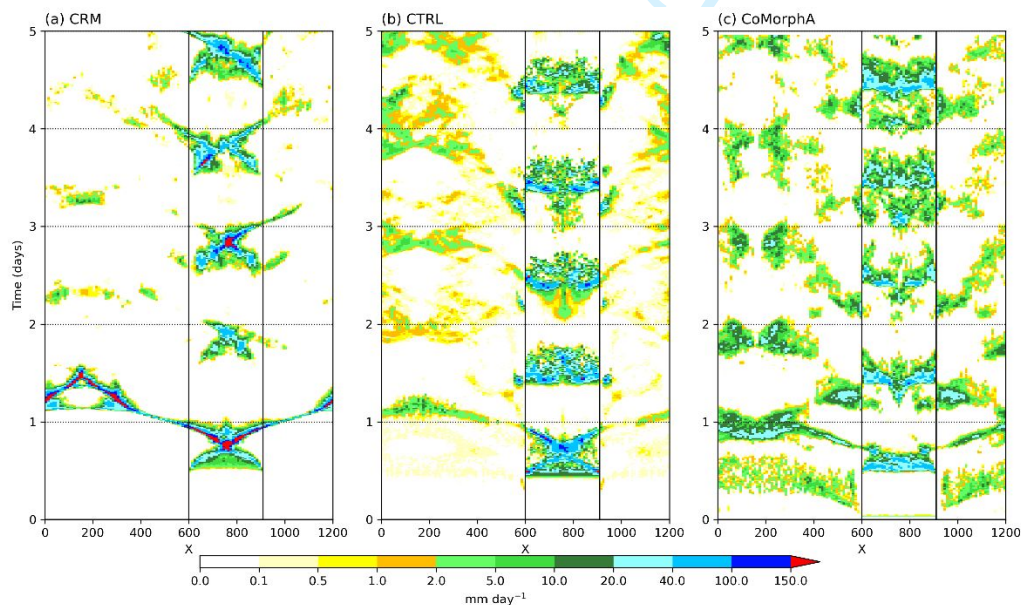
494 **Fig 8. Island case. Snapshots of precipitation [mm day⁻¹] at (a – c) 11 and (d-f) 23 UTC on**
 495 **day 3 of the island simulation with a 5 m s⁻¹ background wind ($U=5$) for (a, d) the CRM;**
 496 **regridDED to 10 km, (b, e) CTRL and (c, f) CoMorph-A. Hovmöller of precipitation [mm**
 497 **day⁻¹] averaged over full y-domain from (g) CRM (250 m; regridDED to 10 km), (h) CTRL**
 498 **and (i) CoMorph-A. The vertical black lines show the location of land ($x = 600\text{—}900$ km).**
 499 **The diagonal black line shows the background wind (5 m s⁻¹) with the grey line showing 20**
 500 **m s⁻¹. Red dashed lines show the times of the snapshots in (a-f).**

501 The Maritime Continent is difficult to represent accurately, with the initiation of convection
 502 by the convergence of sea-breeze circulations (Birch et al. 2015) and offshore gravity waves
 503 (Love et al. 2011) being vital for simulation of the region. An idealised island case has been
 504 developed to analyse this behaviour and examine the ability of propagation of convection

both on and off land. This new setup has an idealised island set at the equator, with interactive radiation and a real sandy land surface with plenty of moisture initially. It has been run with ($U=5 \text{ m s}^{-1}$; Fig 8) and without a background wind ($U=0 \text{ m s}^{-1}$; Fig 9). The case with the wind has a gravity wave propagating off the land initiating convection over the sea due to the heating profile of late afternoon convection over the land. The case with no wind illustrates the impact of land sea breezes.

With a background wind (Fig 8), snapshots of precipitation rate at 11am and 11pm show the location of precipitation in each simulation. At 11am on day 3 there is much more rain over land in the parameterized runs than the high-resolution CRM (Figs 8a—c), although there is a line of precipitation over the ocean in all three simulations. At 11pm (Figs 8d—f) there is a distinct line of precipitation associated with the gravity wave in the CRM. The CTRL has convection just off-land which isn't evident in CoMorph-A.

Propagation in the CRM (Fig 8g) is much quicker ($\sim 20 \text{ m s}^{-1}$) than the lower-resolution parametrized convection runs (Fig 8h,i) which propagate at a similar speed to the background wind (5 m s^{-1}), particularly over the ocean. CoMorph-A propagates at this higher speed over land but struggles to propagate off the land, unlike CTRL which is better at capturing this. CoMorph-A has widespread mid-intensity precipitation but not the very high intensities shown in CTRL.



523

524 **Fig 9. Island case. Hovmöller (averaged over full y-domain) of precipitation [mm day^{-1}] from (a)**
 525 **CRM (250 m; regridded to 10km), (b) CTRL and (c) CoMorph-A from simulations of the**
 526 **idealised island with no background wind ($U=0$).**

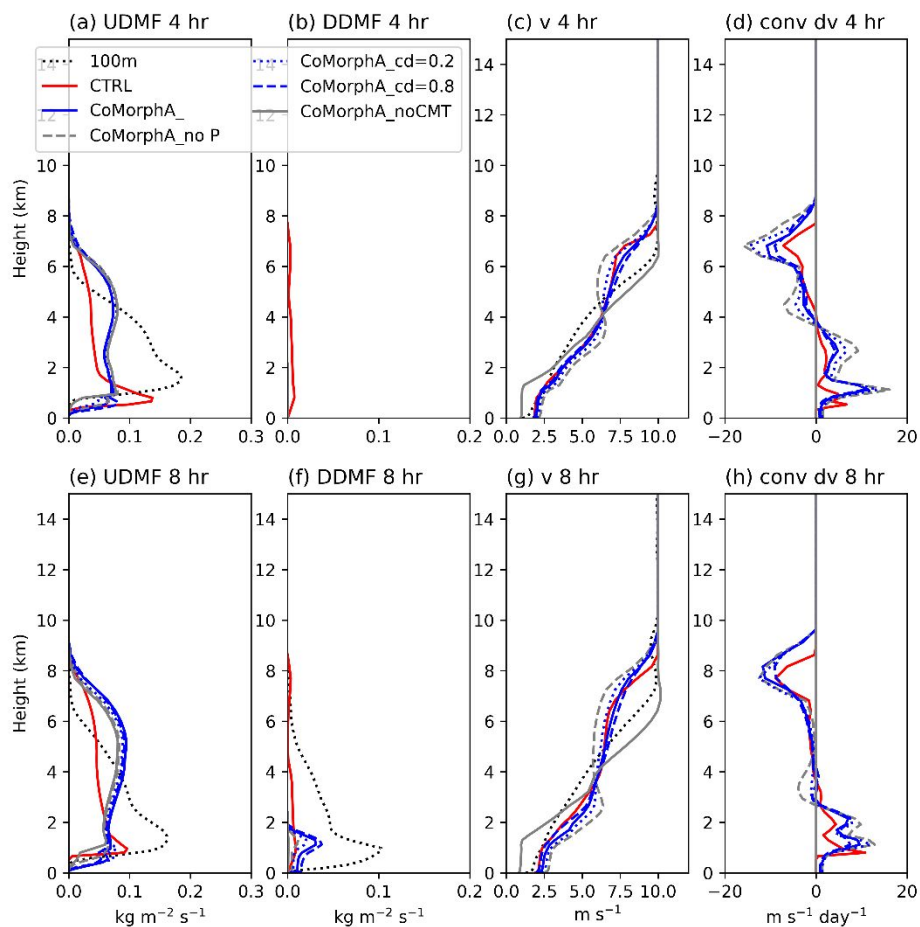
1
2
3 527 The case with no background wind (Fig 9a) shows precipitation over the island tending to
4 528 start close to the coasts, likely initiated by sea breezes, and gradually moving inland. Later in
5 529 the day the convection tends to become more widespread over the land. On some days
6 530 convection propagates for a small distance off land which is possible evidence of cold pools
7 531 and land-sea breezes. Both CTRL and CoMorph-A (Figs 9b,c) show no evidence of the
8 532 convection over land starting at the coasts, instead there is some evidence of convection in
9 533 the centre of the island starting far too early. This island setup shows some more work is
10 534 needed to correctly represent the interaction with sea breezes in CoMorph-A and will be a
11 535 useful testbed during future development of the scheme.

12
13
14
15
16
17
18
19
20 536 In the final case, we show the impact of different tunings on the representation of CMT and
21 537 the utility of idealised cases to inform tunings of the GCM.

22 23 24 538 3.7 Convective momentum transport

25
26
27 539 The transport of momentum vertically by convection (i.e. CMT) is an important process,
28 540 significantly affecting upper-level wind speeds in global models (e.g. Gregory et al. 1997),
29 541 and needs to be parametrized. The cold air outbreak case
30
31
32
33 542 from Kershaw & Gregory (1997) is used to test CoMorph's CMT behaviour. The CRM
34 543 profiles (black dotted, Fig 10) are similar to the results documented in the original paper (Figs
35 544 7,9 in Kershaw & Gregory 1997). The mass flux profiles (Fig 10a, b, e, f) differ between the
36 545 parametrized and CRM results with CoMorph-A having a secondary peak in updraught mass
37 546 flux at 5—6 km altitude compared with CTRL and CRM where there is a single peak just
38 547 above cloud base (Figs 10a, e). The CTRL downdraft mass flux remains fairly uniform with
39 548 height whereas both CoMorph-A and CRM show a peak at 1 km. Since the mass flux
40 549 profiles are different between the simulations, we do not expect to have the same wind
41 550 profile; however, by changing the CMT calculation we can see the effect on these profiles.
42 551 The shallower updraught mass flux profile in the CRM than the parametrized runs results in
43 552 the winds reaching the maximum value at lower altitude. Without the inclusion of CMT the
44 553 resulting winds are too weak at low levels and too strong above 2 km (grey solid line; Fig
45 554 10c, g). Originally the CMT was applied without a pressure gradient term to account for the
46 555 difference between in-cloud and environmental momentum, resulting in the overly strong
47 556 damping of the upper-level winds (grey dotted line; Fig 10c, g) which was also evident in
48 557 global simulations (not shown). Adding in a pressure gradient term with a quadratic drag law
49
50
51
52
53
54
55
56
57
58
59
60

558 leads to damping of the winds to an appropriate level, taking into consideration that the mass
 559 flux profile does not compare perfectly with the CRM. The sensitivity to the value of the
 560 drag coefficient in the pressure gradient term is also shown with a lower drag (dashed lines)
 561 resulting in convection being more efficient at transporting momentum in the vertical (e.g.
 562 Fig 8c,d,g,h). The magnitude of the convective increment to meridional winds are similar
 563 between CTRL and CoMorph-A.



564

565 **Fig 10. CMT. Profiles at 4 hours of (a) updraught mass flux [$\text{kg m}^{-2} \text{s}^{-1}$], (b) downdraught**
 566 **mass flux [$\text{kg m}^{-2} \text{s}^{-1}$], (c) meridional wind [m s^{-1}] and (d) the increment in meridional wind**
 567 **due to convection [$\text{m s}^{-1} \text{day}^{-1}$] in the parameterized runs for the cold air outbreak case. (e-h)**
 568 **as (a-d) but 8 hours into the run. Results shown for the 100 m CRM (black), CTRL (red)**
 569 **and various configurations of CoMorph: CoMorph-A (blue, solid), CoMorph-A with no**
 570 **CMT (grey), CoMorph-A but no pressure term in the CMT calculation (grey, dashed), drag**
 571 **coefficient of 0.2 (blue, dotted) and 0.8 (blue, dashed).**

1
2
3 572 This final case has shown the impact of different formulations and tunings of the
4 parameterization on the results. The following section will bring all these cases together and
5 573 summarise the results.
6
7 574

9 575 4.Summary & Conclusions

10
11
12 576 CoMorph is a new convection scheme developed for the UM, a model which is used
13 extensively across the globe by various institutions. The CoMorph-A package has been
14 577 shown to perform well in a global configuration, with a reduction of biases under climate
15 578 configuration and improved NWP performance (A. Lock, submitted work). Although
16 579 ultimately it is the GCM performance that determines if a scheme becomes operational,
17 580 throughout development the scheme has been tested using a 3D idealised UM which uses the
18 581 same science configuration as the full GCM but is substantially cheaper to run. This has
19 582 allowed us to understand in detail how the model behaves as a function of regime. The
20 583 present study has documented the performance of CoMorph-A in a selection of idealised
21 584 experiments, ranging from highly idealised with only high-resolution convection-resolving
22 585 data as a reference to those based on observational field campaigns with real data and
23 586 previous intercomparison studies to compare against. Although a number of these cases were
24 587 initially designed for SCM comparisons, the use of the 3D idealised model has several
25 588 advantages: Evaluation at higher resolutions with the same physics, dynamics and coupling
26 589 as used in the full GCM, comparison of the emergent organisation and spatial structures, and
27 590 allowing interaction with the winds leading to propagation of convection (Section 3.6). The
28 591 results are designed to serve as a baseline for others to compare against, and for assessing
29 592 performance as CoMorph evolves over the coming years.
30
31
32
33
34
35
36
37
38
39
40
41
42
43

44 594 CoMorph-A showed some organisation of convection when in RCE, consistent with the
45 595 majority of models compared in RCEMIP (Wing et al. 2020). The structures from the
46 596 sensitivity to humidity case showed the emergence of cellular behaviour that was observed in
47 597 the high-resolution reference. However, both parameterized runs produce too widespread
48 598 precipitation throughout the domain compared to the CRM. Profiles of updraught mass flux
49 599 have shown that the peak value is consistently greater in the high-resolution simulations than
50 600 the parameterised runs, although with lower associated precipitation rates. This may point to
51 601 a need for stronger downdraught representation in CoMorph in future. The sharper inversion
52 602 and low termination of updraught mass flux relative to the CRM also suggest the need for a
53 603 representation of overshoots.
54
55
56
57
58
59
60

1
2
3 604 All three diurnal cycle experiments (Section 3.3) show improvements in the timing of the
4
5 605 triggering and peak in precipitation over CTRL but still trigger too early relative to high
6
7 606 resolution simulations. This is consistent with the results from global simulations (A. Lock,
8
9 607 submitted work) where, although some regions such as parts of Africa have a degradation in
10
11 608 the diurnal cycle compared to the control, other regions are improved but still precipitate too
12
13 609 early in the day. The peak precipitation is too high across the three cases, with the mass flux
14
15 610 showing convection is too deep in most cases. Use of the memory function (Section 3.4)
16
17 611 shows CoMorph-A has a more realistic response to earlier precipitation than CTRL. A
18
19 612 number of cases (Figs 4,5,10) show CoMorph has a more top-heavy mass-flux profile than
20
21 613 CTRL. This is likely due to convection triggering from multiple different heights in the
22
23 614 column as well as differences in the detrainment and entrainment formulation.

24
25 615 Overall, CoMorph-A is shown to perform competitively against the existing science
26
27 616 configuration. However, as might be expected with the development of a new convection
28
29 617 scheme there are still areas for improvement. In addition to the timing and amplitude of the
30
31 618 diurnal cycle of precipitation mentioned above, difficulties in simulating the propagation of
32
33 619 convection off land and representing sea breezes in CoMorph-A are made evident using the
34
35 620 idealised island case (Section 3.6). CoMorph-A is shown to have too little sensitivity to
36
37 621 humidity using the Derbyshire et al. (2004) experimental setup (Fig 2) with little variation in
38
39 622 the mass flux profiles. These results suggest the need to suppress convection at lower
40
41 623 humidities (e.g Hirons et al. 2013) and based on this experiment it is perhaps surprising that
42
43 624 CoMorph-A shows improvements in the representation of the MJO (A. Lock, submitted
44
45 625 work). However, the mass flux profiles do vary greatly between the wet and dry periods of
46
47 626 the TWP-ICE experiment (Fig 7) suggesting this sensitivity may be increased under a
48
49 627 different experimental setup. Using a SCM, Daleu et al. (2023) found the relationship
50
51 628 between precipitation and column relative humidity was well represented by CoMorph-A in
52
53 629 dry environments but breaks down above 70% relative humidity. This sensitivity and the
54
55 630 difference in results depending on the experiment needs to be investigated further using
56
57 631 additional tests.

58
59 632 Many of the convective-scale processes parameterised in CoMorph carry significant
60
61 633 uncertainties. In recognition of this, many of the formulae within the scheme are scaled by
62
63 634 dimensionless “tuning factors” which can be easily changed. CoMorph has around 30 of
64
65 635 these tuneable parameters, scaling the initial parcel perturbations, entrainment (and its

1
2
3 636 sensitivity to convective organisation), detrainment, various in-plume microphysical
4 637 processes, the area-fractions of convective cloud and precipitation passed to other parts of the
5 638 model, and other processes. In CoMorph A, many of these parameters have been tuned over
6 639 successive versions to ensure both model-stability and good global performance. Section 3.7
7 640 illustrates the need for a convection scheme to consider the sub-grid transport of momentum
8 641 by convection without which the upper-level winds are too strong. How the CMT is
9 642 parameterized, and the sensitivity to the drag coefficient, required careful consideration to
10 643 perform well in both global and idealised simulations. This is the only section where the
11 644 sensitivity of the results to parameters within CoMorph has been discussed. However, it is
12 645 worth noting that the CoMorph-A entrainment rate is variable depending on the previous
13 646 time-step precipitation rate, a development that was included based on global testing and is
14 647 found to improve the performance in climate simulations. Many of the idealised cases have
15 648 additionally been run with a fixed (high or low) entrainment rate. The higher entrainment
16 649 rate is found to be beneficial for some cases such as increasing the sensitivity to humidity and
17 650 the timing of triggering of precipitation in the diurnal cycle experiments, but the lower
18 651 entrainment is necessary for TWP-ICE and capturing the secondary enhancement of
19 652 convection in the convective memory (not shown). Global analysis suggests the tropical
20 653 mean temperature profiles are particularly sensitive to the parameters controlling
21 654 entrainment, detrainment and in-plume ice processes. Sub-tropical light rain (which exerts a
22 655 strong influence on climate sensitivity) is very sensitive to the in-parcel cloud-to-rain
23 656 autoconversion and precipitation fraction parameters. A more detailed analysis of the
24 657 sensitivity to a range of parameters may form the basis of future work.

25
26
27
28
29
30
31
32
33
34
35
36
37
38
39
40
41
42 658 There are several proposed improvements to CoMorph to help address the discussed
43 659 deficiencies. These include the representation of a second updraught type such that both
44 660 surface-driven and cold-pool forced convection are represented and allow the proportion of
45 661 cold-pool forced updraughts to grow more gradually as more deep clouds are initiated. This,
46 662 along with various additional scientific improvements, including the representation of
47 663 overshoots and formulation of downdraughts highlighted in this study, will be included in a
48 664 future release of CoMorph. At the time of writing, the next release of CoMorph is
49 665 undergoing extensive testing over a range of experiments, including the idealised experiments
50 666 discussed in the current study. Subsequently, the aim is to couple CoMorph with the C-POOL
51 667 prognostic cold-pool scheme (Rooney et al. 2022) and enhance the scale-aware properties of
52 668 the scheme for running at higher (< 10 km) resolutions.
53
54
55
56
57
58
59
60

669

670 *Acknowledgements*

671 SLL is funded through the Northern Australia Climate Program (NACP), funded by Meat and
672 Livestock Australia, the Queensland Government through the Drought and Climate
673 Adaptation Program, and the University of Southern Queensland. CD, RP and J-FG
674 gratefully acknowledge funding from NERC grant NE/N013743/1 as part of the ParaCon
675 programme (<https://www.metoffice.gov.uk/research/approach/collaboration/paracon>). The
676 authors thank two anonymous reviewers for their detailed and insightful comments that
677 helped to improve the manuscript.

678 *Author Contributions*

679 SLL: Formal analysis; data curation; methodology; investigation, software; visualization;
680 writing – original draft; writing – review and editing. AJS: Conceptualization; supervision;
681 writing – review and editing. MW: Software; writing – review and editing. RS: Data curation;
682 methodology; software; investigation, writing - review and editing. CLD: Formal analysis;
683 data curation; methodology; investigation, software; writing – review and editing. RSP:
684 Writing - review and editing. AL: Writing - review and editing. J-FG: Methodology; writing -
685 review and editing.

686 *Data Availability Statement*

687 The data generated from the model simulations used in this paper can be made available by
688 the lead author and Met Office co-authors.

689 **References**

- 690 Ahn, M.-S., Kim, D., Kang, D., Lee, J., Sperber, K. R., Gleckler, P. J., et al. (2020). MJO propagation
691 across the Maritime Continent: Are CMIP6 models better than CMIP5 models? *Geophysical Research*
692 *Letters*, 47, e2020GL087250. <https://doi.org/10.1029/2020GL087250>
- 693 Arakawa, A., and Schubert, W. H. (1974), Interaction of a cumulus cloud ensemble with the large-
694 scale environment, Part I. *J. Atm Sci*, 31.3, 674-701.
- 695 Birch, C. E., Roberts, M. J., Garcia-Carreras, L., Ackerley, D., Reeder, M. J., Lock, A. P. and
696 Schiemann, R. (2015) Seabreeze dynamics and convection initiation: the influence of convective

- 1
2
3 697 parameterization in weather and climate model biases. *Journal of Climate*, 28 (20). pp. 8093-8108.
4
5 698 ISSN 1520-0442 doi: <https://doi.org/10.1175/JCLI-D-14-00850.1>
6
7 699 Brown, A.R., Cederwall, R. T., Chlond, A., Duynkerke, P.G., Golaz, J.-C., Khairoutdinov, M.,
8
9 700 Lewellen, D. C., Lock, A. P., Macvean, M. K., Moeng, C.-H., Neggers, R.A.J., Siebesma, A. P. and
10
11 701 Stevens B. (2002) Large-eddy simulation of the diurnal cycle of shallow cumulus convection over
12
13 702 land. *Q.J.R. Meteorol. Soc.* 128, 1075-1093.
14
15 703 Brown, A., Milton, S., Cullen, M., Golding, B., Mitchell, J. and Shelly, A. (2012) Unified modeling
16
17 704 and prediction of weather and climate: a 25 year journey. *Bulletin of the American Meteorological*
18
19 705 *Society*, 93, 1865–1877. <https://doi.org/10.1175/BAMS-D-12-00018.1>
20
21 706 Brown, N., Weiland, M., Hill, A., Shipway, B., Maynard, C., Allen, T., & Rezný, M. (2015). A highly
22
23 707 scalable Met Office NERC Cloud model. In *Proceedings of the 3rd International Conference on*
24
25 708 *Exascale Applications and Software* (pp. 132– 137).
26
27 709 Bush, M., Boutle, I., Edwards, J., Finnenkoetter, A., Franklin, C., Hanley, K., Jayakumar, A., Lewis,
28
29 710 H., Lock, A., Mittermaier, M., Mohandas, S., North, R., Porson, A., Roux, B., Webster, S., and
30
31 711 Weeks, M. (2023) The second Met Office Unified Model–JULES Regional Atmosphere and Land
32
33 712 configuration, RAL2, *Geosci. Model Dev.*, 16, 1713–1734, [https://doi.org/10.5194/gmd-16-1713-](https://doi.org/10.5194/gmd-16-1713-2023)
34
35 713 [2023](https://doi.org/10.5194/gmd-16-1713-2023)
36
37 714 Chaboureaud, J.-P., Guichard, F., Redelsperger, J.-L. and Lafore, J.-P. (2004), The role of stability
38
39 715 and moisture in the diurnal cycle of convection over land. *Q.J.R. Meteorol. Soc.*, 130: 3105-3117.
40
41 716 <https://doi.org/10.1256/qj.03.132>
42
43 717 Chen, S. S., Houze, R. A., Jr., and Mapes, B. E. (1996). Multiscale Variability of Deep Convection in
44
45 718 Relation to Large-Scale Circulation in TOGA COARE. *Journal of Atmospheric Sciences* 53, 10,
46
47 719 1380-1409, [https://doi.org/10.1175/1520-0469\(1996\)053<1380:MVODCI>2.0.CO;2](https://doi.org/10.1175/1520-0469(1996)053<1380:MVODCI>2.0.CO;2)
48
49 720 Christopoulos, C., & Schneider, T. (2021). Assessing biases and climate implications of the diurnal
50
51 721 precipitation cycle in climate models. *Geophysical Research Letters*, 48, e2021GL093017.
52
53 722 <https://doi.org/10.1029/2021GL093017>
54
55 723 Couvreux, F., Rio, C., Guichard, F., Lathon, M., Canut, G., Bounou, D. and Gounou, A. (2012)
56
57 724 Initiation of daytime local convection in a semi-arid region analysed with high resolution simulations
58
59 725 and AMMA observations. *Q.J.R. Meteorol. Soc.*, 138, 56-71.
60
61 726 Couvreux, F., Roehrig, R., Rio, C., Lefebvre, M.-P., Caian, M., Komori, T., Derbyshire, S., Guichard,
62
63 727 F., Favot, F., D'Andrea, F., Bechtold, P. and Gentine, P. (2015), Representation of daytime moist

- 1
2
3 728 convection over the semi-arid Tropics by parametrizations used in climate and meteorological models.
4
5 729 Q.J.R. Meteorol. Soc, 141: 2220-2236. <https://doi.org/10.1002/qj.2517>
6
7 730 Daleu, C.L., Plant, R.S., Stirling, A.J. & Whittall, M.(2023) Evaluating the CoMorph-A
8
9 731 parametrization using idealized simulations of the two-way coupling between convection and large-
10
11 732 scale dynamics. Quarterly Journal of the Royal Meteorological Society, 1–23.
12
13 733 <https://doi.org/10.1002/qj.4547>
14
15 734 Daleu, C. L., Plant, R. S., Woolnough, S. J., Stirling A.J. and Harvey N.J. (2020) Memory Properties
16
17 735 in cloud-resolving simulations of the diurnal cycle of deep convection. JAMES 12
18
19 736 doi:10.1029/2019MS001897
20
21 737 Derbyshire, S.H., Beau, I., Bechtold, P., Grandpeix, J.-Y., Piriou, J.-M., Redelsperger, J.-L. and
22
23 738 Soares, P.M.M. (2004), Sensitivity of moist convection to environmental humidity. Q.J.R. Meteorol.
24
25 739 Soc., 130: 3055-3079. doi:10.1256/qj.03.130
26
27 740 Fridlind, A.M., Ackerman, A.S., Chaboureau, J.-P., Fan, J., Grabowski, W.W., Hill, A.A., Jones,
28
29 741 T>R., Khaiyer, M.M, Liu, G., Minnis, P., Morrison, H., Nguyen, L., Park, S., Petch, J.C., Pinty, J.-P.,
30
31 742 Schumacher, C., Shipway, B.J., Varble, A.C., Wu, X., Xie, S. and Zhang, M. (2012) A comparison of
32
33 743 TWP-ICE observational data with cloud-resolving model results. J. Geophys. Res.
34
35 744 117, doi:10.1029/2011JD016595.
36
37 745 Gregory, D. and Guichard, F. (2002), Aspects of the parametrization of organized convection:
38
39 746 contrasting cloud-resolving model and single-column model realizations. Q.J.R. Meteorol. Soc., 128:
40
41 747 625-646. <https://doi.org/10.1256/003590002321042126>
42
43 748 Gregory, D. and Rowntree, P. R. (1990) A mass-flux convection scheme with representation of cloud
44
45 749 ensemble characteristics and stability dependent closure. Mon. Weather Rev., 118, 1483–1506.
46
47 750 Guichard, F., Petch, J.C., Redelsperger, J.-L., Bechtold, P., Chaboureau, J.-P., Cheinet, S.,
48
49 751 Grabowski, W., Grenier, H., Jones, C.G., Köhler, M., Piriou, J.-M., Tailleux, R. and Tomasini, M.
50
51 752 (2004), Modelling the diurnal cycle of deep precipitating convection over land with cloud-resolving
52
53 753 models and single-column models. Q.J.R. Meteorol. Soc., 130: 3139-3172.
54
55 754 <https://doi.org/10.1256/qj.03.145>
56
57 755 Hirons, L.C., Inness, P., Vitart, F. and Bechtold, P. (2013), Understanding advances in the simulation
58
59 756 of intraseasonal variability in the ECMWF model. Part II: The application of process-based
60
757 758 diagnostics. Q.J.R. Meteorol. Soc., 139: 1427-1444. <https://doi.org/10.1002/qj.2059>

- 1
2
3 758 Kershaw, R. and Gregory, D. (1997) Parametrization of momentum transport by convection. I:
4 759 Theory and cloud modelling results. *Q.J.R. Meteorol. Soc.*, **123**, 1133-1151.
5
6
7 760 Kim, D., Kug, J., and Sobel, A.H. (2014): Propagating versus Nonpropagating Madden–Julian
8 761 Oscillation Events. *J. Climate*, **27**, 111–125, <https://doi.org/10.1175/JCLI-D-13-00084.1>.
9
10
11 762 Lenderink, G., Siebesma, A.P., Cheinet, S., Irons, S., Jones, C.G., Marquet, P., Müller, F., Olmeda,
12 763 D., Calvo, J., Sánchez, E. and Soares, P.M.M. (2004), The diurnal cycle of shallow cumulus clouds
13 764 over land: A single-column model intercomparison study. *Q.J.R. Meteorol. Soc.*, 130: 3339-3364.
14 765 <https://doi.org/10.1256/qj.03.122>
15
16
17
18 766 Love, B.S., Matthews, A.J. and Lister, G.M.S. (2011), The diurnal cycle of precipitation over the
19 767 Maritime Continent in a high-resolution atmospheric model. *Q.J.R. Meteorol. Soc.*, 137: 934-947.
20 768 <https://doi.org/10.1002/qj.809>
21
22
23
24 769 May, P. T., J. H. Mather, G. Vaughan, and C. Jakob (2008), Characterizing oceanic convective cloud
25 770 systems—The Tropical Warm Pool International Cloud Experiment, *Bull. Am. Meteorol. Soc.*, 154,
26 771 153–155, doi:10.1175/BAMS-89-2-153.
27
28
29
30 772 McIntyre, W.A., Efstathiou, G.A. & Thuburn, J.(2022) A two-fluid single-column model of turbulent
31 773 shallow convection. Part III: Results and parameter sensitivity. *Q.J.R. Meteorol. Soc.*, 1–20.
32 774 <https://doi.org/10.1002/qj.4390>
33
34
35
36 775 Petch, J., Hill, A., Davies, L., Fridlind, A., Jakob, C., Lin, Y., Xie, S. and Zhu, P. (2014), Evaluation
37 776 of intercomparisons of four different types of model simulating TWP-ICE. *Q.J.R. Meteorol. Soc.*,
38 777 140: 826-837. <https://doi.org/10.1002/qj.2192>
39
40
41
42 778 Roberts, N. M., (2001), Results from simulations of an organised convective event using the New
43 779 Dynamics at 12, 4 and 2 km resolution. *NWP Technical Report No. 344*. Joint Centre for Mesoscale
44 780 Meteorology, University of Reading, PO Box 243, Reading, Berkshire RG6 2BB, UK
45
46
47
48 781 Rooney, G.G., Stirling, A.J., Stratton, R.A., and Whittall, M.(2022) C-POOL: A scheme for modelling
49 782 convective cold pools in the Met Office Unified Model. *Q J R Meteorol Soc*, 962– 980.
50 783 <https://doi.org/10.1002/qj.4241>
51
52
53 784 Smith, R. N. B., (1990), A scheme for predicting layer clouds and their water content in a general
54 785 circulation model. *Quart. J. Roy. Meteor. Soc.*, 116, 435–460, doi:10.1002/qj.49711649210.
55
56
57
58
59
60

- 1
2
3 786 Tomassini, L., Parker, D.J., Stirling, A., Bain, C., Senior, C. and Milton, S. (2017), The interaction
4 787 between moist diabatic processes and the atmospheric circulation in African Easterly Wave
5 788 propagation. *Q.J.R. Meteorol. Soc.*, 143: 3207-3227. doi:[10.1002/qj.3173](https://doi.org/10.1002/qj.3173)
- 6
7
8
9 789 Walters, D., Baran, A. J., Boutle, I., Brooks, M., Earnshaw, P., Edwards, J., Furtado, K., Hill, P.,
10 790 Lock, A., Manners, J., Morcrette, C., Mulcahy, J., Sanchez, C., Smith, C., Stratton, R., Tennant, W.,
11 791 Tomassini, L., Van Weverberg, K., Vosper, S., Willett, M., Browse, J., Bushell, A., Carslaw, K.,
12 792 Dalvi, M., Essery, R., Gedney, N., Hardiman, S., Johnson, B., Johnson, C., Jones, A., Jones, C.,
13 793 Mann, G., Milton, S., Rumbold, H., Sellar, A., Ujiie, M., Whittall, M., Williams, K. and Zerroukat, M.
14 794 (2019) The Met Office Unified Model Global Atmosphere 7.0/7.1 and JULES Global Land 7.0
15 795 configurations. *Geoscientific Model Development*, 12 (5). pp. 1909-1963.
16 796 <https://doi.org/10.5194/gmd-12-1909-2019>
- 17
18 797 Whittall, M., Stirling, A., Lock, A., Lavender, S., Stratton, R., Matsubayashi, K. (2022) The CoMorph
19 798 convection scheme. UM Documentation Paper 043.
- 20
21
22 799 Willett, M. R., & Whittall, M. A. (2017). A simple prognostic based convective entrainment rate for
23 800 the unified model: Description and tests (technical report no. 617). Met Office.
- 24
25
26 801 Williams, K. D., Copsey, D., Blockley, E. W., Bodas-Salcedo, A., Calvert, D., Comer, R., ... Xavier,
27 802 P. K. (2017). The Met Office Global Coupled model 3.0 and 3.1 (GC3.0 and GC3.1) configurations.
28 803 *Journal of Advances in Modeling Earth Systems*, 10, 357–380.
29 804 <https://doi.org/10.1002/2017MS001115>
- 30
31
32 805 Wilson, D. R., Bushell, A. C., Kerr-Munslow, A. M., Price, J. D., and Morcrette, C. J. (2008) PC2: A
33 806 prognostic cloud fraction and condensation scheme. I: Scheme description, *Q. J. Roy. Meteorol. Soc.*,
34 807 134, 2093–2107, <https://doi.org/10.1002/qj.333>
- 35
36
37 808 Wing, A. A., Reed, K. A., Satoh, M., Stevens, B., Bony, S., and Ohno, T. (2018) Radiative–
38 809 convective equilibrium model intercomparison project, *Geosci. Model Dev.*, 11, 793–813,
39 810 <https://doi.org/10.5194/gmd-11-793-2018>
- 40
41
42 811 Wing, A. A., Stauffer, C. L., Becker, T., Reed, K. A., Ahn, M.-S., & Arnold, N. P., et al. (2020).
43 812 Clouds and convective self-aggregation in a multimodel ensemble of radiative-convective equilibrium
44 813 simulations. *Journal of Advances in Modeling Earth Systems*, 12, e2020MS002138.
45 814 <https://doi.org/10.1029/2020MS002138>
- 46
47
48 815 Yang, G. Y., & Slingo, J. (2001). The diurnal cycle in the tropics. *Monthly Weather Review*, 129,
49 816 784–801.
- 50
51
52
53
54
55
56
57
58
59
60

1
2
3 The authors thank both reviewers for their positive comments regarding the revised manuscript. We
4 have addressed all minor comments, and point-by-point responses are included below.
5

6 We have additionally gone through and addressed all areas where unpublished work (the Lock et al.
7 paper) was cited. Where appropriate we have included the additional necessary information and
8 when referring to results from that paper, we have cited the unpublished work (in the text only)
9 according to Wiley guidelines.
10
11

12
13 Referee(s)' Comments to Author:
14

15 Reviewer: 1
16

17 Comments to the Author

18 It is good to see that the authors have followed both reviewers comments, mostly a wise decision,
19 including dropping two case studies. The manuscript reads now much better with a clearer line of
20 thought. Just a few more minor clarifications are needed
21
22

23 Many thanks for your positive response to the changes we made and your subsequent comments
24 that help clarify the text.
25

26 -line 82 make a paragraph before "A selection.." Thanks for the suggestion – the paragraph now split
27
28

29 -line 92 "CoMorph has around 30 tuneable parameters" This is quite huge number. You just
30 discussed/tested two here, for entrainment and momentum drag, could you add at least in
31 conclusion/outlook which are the other most important and could have affected results here (ie
32 heating profiles)
33

34 It is worth noting that many other convection schemes have a similar or larger numbers of free
35 parameters. We have declared such parameters centrally in the code and allow them to be set via
36 the namelist; other convection codes like the 6A scheme have many uncertain values hardwired
37 within the source-code, so that the number of free parameters in the scheme is not obvious and
38 aren't easily modified without changing the source code.
39
40

41 We have added in the additional information:

42 "Many of the convective-scale processes parameterised in CoMorph carry significant
43 uncertainties. In recognition of this, many of the formulae within the scheme are scaled by
44 dimensionless "tuning factors" which can be set via the namelist. CoMorph has around 30 of these
45 tuneable parameters, scaling the initial parcel perturbations, entrainment (and its sensitivity to
46 convective organisation), detrainment, various in-plume microphysical processes, the area-fractions
47 of convective cloud and precipitation passed to other parts of the model, and other processes. In
48 CoMorph A, many of these parameters have been tuned over successive versions to ensure both
49 model-stability and good global performance. " and

50 "The Tropical mean temperature profiles are particularly sensitive to the parameters controlling
51 entrainment, detrainment and in-plume ice processes. Sub-Tropical light rain (which exerts a strong
52 influence on climate sensitivity) is very sensitive to the in-parcel cloud-to-rain autoconversion and
53 precipitation fraction parameters."
54
55

56 -are the CTL forecast also using prognostic entrainment? This was not clear in text and should be
57 made clearer
58
59
60

1
2
3 Apologies this wasn't clear in the text. Yes, the CTRL has prognostic entrainment (CoMorph does
4 not). "For the control run (CTRL) using GAL8 as officially defined i.e., with the current UM convection
5 scheme, there have been significant changes to the existing convection scheme **including the use of**
6 **a prognostic entrainment rate to allow some memory of recent convection** (Willett & Whitall,
7 2017). "

8
9
10 -l146 "When surface-triggered convection occurs, the cloud-base height emerges from the scheme
11 when the modelled bulk plume rises high enough to reach saturation." what do you do then for
12 non-surface triggered convection? the LFC should still be obtained the same way normally
13 Dry-statically-unstable layers usually only occur near-surface. Convection also triggers from moist-
14 unstable (but dry-stable) layers at other heights, but only if the model's large-scale cloud scheme
15 predicts cloud is present. In this case, the convection triggers from within already-cloudy air, so the
16 cloud-base is at or below the parcel's triggering height (and the initial parcel is set to be already
17 saturated). But yes, in the rare event that convection triggers from an elevated dry-statically-
18 unstable layer, the cloud-base height would emerge naturally in the same way as for surface-
19 triggered convection.
20

21
22 To clarify this, we have altered the sentence to "**When convection triggers from non-cloudy model-**
23 **levels**, the cloud-base height emerges from the scheme when the modelled bulk plume rises high
24 enough to reach saturation."
25

26
27 Figures 4, 5,7, 10: you didn't discuss this this but it is important that CoMorph seems to produce
28 more top heavy (too top heavy?) profiles, is this linked to the lack of entrainment or a too
29 "stratiforme" heating/condensation profile?

30 We have not investigated in-detail why CoMorph A produces more top-heavy mass-flux profiles than
31 GA8 in these tests. There are several possibilities:

- 32 - CoMorph allows convection triggering from multiple different heights in the column to co-exist
33 higher in the column (this is arbitrarily not permitted in GA8, due to the code structure not
34 allowing "mid-level" convection to trigger at heights where a plume from below has not yet
35 terminated, however small its mass-flux and however unstable the layer is).
- 36 - CoMorph's detrainment formulation maybe more sensitive to environment stability; it can
37 produce zero detrainment where the profile is exceptionally unstable (which is the case in
38 EUROCS), so that the mass-flux increases with height via entrainment.
- 39 - Differences in entrainment formulation may play a role too, as you suggest.

40 Have included the following in the text:

41 "A number of cases (Figs 4,5,10) show CoMorph has a more top-heavy mass-flux profile than CTRL.
42 This is likely due to convection triggering from multiple different heights in the column as well as
43 differences in the detrainment and entrainment formulation."
44
45
46
47

48 -page 19: here you often talk talk about "convection produced after triggering". It should be
49 explained once on top of page what you really mean by this

50 Thanks for this useful suggestion. For these cases triggering is taken as the time the first
51 precipitation occurs. This is now clarified where it is first mentioned.
52
53

54 -l613 "based on this it is perhaps surprising that CoMoroh shows improvements in the
55 representation of the MJO". This is an honest but not very scientific statement. It would be helpful
56 and appreciated if you could cite here Hiron et al. 2012 (who had done all this already)
57 <https://eur01.safelinks.protection.outlook.com/?url=https%3A%2F%2Frmets.onlinelibrary.wiley.com%2Fdoi%2Ffull%2F10.1002%2Fqj.2059&data=05%7C01%7Csally.lavender%40metoffice.gov.uk%7C15f395d99c4449cb588508dbf37f5b65%7C17f1816120d7474687fd50fe3e3b6619%7C0%7C0%7C63837>
58
59
60

[1500548354359%7CUnknown%7CTWFpbGZsb3d8eyJWljojMC4wLjAwMDAiLCJQIjoiV2luMzliLCJBTiI6I
k1haWwiLCJXVCI6Mn0%3D%7C3000%7C%7C%7C&sdata=F4ov9LyZEimwHYqgcZntLY0BMYGKL%2FVR
AaRHF%2F0xg4Q%3D&reserved=0](#)

as already suggested that allows to lift these ambiguities. In addition, you could mention here the link to your top heavy heating profile

We've changed this sentence to reference the suggested paper:

"These results suggest the need to suppress convection at lower humidities (e.g Hiron et al. 2013) and based on this experiment it is perhaps surprising that CoMorph-A shows improvements in the representation of the MJO (A. Lock, submitted work)."

We have additionally added in a reference to the above paper earlier where the MJO and moisture sensitivity was introduced. This is an area we will be investigating in more detail as we develop CoMorph.

Reviewer: 2

Comments to the Author

Title: The use of idealised experiments in testing a new convective parameterization: Performance of CoMorph-A

Author(s): Lavender et al

Identification: QJ-23-0169.R1

Paper Summary:

This is the second review of this manuscript. This manuscript investigates the behaviour of a new convective parameterization over a large set of idealised cases. It defends the idea that the proposed ensemble of cases is suitable to evaluate new development in convective parameterization. I am convinced that having a convective playground to systematically test any development of the convective scheme is a very important objective.

Globally, I am satisfied with this revision that addresses my main major comments. However, I found that there are still quite some minor points that need revision before this paper be accepted in QJRMS.

Recommendation: Minor revision

General comments:

[Many thanks for your detailed review and positive response to the changes we made to the manuscript.](#)

Minor Comments:

Abstract:

1. L15-19: "Use of a three-dimensional idealised model enables controlled tests of the performance of the scheme..." this is a very long sentence conveying different messages. You should split into two sentences.

[Thanks for this suggestion. We've split in two sentences at "...regimes. This includes...."](#)

Introduction:

1. L37 'Since this motion can't accurately...' change to 'cannot'. [Changed, thanks.](#)
2. L62-63 'Lock et al 2023' is still quoted while not yet reviewed. [This is changed to \(A. Lock, submitted work\) based on the wiley guidelines.](#)
3. L76-77 'the more THE organised convection becomes ...' please rephrase.

We've changed this sentence to "In a recent study, Hwong et al. (2022) found that as convection becomes more organised, there are larger differences in results between one- and three-dimension (3D) simulations."

4. L 91-92 '... are presented alongside high-resolution (1 km or higher)' Please update as now all your CRM runs use hectometric resolution. Thanks for pointing out – we've changed to 250 m Model Experiments:

1. L 116 'including the inclusion of' change to including the prognostic entrainment. This sentence has been altered in response to Rev1

Focused Testing of CoMorph-A:

1. Table 1. Explain why these values vary among different cases. in 3.5 change 'casecases' to 'cases'

Apologies, it isn't clear what you are referring to by values – do you mean domain size? These are based on the original cases where appropriate – we have changed the wording to add further clarification "Since many of these cases are based on field campaigns, where the large-scale forcings have been observed/evaluated for specific areas, the domain sizes are chosen to be the same as those original cases. Where the original domain was smaller than $100 \times 100 \text{ km}^2$ this has been increased to allow large-scale circulations to form in the parametrized cases."

Thanks for pointing out the typo.

2. Section 3.1: L.199-200: 'The 200m simulation has a cooler troposphere': cooler compared to what? The CRM is it compared to the ensemble of the runs in RCE-MIP or only to the parameterized run. Similarly when describing the parameterized runs, it is implicit that the comparison is with the CRM. Should be explicit.

Thanks for pointing out that this wasn't clear. We have amended these sentences: "The parameterized runs have a warmer troposphere and higher altitude inversion than the CRM, leading to a higher termination of the updraft mass flux. CoMorph-A has a slightly warmer mid to upper-troposphere than CTRL and both parameterizations have a sharper inversion at cloud top than the CRM, with CoMorph-A slightly sharper than CTRL, possibly due to the current lack of representation of overshoots that would smooth out the inversion."

3. Figure 1: you may want to plot a vertical line at day=50 in (g) to indicate at what time the horizontal cross-sections of precipitation are shown on d-f. Also please adjust the plots in (d-f) in order to show the exact same horizontal domain.

Thanks for pointing this out - we have rerun the RCE in 200 km domain so that all domains are the same and replotted all plots. Additionally, we have included a vertical line to show the timing of the snapshot and adjusted the caption accordingly as suggested.

4. L 227–228; Please check this sentence 'the dependence of f_{sub} on the size of the domain... and the values were found similar' sounds bizarre.

Thanks, reworded to: "Using the large domain, the dependence of f_{sub} on the size of the blocks ($10 \times 10 \text{ km}^2$ compared to $100 \times 100 \text{ km}^2$ as used in the original study) was investigated and the values of f_{sub} were found to be similar."

5. L256-257 'While the CRM results show a similar overall sensitivity'. Please explicit 'similar to what? To the Derbyshire results?'

Have clarified "While the CRM results show a similar overall increase in precipitation rate from 25% to 90% humidity as documented in Derbyshire et al. (2004)"

6. L 309 'and consequently has a lower vertical resolution': can you describe more precisely the difference in terms of vertical resolution

We have now included more detail: "The original paper had a very small domain ($6.4 \times 6.4 \text{ km}^2$) domain with a low model top depth (4.4 km) and 40 m vertical resolution. Here, the same operational global and regional stretched grid vertical levels (Bush et al. 2023) are used with a 40 km model top and consequently the vertical resolution above the near-surface layer is lower. "

1
2
3 7. L 355: “Shown for each ensemble member...” maybe could be included just after CoMorph-A
4 (blue) in the previous sentence. [Have rearranged caption as suggested.](#)

5 8. L 357 “but FOR a different day” [Thanks, changed.](#)

6
7 9. L361-364: “earlier start time of 6 hours”... how this is accounted for? In the original version there
8 is a interactive radiation scheme? At the beginning of the diurnal case it is mentioned that no
9 radiation is included in none of those cases. How this affects the result for this case?

10 [This is purely a shift in the timeseries of 6 hours – this is already accounted for in the text when
11 comparing the results and have reworded to clarify this “...which is accounted for...”](#)

12 [Additionally, we have clarified that it uses the same experimental setup of Daleu who used this
13 radiative cooling applied to potential temperature – we have further clarified this in the text “... with
14 a prescribed radiative cooling applied to the potential temperature \(Daleu et al. 2020\).”](#)

15 [Based on the results of Guichard et al. 2004 \(and Petch et al. 2004\) who experimented with and
16 without interactive radiation we would not expect this to have much impact on the results but
17 instead allows a cleaner comparison of the different model comparisons without the additional
18 radiative variability.](#)

19
20 10. L 415-416: ‘but rainfall remains higher for longer’ better if changed to ‘...for longer time’ other
21 the sentence seems incomplete. [Thanks, changed](#)

22 11. L 432-433: ‘The suppression of convection (second phase) in MONC starts within 1.5 hours for
23 convection produced 2.5 hours after triggering (Fig 6c).’ MONC is not shown anymore please update
24 this sentence. [Thanks for pointing out – changed to the CRM](#)

25 12. L 438 ‘and IS only evident after’ [thanks, changed.](#)

26 13. L 449 ‘using time-varying FORCING based on observations’ [Thanks, altered.](#)

27
28 14. L470-471: ‘Like that case, CoMorph-A has a higher mass flux than CTRL with both lower than
29 the CRM peak.’ please change the end of the sentence for example => ‘While both lower than...’
30 [Changed as suggested.](#)

31 15. L 485: Inland propagation: please document the lateral boundary conditions used for this case,
32 cyclic? [This is already included in Section 2.1 “In the idealised configuration the model has bicyclic
33 boundary conditions over a limited area domain on a flat, cartesian grid.” This applies to all cases.](#)

34 16. L 487: caption of Fig 8: ‘CoMorph-A for the idealised island case.’ ‘for the idealised island case’
35 is not needed as already indicated at the beginning of the caption. Location of land (x=600-850 km)
36 [Thanks for pointing out this error in the location of land - have altered the caption in response to
37 both these points.](#)

38
39 Summary and Conclusions:

- 40 1. L 571-572: Lock et al 2023 and Zhu et al 2023 (here and elsewhere in the Conclusion) is
41 just submitted so this is an issue for referring to it.

42 [We have removed the Zhu citation. Where appropriate we have included the additional necessary
43 information from Lock et al. 2023 and when referring to results from that paper we have cited the
44 unpublished work \(in the text only\) according to Wiley guidelines.](#)

45 2. L 585-586: ‘agains as CoMorph evolves...’ erase the ‘and’ [This changes the meaning of the
46 sentence – we have instead reworded for additional clarification “The results are designed to serve
47 as a baseline for others to compare against, and for assessing performance as CoMorph evolves over
48 the coming years.”](#)

- 49
50
51 2. L 600 : ‘although some regions such as Africa have a degradation’ how this is consistent
52 with the AMMA case representative of local convection initiated over West Africa?

53 [Have added in “parts of Africa” since this degradation is worse in other regions of the
54 continent than West Africa. It isn’t comparing the same measure since the global paper
55 looks at the timing of the peak in the maximum diurnal harmonic rather than the time of
56 initiation of precip.](#)

- 57 4. L 636-637: change ‘the deficiencies discussed’ to ‘the discussed deficiencies’ [Thanks,](#)

58
59 [Altered](#)

60

1
2
3
4
5
6
7
8
9
10
11
12
13
14
15
16
17
18
19
20
21
22
23
24
25
26
27
28
29
30
31
32
33
34
35
36
37
38
39
40
41
42
43
44
45
46
47
48
49
50
51
52
53
54
55
56
57
58
59
60

For Peer Review

1
2
3
4
5
6
7
8
9
10
11
12
13
14
15
16
17
18
19
20
21
22
23
24
25
26
27
28
29
30
31
32
33
34
35
36
37
38
39
40
41
42
43
44
45
46
47
48
49
50
51
52
53
54
55
56
57
58
59
60

1 **The use of idealised experiments in testing a new convective**
2 **parameterization: Performance of CoMorph-A**

3 Sally L. Lavender^{1,2}, Alison J. Stirling², Michael Whitall², Rachel Stratton², Chimene L.
4 Daleu³, Robert S. Plant³, Adrian Lock², Jian-Feng Gu^{3,4}

5 ¹ *Centre for Applied Climate Sciences, University of Southern Queensland, Toowoomba, Australia*

6 ² *Met Office, Fitzroy Road, Exeter, UK*

7 ³ *Department of Meteorology, University of Reading, Reading, UK*

8 ⁴ *Key Laboratory of Mesoscale Severe Weather, Ministry of Education, and School of Atmospheric Sciences,*
9 *Nanjing University, Nanjing, China*

10
11
12 *Corresponding author: Sally Lavender, Sally.lavender@usq.edu.au*

13 ABSTRACT

14 CoMorph is a new mass-flux convection parameterization under development at the Met
15 Office designed for use within the Unified Model and its successor model, LFRic. Use of a
16 three-dimensional idealised model enables controlled tests of the performance of the scheme
17 across different regimes. This, including the interaction between the physical
18 parametrizations and the resolved dynamics, allowing study of the emergent organisation of
19 convection on the resolved scale. A selection of well-known cases is revisited here, with the
20 purpose of documenting the extent to which CoMorph captures a range of important, but
21 challenging behaviour such as the diurnal cycle and sensitivity to tropospheric moisture.
22 Simulations using CoMorph-A, a new physics package, that has been demonstrated to
23 perform well at NWP and climate scales, are compared against the current global atmosphere
24 configuration and high-resolution results. In addition to an entirely new convection scheme,
25 the package of changes includes significant changes to the cloud, microphysics, and boundary
26 layer parametrizations. Recognising that CoMorph-A is the first version of a scheme that
27 will continue to be substantially developed and to obtain good performance, compromises in
28 tuning have had to be made. These idealised tests therefore show what works well in this
29 configuration, and what areas will require further work. As such, it is quite a demanding
30 testbed and could be viewed as some of the equipment required for a 'convective
31 playground'.

32 **KEYWORDS:** convection parameterization, idealised modelling, cloud resolving models,
33 climate models, diurnal cycle

35 1. Introduction

36 Convective clouds act to transport heat, moisture and mass upwards, fuelled by the latent heat
37 release of condensing water from rising air parcels. Since this motion cannot accurately be
38 represented on the resolved model grid, a convection parameterization needs to represent the
39 effects of this dynamical process by estimating its influence on the temperature, moisture and
40 horizontal winds of the atmosphere, in addition to predicting the precipitation generated. The
41 subsequent adjustment of the temperature profile by the resolved scale has an influence on
42 the wider circulation patterns. As such, whether the convection scheme in a model adequately
43 represents the spatial and temporal distribution of convective precipitation and diabatic

1
2
3 44 heating has implications not only for local precipitation accumulations but also for global
4
5 45 circulation patterns through convective-dynamical coupling.
6

7
8 46 The Met Office Unified Model (UM; Brown et al. 2012) is used extensively across the world
9
10 47 with partnership institutions including the Australian Bureau of Meteorology, the National
11
12 48 Centre for Medium Range Weather Forecasting (NCMRWF) in India and the Meteorological
13
14 49 Service Singapore. For over 30 years, the Met Office convection scheme has been based on
15
16 50 the mass-flux approach of Arakawa and Schubert (1974), in which the role of the convection
17
18 51 scheme is to stabilise atmospheric profiles via the removal of CAPE (convectively available
19
20 52 potential energy) through subsidence within a grid column. The existing scheme, based on
21
22 53 Gregory and Rowntree (1990), lacks much of the structural flexibility required to address
23
24 54 systematic biases generated by convection in the UM (e.g. Walters et al. 2019). To address
25
26 55 this, a new convection scheme, CoMorph, has been developed (see Whitall et al. 2022 for full
27
28 56 details). Whilst still a bulk mass-flux scheme, CoMorph removes previously hardwired
29
30 57 structural assumptions such as initiation from a pre-determined cloud-base height and the use
31
32 58 of separate schemes for shallow, deep and mid-level convection which must be pre-
33
34 59 diagnosed. CoMorph has been written in a way that allows the inclusion of additional
35
36 60 physics and couples more fully and consistently to other physics components of the model
37
38 61 (see Section 2.2). A package of changes called CoMorph-A has been released and
39
40 62 simulations in a full global circulation model (GCM) have shown the positive impact of
41
42 63 including this package in the GCM ([A. Lock, submitted work](#)) ([Loek et al. 2023](#)). These
43
44 64 benefits include a reduction in radiative flux biases across the tropics, improvements in
45
46 65 tropical and extratropical cyclone statistics, strengthening of the Madden Julian oscillation
47
48 66 (MJO) and other tropical waves as well as improvements in overall scores in numerical
49
50 67 weather prediction trials.
51

52
53 68 It is common to use single column models (SCMs) alongside convection resolving models
54
55 69 (CRM) or large-eddy simulation (LES) together with field observations whilst developing
56
57 70 and testing parameterizations (e.g. Lenderink et al., 2004; Grabrowski et al. 2006; Couvreur
58
59 71 et al., 2015). However, SCMs are unable to capture feedbacks between subgrid- and grid-
60
61 72 scale processes which can lead to different behaviour than the full GCM. For example, SCM
62
63 73 cases have been successfully used to develop improvements to convective parameterizations to
64
65 74 represent the diurnal cycle of convection over land (e.g. Rio et al., 2009) but additional
66
67 75 modifications may be needed to perform well in the GCM due to interactions not originally
68

1
2
3 76 exposed by the SCM (e.g. Rio et al., 2013). In a recent study, Hwong et al. (2022) found that
4
5 77 ~~as convection becomes more the more~~organised, ~~-there are larger differences in convection~~
6
7 78 ~~becomes the more the~~results between one- and three-dimension (3D) simulations ~~differ~~.
8
9 79 Although the UM SCM has been used extensively during development of CoMorph, this
10
11 80 study uses the ~~three-dimensional (3D)~~ idealised UM. While still being substantially cheaper
12
13 81 to run than the full GCM, this enables controlled tests of the interaction between the physical
14
15 82 parametrisations and the resolved dynamics, enabling more comprehensive testing of the
16
17 83 scheme, including the emergent organisation of convection on the resolved scale.

18 84 A selection of well-known cases is revisited here, with the purpose of documenting the extent
19
20 85 to which CoMorph-A captures a range of important, but challenging behaviour. These
21
22 86 idealised cases have the advantage that they can be accompanied by high-resolution
23
24 87 analogues, where the convection is well captured by the resolved grid. Many of these cases
25
26 88 were originally designed for use in a SCM for testing parameterizations over a grid box of
27
28 89 order 100—200 km² however the UM, along with many other GCMs, is now routinely run at
29
30 90 much higher resolutions of order of 10—50 km. Using the idealised UM configured to use
31
32 91 the same physics as in the full GCM allows some exploration of how the model will behave
33
34 92 at these higher resolutions. Results from a coarser resolution (10 km and lower) model setup
35
36 93 with parameterized convection (with and without CoMorph-A) are presented alongside high-
37
38 94 resolution (~~250-4~~km or higher) CRM results. CoMorph has around 30 tuneable parameters,
39
40 95 so many different versions have been tested in the development of a package that performs
41
42 96 well operationally. Recognising that CoMorph-A is the first version of a scheme that will
43
44 97 continue to be substantially developed, compromises in tuning have had to be made in order
45
46 98 to obtain good performance. These idealised tests evaluate where this configuration performs
47
48 99 well and identifies any deficiencies that require further work. This testbed is designed to
49
50 100 serve as a reference for others to replicate, and could be viewed as some of the equipment
51
52 101 required for a 'convective playground'; a platform to enable testing of convection
53
54 102 parametrizations with differing levels of complexity, from simple idealized tests through to
55
56 103 comparisons with field campaigns.

57 104 The following section describes the idealised UM and details of the CoMorph-A package of
58
59 105 changes. Section 3 gives an overview of multiple experiments and documents the
60
61 106 performance of CoMorph-A. The results are summarised in Section 4.

107 2. Model experiments

2.1. Model overview

The atmospheric model used is version 12.1 of the UM. In the idealised configuration the model has bicyclic boundary conditions over a limited area domain on a flat, cartesian grid.

The full science setup with parameterized convection is based on the current operational global atmosphere and land configuration, GAL8. This configuration is based on that described by Walters et al. (2019) with updates to some of the physics. These include the addition of a drag package, changes to the boundary layer scheme to improve representation of shear-driven boundary layers as well as the numerical stability of stable boundary layers, and a new riming parameterization in the large-scale precipitation scheme. For the control run (CTRL) using GAL8 as officially defined i.e., with the current UM convection scheme, there have been significant changes to the existing convection scheme including the use of a prognostic entrainment rate to allow some memory of recent convection (Willett & Whittall, 2017; see Loek et al. 2023 for full details). The additional changes in replacing the convection scheme with CoMorph-A are detailed in Section 2.2.

For the CRM with only explicit convection, the tropical regional atmosphere configuration, RAL2-T, is used as described in detail by Bush et al. (2023) -but using the Smith (1990) cloud parameterization scheme and; the same higher order interpolation scheme for dry potential temperature and moisture, and with the addition of the Fountain Buster scheme (Loek et al., 2023). Tests have shown benefits of using the Smith (1990) diagnostic cloud parameterization scheme, as in the RAL2-M configuration (Bush et al., 2023) instead of the PC2 scheme (Wilson et al., 2008) when running at sub-km resolutions. Additionally, the Fountain Buster scheme is used which modifies the semi-lagrangian advection scheme to address local conservation errors caused by unrealistically intense updrafts. Unless specified in the text, updraught mass fluxes from the CRM are calculated over buoyant cloudy updrafts whereby sub-grid velocity is upwards relative to the layer mean ($w' > 0$ m/s), cloudy points are defined by a cloud condensate mixing ratio greater than 1×10^{-5} (kg kg⁻¹) and are positively buoyant relative to the layer mean ($\theta'_v > 0$).

A selection of idealised experiments has been used to develop and test the performance of CoMorph-A. Rather than provide details of all the idealised experiments here, these are described in Table 1 and the relevant results section where they are first mentioned. The reader is directed to the original papers for full details but any divergence from the original

139 experiments is outlined. Where available, the results are compared against the CRM and
140 previously documented results and observations.

141 2.2. The CoMorph-A physics package

142 The CoMorph convection scheme is detailed in Whitall et al (2022). Here we briefly
143 describe some of the fundamental components of the scheme and detail differences from the
144 existing scheme.

- 145 • In the previous scheme, updrafts are prescribed from a predetermined cloud-base
146 height with a CAPE closure assumption to calculate the mass flux at cloud base. In
147 CoMorph, mass-flux is allowed to initiate independently from all heights where there
148 is local vertical instability (dry-statically unstable layers such as near a heated surface,
149 or moist stratiform cloud layers which become moist-unstable layers such as from
150 large-scale cloud). When ~~convection triggers from non-cloudy model-levels~~
151 ~~surface-triggered convection occurs~~, the cloud-base height emerges from the scheme when the
152 modelled bulk plume rises high enough to reach saturation. The amount of mass
153 initiated is set to depend on the vertical instability, and this is effectively the “closure”
154 for the scheme. The cloud-base mass -flux then becomes determined by the balance of
155 entrainment versus detrainment in the layer below cloud-base.
- 156 • Entrainment rate scales with the inverse “parcel radius”, which is based on a
157 boundary-layer turbulence length-scale in the parcel’s source-layer. The parcel radius
158 in CoMorph-A is also scaled by an ad-hoc function of the previous time step
159 precipitation rate allowing a crude representation of increased organisation of
160 convection by precipitation-driven cold pools.
- 161 • The detrainment rate is based on a power-law ~~probability distribution function~~ PDF of
162 in-plume buoyancy and other properties, with the core (lower entrainment rate) and
163 mean properties of the plume treated separately. The ascent terminates at the level at
164 which the parcel core is negatively buoyant. This detrainment calculation also uses an
165 implicit method to ensure it evolves smoothly over successive timesteps.
- 166 • CoMorph includes a microphysics parameterization allowing formation of different
167 hydrometeors within the parcel and allows the parcel and detrained air to remain
168 supersaturated with respect to ice. All convectively generated precipitation is passed
169 on the model-level where it falls out of the parcel to the “large-scale” microphysics
170 scheme, which then simulates the fall to the surface, evaporation, melting etc. To aid

171 coupling between CoMorph and the large-scale microphysics at coarse resolution,
 172 both schemes update a prognostic precipitation fraction, so that convection can
 173 modify rain mass and area fraction consistently.

- 174 • CoMorph represents convective momentum transport (CMT) by transporting the
 175 zonal and meridional wind components within the bulk plume and allowing the
 176 exchange of momentum between the plume and environment with a parameterisation
 177 of the horizontal pressure gradient force based on a quadratic drag law.

178 Compared to the previous UM convection scheme, CoMorph is much more closely coupled
 179 to the model's boundary layer, large-scale microphysics and prognostic cloud schemes and
 180 modifications to all four schemes have been required to ensure they operate consistently
 181 together. ~~These are detailed in Lock et al. (2023).~~ The improved coupling between CoMorph
 182 and the resolved dynamics enables organised convective structures to develop over a range of
 183 scales.

184 3. Focussed testing of CoMorph-A

185 In this section we focus on the performance of CoMorph-A in a range of different
 186 experiments targeting different model behaviours. An overview of all the test cases is given
 187 in Table 1 along with a summary of the rationale for selection of these cases. Since many of
 188 these cases are based on field campaigns, where the large-scale forcings have been
 189 observed/evaluated for specific areas, the domain sizes are chosen to be ~~consistent the same~~
 190 ~~as with~~ those original cases. Where the original domain was smaller than 100×100 km² this
 191 has been increased to ~~whilst still allowing~~ large-scale circulations to form in the parametrized
 192 cases. In cases where the ~~parameterized~~ domain size is 100 – 200 km², the runs have been
 193 repeated to check for any domain dependence. In all cases a discussion of the CRM results
 194 compared to other high-resolution results will be discussed and, where appropriate, plots are
 195 shown in a form that can be directly compared with earlier papers describing the case.

Section	Case title	Original reference	Domain (& resolution)	Interactive radiation?	Additional details	Scientific rationale
3.1. Mean State	RCE	Wing et al. (2018)	GA: 2040×2040 km ² , 6000×400 km ² (10 km) CRM: 200×200 km ² (200m)	Yes	SST= 300K.	Analysis of the mean-state and organisation of convection under radiative-convective equilibrium (RCE)

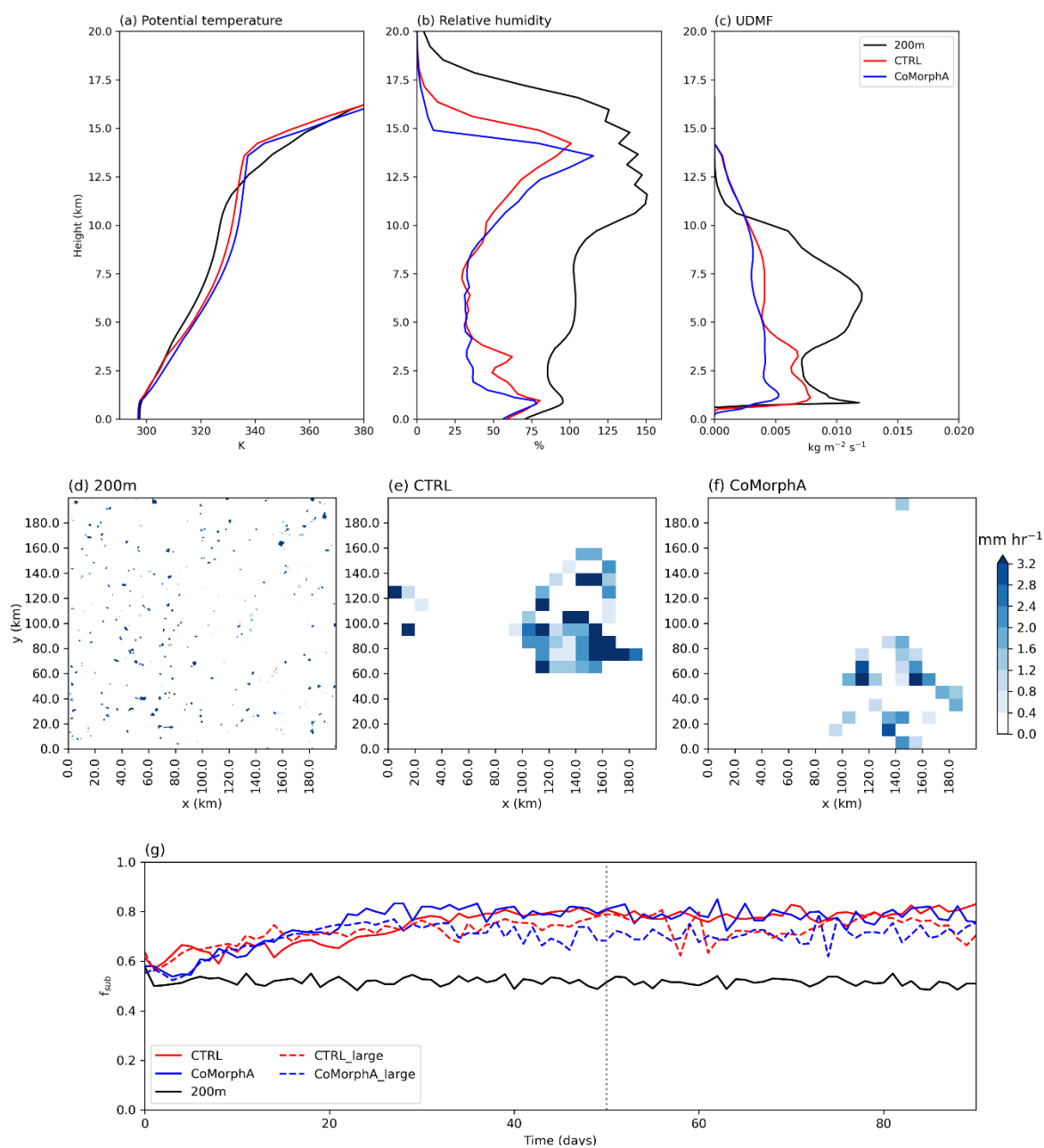
3.2 Sensitivity to tropospheric humidity	EUROCS	Derbyshire et al. (2004)	Multiple - see text.	No	Relax (1 hour timescale) to theta, wind and relative humidity profiles. 4 different humidity profiles.	Examining the moisture-convection relationship, shown to be important for simulating the MJO.
3.3 Diurnal cycle	Shallow ARM	Brown et al. (2002), Lenderink et al. (2004)	GA: 160×160 km ² (10 km) CRM: 160×160 km ² (100m)	No	Prescribed surface fluxes, geostrophic wind of (u,v)=(10,0) m s ⁻¹ .	Development of shallow cumulus over land with no transition to deep convection.
	AMMA	Couveux et al. (2012, 2015)	GA: 100×100 km ² (10 km) CRM: 100×100 km ² (100m)	No	Prescribed surface fluxes and temperature, moisture and vertical velocity tendencies.	Large amplitude diurnal cycle with deep, dry boundary layer. Transition from shallow to deep convection.
	Deep ARM	Guichard et al. (2004)	GA: 100×100 km ² (10 km) CRM: 100×100 km ² (200 m)	No	Prescribed surface fluxes and temperature tendencies. Relax to zero wind.	Idealised diurnal cycle case representing transition from dry to shallow to deep convection. Forced with the same cycle over 10 days.
3.4 Memory in diurnal cycle	As above (Deep ARM)	Daleu et al. (2020)	As above.		As above.	Quantifying the memory of the system in terms of the development of convection being influenced by previous convection
3.5 Multi-day tropical cases	TWP-ICE	Fridlind et al. (2012)	GA: 200×200 km ² (10 km), CRM: 200×200 km ² (100 m)	Yes	SST = 302.15, nudging of horizontal winds, moisture and temperature.	Performance when simulating convective systems over multiple days. A well-documented case with interactive radiation.
3.6 Inland propagation and nocturnal convection	Island case	N/A	GA: 1200 × 300 km ² , CRM: 1200 × 300 km ² (250 m.)	Yes	Island 300 km in x-dimension, real, flat, sandy land surface with plenty of moisture initially. u=0 m s ⁻¹ and u=5 m s ⁻¹ .	A newly developed case based on an island in the maritime continent to examine the initiation of convection by sea-breeze circulation and propagation of convection.
3.7 Convective momentum transport	Cold-air outbreak	Kershaw & Gregory (1997)	GA: 200×200 km ² (10 km), CRM: 200×200 km ² (100 m)	No	<u>Prescribed, constant surface fluxes. u=0 m s⁻¹ and v linearly varies from 0 m s⁻¹ at the surface to 10 m s⁻¹ at 6 km.</u> <u>Prescribed, constant surface fluxes. u=0 m s⁻¹ and v linearly varies from 0 m s⁻¹ at the surface to 10 m s⁻¹ at 6 km.</u>	Sensitivity to different parameterizations of convective momentum transport

196 **Table 1: Summary of the experiments used in this paper to evaluate the performance of**
197 **CoMorph-A.**

198 3.1. Modelled mean state

199 To give an idea of the mean state, radiative-convective equilibrium (RCE) experiments were
200 performed based on the RCEMIP setup (Wing et al. 2018) with a sea surface temperature of
201 300 K. The simulations are run for 100 days, reaching equilibrium after 20 days. The
202 original RCEMIP CRM simulations show a large range of results. Figure 1a-c shows
203 profiles of potential temperature, relative humidity and updraught mass flux averaged over

204 the final 70 days of the simulation. The parameterized runs have a warmer troposphere and
 205 higher altitude inversion than the CRM, leading to a higher termination of the 200-m CRM
 206 simulation has a cooler troposphere and much lower altitude inversion leading to lower
 207 termination of the updraft mass flux. The parameterized runs have a similar potential
 208 temperature profile to one another, although CoMorph-A has a slightly warmer mid to upper-
 209 troposphere than CTRL and—B both parameterizations have a sharper inversion at cloud top
 210 than the CRM, with CoMorph-A slightly sharper than CTRL, possibly due to the current lack
 211 of representation of overshoots that would smooth outweaken the inversion.



212

1
2
3 **Fig 1.RCE. Profiles of (a) potential temperature [K], (b) relative humidity [%], with respect to**
4 **water (ice) above (below) 0 °C, and (c) updraught mass flux, averaged over the final 70 days of**
5 **simulation. Snapshot of surface precipitation rate [mm hr⁻¹] on day 50 of the simulations from**
6 **(d) 200m CRM (native resolution), (e) CTRL and (f) CoMorph-A, both 10 km resolution, (g)**
7 **time series of f_{sub} , calculated as in the text, for the CRM, CTRL and CoMorph-A. The dashed**
8 **lines are the CTRL and CoMorph-A results over the large 6000 × 400 km² domain. The vertical**
9 **grey dotted line in f shows the timing of the snapshots in a-d.**
10
11
12
13
14

15
16 Consistent with other model results in Wing et al. (2020), the mid-tropospheric humidity in
17
18 the parameterized runs is much lower than in the CRM where it remains ~~at~~ above 75% in
19
20 both simulations and becomes supersaturated with respect to ice above 8 km. This may
21
22 suggest not enough detrainment in the plume formulation in both parameterizations. The
23
24 CRM has a higher mass flux near cloud base and in the mid-troposphere but terminates at a
25
26 lower altitude than both CTRL and CoMorph-A. CoMorph-A is drier than CTRL in the low
27
28 to mid-troposphere with a resulting smaller mass flux.

29
30 A snapshot of the surface precipitation from day 50 of the 200 m CRM, CTRL and
31
32 CoMorph-A simulations are shown in Fig 1d-f. Both parameterized runs show some
33
34 aggregation of convection that isn't so evident in the CRM simulation. The degree of
35
36 aggregation in each simulation is quantified by calculating the subsidence fraction (f_{sub}), the
37
38 fraction of the domain where there is subsidence, as in Wing et al. (2020) using daily 500 hPa
39
40 vertical velocity averaged over 10×10 km² blocks. The parameterized simulations were
41
42 repeated using a domain of 6000×~~400~~ km² to check how the spatial organisation compares
43
44 with the smaller domain. Using the large domain, the dependence of f_{sub} on the size of the
45
46 blocks (10×10 km² compared to 100×100 km² as used in the original study) was investigated
47
48 and the values of f_{sub} were found to be similarsimilar. The values of f_{sub} in the CRM range
49
50 from 0.5—0.6 compared to 0.7—0.8 in the parameterized runs, suggesting that there is
51
52 greater organisation in the parameterized runs which may be excessive. However, these
53
54 higher values of f_{sub} are within the same range as other CRM models analysed in RCEMIP
55
56 (Fig 12 in Wing et al. 2020).
57
58
59
60

241 This section has shown the mean profiles under RCE and how convection self-aggregates
242 using CoMorph-A, with similar performance to CTRL. The following section will examine
243 how convection is related to mid-tropospheric humidity and the organisation of convection in
244 the different simulations will be revisited.

3.2. Sensitivity to tropospheric humidity

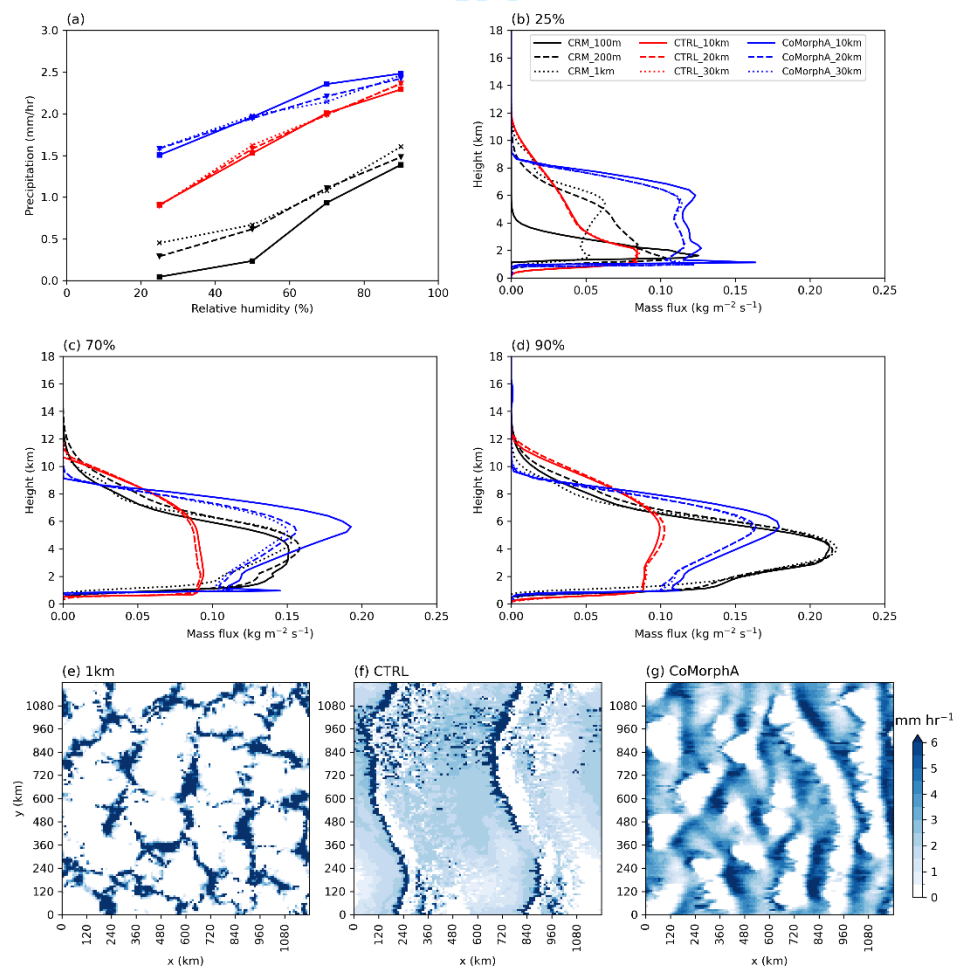
For models to adequately represent convective clouds, they must capture the interaction between convection and mid-tropospheric humidity. This moisture-convection relationship has been found to be important for simulating the MJO (e.g. Kim et al. 2014, [Hirons et al. 2013](#)), but is poorly simulated in the UM, in terms of amplitude and propagation across the maritime continent (Ahn et al. 2020, Williams et al. 2017).

The experimental setup has been kept as similar to Derbyshire et al. (2004) as possible, although accounting for a higher model top in more recent versions of the model. The model is initialised and above 1 km is relaxed back to fixed profiles of potential temperature, zonal wind and relative humidity (RH) with a relaxation timescale of 1 hour. Between 2 km and 16 km there are 4 different experiments with reference values of RH of 25%, 50% 70% and 90%. The simulation is run for 5 days with the initial day discarded from the analysis. The 3D idealised setup of this case has been useful for investigating propagating convective bands that have been seen in earlier versions of the UM (e.g. Roberts 2001; Tomassini et al. 2017). In addition to the results shown here for $50 \times 50 \text{ km}^2$ (CRM) and $1200 \times 1200 \text{ km}^2$ domains, the CRM has been run at 100 m, 200 m, 500 m and 1 km resolution over $25 \times 25 \text{ km}^2$, $50 \times 50 \text{ km}^2$ and $100 \times 100 \text{ km}^2$ domains and CTRL and CoMorph-A at 10 km, 20 km, 30 km and 60 km resolutions over $100 \times 100 \text{ km}^2$ (10 km resolution only), $600 \times 600 \text{ km}^2$ and $1200 \times 1200 \text{ km}^2$ domain sizes.

The original paper showed the sensitivity to humidity was highly variable depending on the single-column model analysed. While the CRM results show a similar overall ~~sensitivity and~~ increase in precipitation rate from 25% to 90% humidity as documented in ~~the original~~ [Derbyshire et al. \(2004\) paper](#), there is clear variation with resolution: The highest resolution (100 m; solid line) tending to have the lowest precipitation values whilst the coarsest resolution (1km; dotted line) has the largest values, with large differences in the mass flux profiles for the 25% experiment (Fig 2b), consistent with the results of the original study (Fig 4 in Derbyshire et al. 2004).

Using this experimental setup, CoMorph-A rapidly responds to the unstable profile and has too high precipitation amounts for all humidity cases (Fig 2a). This is a similar result to the SCMs examined in the original study (see Fig 15 in Derbyshire et al. 2004). The moisture sensitivity is lower in CoMorph-A than CTRL with an increase of 1.0 mm hr^{-1} between the

25% and 90% cases compared to 1.4 mm hr^{-1} in CTRL. CoMorph-A shows more resolution sensitivity than CTRL particularly at the higher humidities but is relatively insensitive to domain size (not shown). The updraught mass flux profiles from the 70% and 90% experiments (Fig 2c, d) show both parameterized runs peaking at too high altitude relative to the CRM with CoMorph-A also terminating too low. The peak values of mass flux are more similar to the CRM in CoMorph-A than CTRL, but this is associated with much higher precipitation rates in CoMorph-A. The CRM has additionally been run over the same $1200\times 1200\text{ km}^2$ domain as CTRL and CoMorph-A but at 1 km resolution. A snapshot of precipitation rate over this large domain after 4 days is shown in Fig 2e-g with the CRM regridded to the same 10 km grid as CTRL and CoMorph-A. Both parameterized runs have too much background precipitation and a less cellular structure than is evident in the CRM although this is arguably improved in CoMorph-A relative to CTRL. Developments to allow a greater sensitivity to relative humidity in future versions of CoMorph will be discussed in Section 4.



290

1
2
3 291 **Fig 2. EUROCS. (a) Precipitation [mm hr^{-1}] against relative humidity and (b-d) Updraught**
4 **mass flux [$\text{kg m}^{-2} \text{s}^{-1}$] for the 25%, 70% and 90% cases. Results for multiple resolutions**
5 **from the $50 \times 50 \text{ km}^2$ domain CRM (black), large (1200 km domain) CTRL (red) and**
6 **CoMorph-A (blue). Snapshot of surface precipitation rate [mm hr^{-1}] on day 4 of the 90%**
7 **case, $1200 \times 1200 \text{ km}^2$ domain simulations from the (e) 1km CRM; regridded to same 10 km**
8 **grid (f) CTRL and (g) CoMorph-A.**
9
10
11
12

13
14 297 This is a highly idealised case which relaxes back to the same profiles and, like the RCE,
15 298 generates a steady state enabling the analysis of mean profiles and precipitation rates as well
16 299 as the emergent spatial structures. In the following section the model uses time-varying
17 300 forcings to represent the initiation and development of convection during the day.
18
19
20

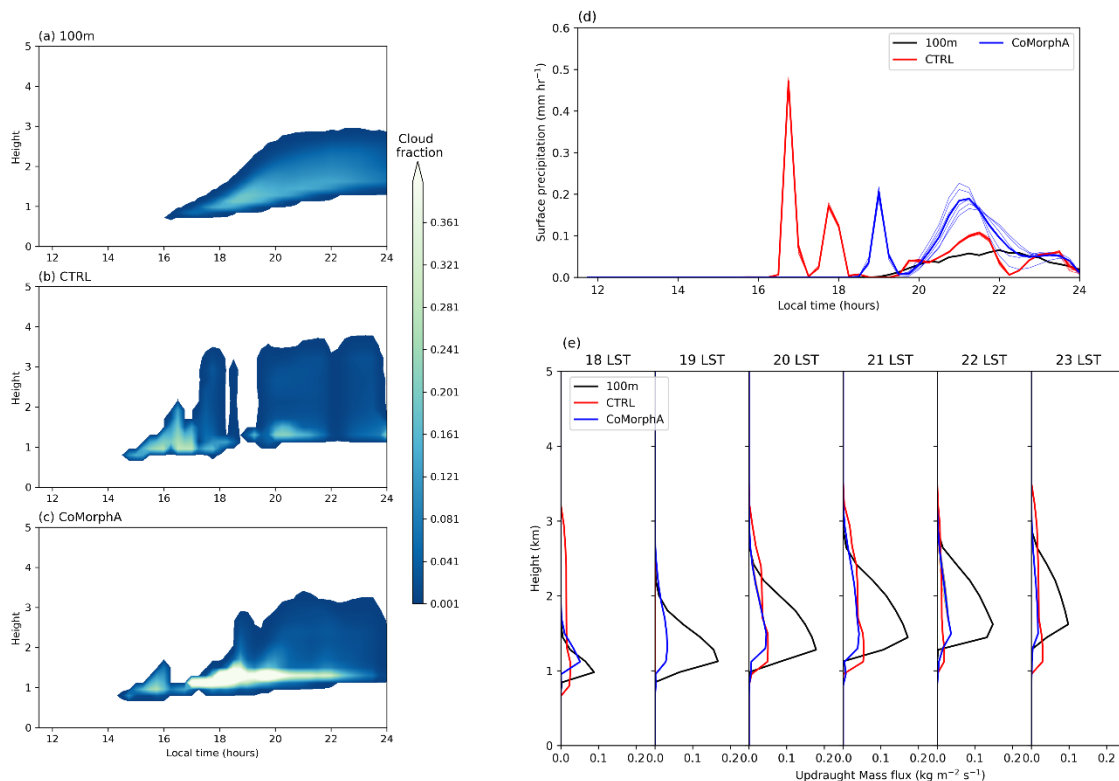
21 301 3.3. Diurnal cycle

22
23
24 302 The failure of models with parameterized convection to fully represent the diurnal cycle is
25 303 well known, with convection often occurring too early in the day, particularly over land (e.g.
26 304 Yang and Slingo 2001). This has been an issue in earlier versions of the UM (e.g.
27 305 Christopoulos and Schneider 2021). Here we examine the performance of CoMorph-A at
28 306 simulating the diurnal cycle using three well-documented experiments examining different
29 307 aspects of the development of convection; a shallow convection case, transition to deep
30 308 convection in a semi-arid environment and a mid-latitude, deep convection case. All three
31 309 cases have interactive radiation turned off. To help understand the sensitivity of the
32 310 parameterized simulations in the single day cases (ARM and AMMA), an ensemble of six
33 311 simulations is performed by perturbing the initial random noise.
34
35
36
37
38
39
40
41

42 312 3.3.1. Shallow ARM case

43
44
45 313 The first diurnal case is based on observations made at the mid-latitude Southern Great Plains
46 314 (SGP) site of the Atmospheric Radiation Measurement (ARM) Program on 21 June 1997
47 315 (Brown et al. 2002, Lenderink et al. 2004), commonly referred to as the ARM case. This
48 316 tests the development of shallow cumulus over land with no development to deep convection.
49
50
51
52 317 Unlike the original paper, had a very small domain ($6.4 \times 6.4 \text{ km}^2$) domain with which had
53 a very low model top depth (4.4 km) and 40 m vertical resolution. Here, this has been run
54 318 with the same operational global and regional stretched grid vertical levels (Bush et al. 2023)
55 319 are used with a 40 km model top but and consequently has lower the vertical resolution above
56 320 the near-surface layer is lower.
57
58
59
60

322 Figs 3a-c show the evolution of the cloud in the three simulations. In the high-resolution run
 323 this is similar to previous studies (Fig 2b in Lenderink et al. 2004; Fig 5 in Brown et al. 2002,
 324 Fig 2a in McIntyre et al. 2022). Both CTRL and CoMorph-A overestimate the cloud fraction
 325 relative to the high resolution, consistent with early SCM results (Lenderink et al. 2004). The
 326 cloud fraction near cloud base is significantly higher in CoMorph-A than both the CRM and
 327 CTRL. The evolution of the height of cloud base is well simulated by both parametrized runs
 328 and both remain shallow although the cloud-top height differs between the runs, with
 329 CoMorph-A increasing more gradually than CTRL. All runs generate precipitation (Fig 3d)
 330 unlike the original simulations where microphysical parameterizations were switched off.
 331 CTRL has a small cloud fraction at 19Z, after precipitating, before increasing again in both
 332 amplitude and altitude. Both parameterized runs also have a rapid reduction in cloud top
 333 height at the end of the simulation once they stop precipitating. Although the cloud fractions
 334 have larger maxima in CTRL and CoMorph-A, the values of updraught mass flux remain
 335 lower than the CRM (Fig 3e) and remain almost identical for the different ensemble
 336 members.



337

338 **Fig 3.ARM.** Time evolution of cloud fraction in (a) 100 m CRM, (b) CTRL and (c) CoMorph-A
 339 simulations of the shallow ARM case. (d) Timeseries of precipitation [mm hr⁻¹] from the three

1
2
3 340 **simulations. (e) Updraught mass flux [$\text{kg m}^{-2} \text{s}^{-1}$] profiles between 1800 and 2300 local time. (d)**
4 **and (e) are shown for each ensemble member (thin lines) and the ensemble mean (thick line).**
5
6

7 342 3.3.2 AMMA case

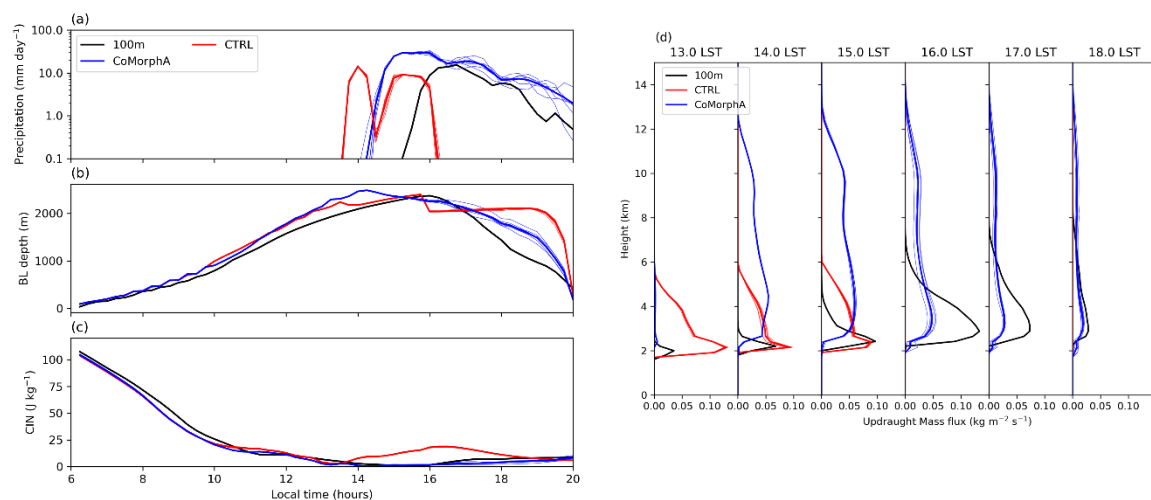
8
9
10 343 The second diurnal case is based on observations from the African Monsoon
11
12 344 Multidisciplinary Analysis (AMMA) showing the development of daytime convection in a
13
14 345 semi-arid region with a much larger amplitude diurnal cycle (Couvreur et al. 2012).

15 346 Comparison of Fig 4a with Fig 2 in Couvreur et al. (2015) shows that the CRM differs
16
17 347 somewhat from the original LES results, with the onset of precipitation and its subsequent
18
19 348 peak occurring approximately 2 hours earlier. CTRL initiates precipitation almost 2 hours
20
21 349 too early relative to the CRM and only persists for 3 hours before abruptly stopping.

22 350 CoMorph-A initiates an hour earlier than the CRM and has almost double the precipitation
23
24 351 rate, which is maintained into the evening.

25
26 352 Observations from the AMMA case-study (Fig 3 in Couvreur et al. 2012) showed the
27
28 353 boundary layer grows throughout the morning reaching 2.5 km in the mid-afternoon
29
30 354 consistent with the present CRM results (Fig 4b). This was associated with a decrease in
31
32 355 convective inhibition (CIN; Fig 4c) during the morning. The CRM shows a decrease in
33
34 356 boundary layer height and slight increase in CIN into the evening. Both CTRL and CoMorph-
35
36 357 A capture the growth of boundary layer height and evolution of CIN although these evolve
37
38 358 too quickly, consistent with the earlier development of precipitation. The positive values of
39
40 359 mass flux (Fig 4d) are confined to lower altitudes in the CRM than CoMorph-A. The CTRL
41
42 360 convective mass flux is zero for 1600 LST with only large-scale precipitation contributing to
43
44 361 the total surface precipitation rate.

45 362
46
47
48
49
50
51
52
53
54
55
56
57
58
59
60



363

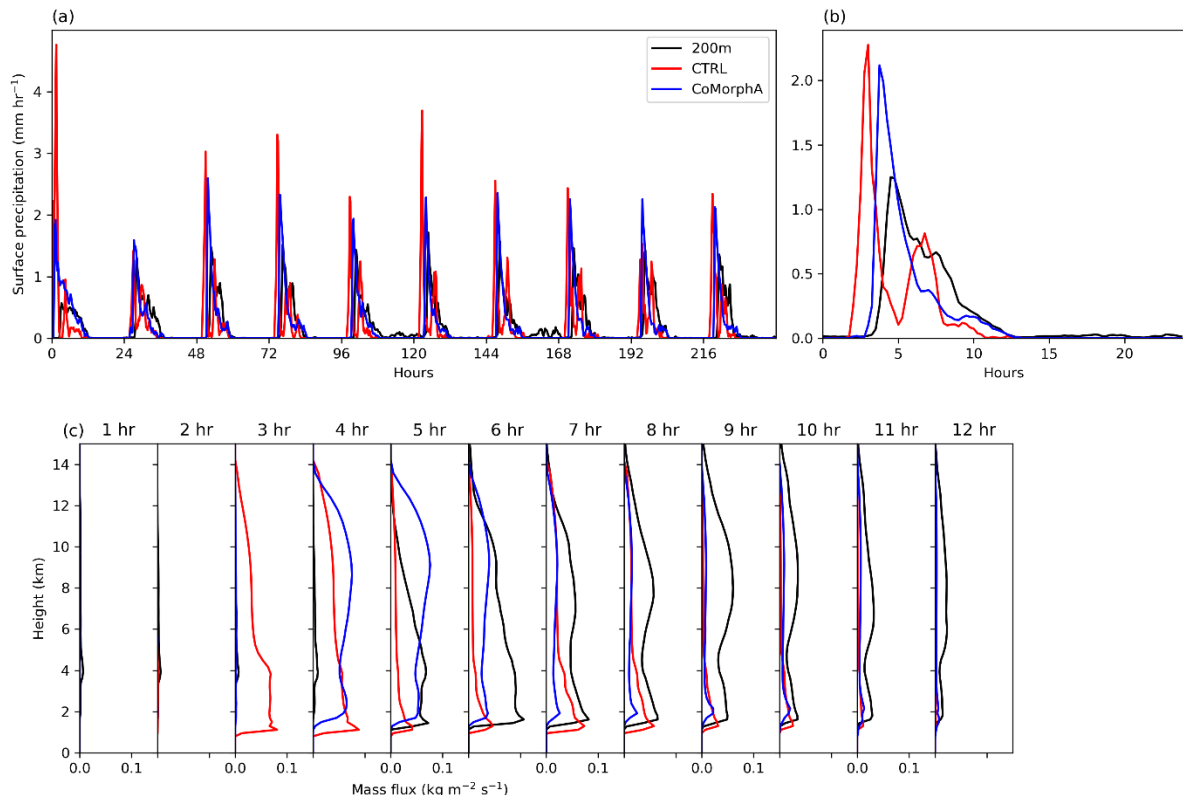
364 **Fig 4.AMMA. Timeseries of (a) surface precipitation [mm day⁻¹], (b) boundary layer depth [m]**
 365 **and (c) CIN [J Kg⁻¹] from the 100m CRM (black), CTRL (red) and CoMorph-A (blue) ensemble**
 366 **members (thin lines) and ensemble mean (thick line) simulations of the AMMA case. (d) Hourly**
 367 **mass flux [kg m⁻² s⁻¹] profiles from 1300 to 1800 local time. ~~Shown for each ensemble member~~**
 368 **~~(thin lines) and the ensemble mean (thick line).~~**

369 3.3.3 Deep ARM case

370 The final diurnal case is based on the same field campaign as 3.3.1 but for a different day
 371 (27th June 1997; Guichard et al. 2004) as using the experimental setup ofed by Daleu et al.
 372 (2020). The model is forced with surface sensible and latent heat fluxes which vary
 373 sinusoidally throughout the day (0-12 hours), reaching a peak at 6 hours and set to zero
 374 overnight (12-24 hours) with a prescribed radiative cooling applied to the potential
 375 temperature (Daleu et al. 2020). The original papers (Guichard et al. 2004 and Chaboureau et
 376 al. 2004) applied the same fluxes but with an earlier start time of 6 hours which must be is
 377 accounted for when comparing the results. This forcing is repeated over 10 days to get the
 378 mean diurnal cycle, with the initial day excluded from the diurnal means.

379 The timeseries of precipitation is shown along with the mean diurnal cycle (Fig 5a,b). All
 380 simulations reach peak precipitation rate prior to the peak in surface fluxes (6 hours into run);
 381 3—4 hours earlier than in the original papers (Figure 3, Guichard et al. 2004 and Figure 2a
 382 Chaboureau et al. 2004). As with the previous cases, CTRL trigger initiates convection earlier
 383 than CoMorph-A and the CRM which is also evident in the updraught mass flux profiles (Fig
 384 5c). CoMorph-A initiates slightly earlier than the CRM and the peak precipitation rate in

385 both parameterized runs is greater than in the high-resolution run. CTRL peaks at hour 3,
 386 decreases until hour 5 before peaking again at hour 8. CoMorph-A precipitation rate reaches
 387 an initial peak after 4 hours and then declines rapidly over the next 3 hours before decreasing
 388 more gradually until 12 hours. The CRM has a higher rate than CoMorph-A between hours 6
 389 and 9, consistent with the higher values of mass flux at these times. but after this the rate
 390 remains similar to CoMorph-A.



391

392 **Fig 5. Deep ARM. (a) Timeseries of precipitation [mm hr⁻¹] over 10 days of the**
 393 **simulation of the deep ARM case, (b) mean diurnal cycle of precipitation [mm hr⁻¹] and**
 394 **(c) mean updraught mass flux [kg m⁻² s⁻¹] profiles shown for the first 12 hours. Means**
 395 **are calculated over the final 9 days of the simulation.**

396 This section has highlighted an improvement in the timing of the diurnal cycle using
 397 CoMorph-A. The following section extends this diurnal cycle analysis by examining how the
 398 development of convection is influenced by previous convection.

399 3.4. Memory in the diurnal cycle

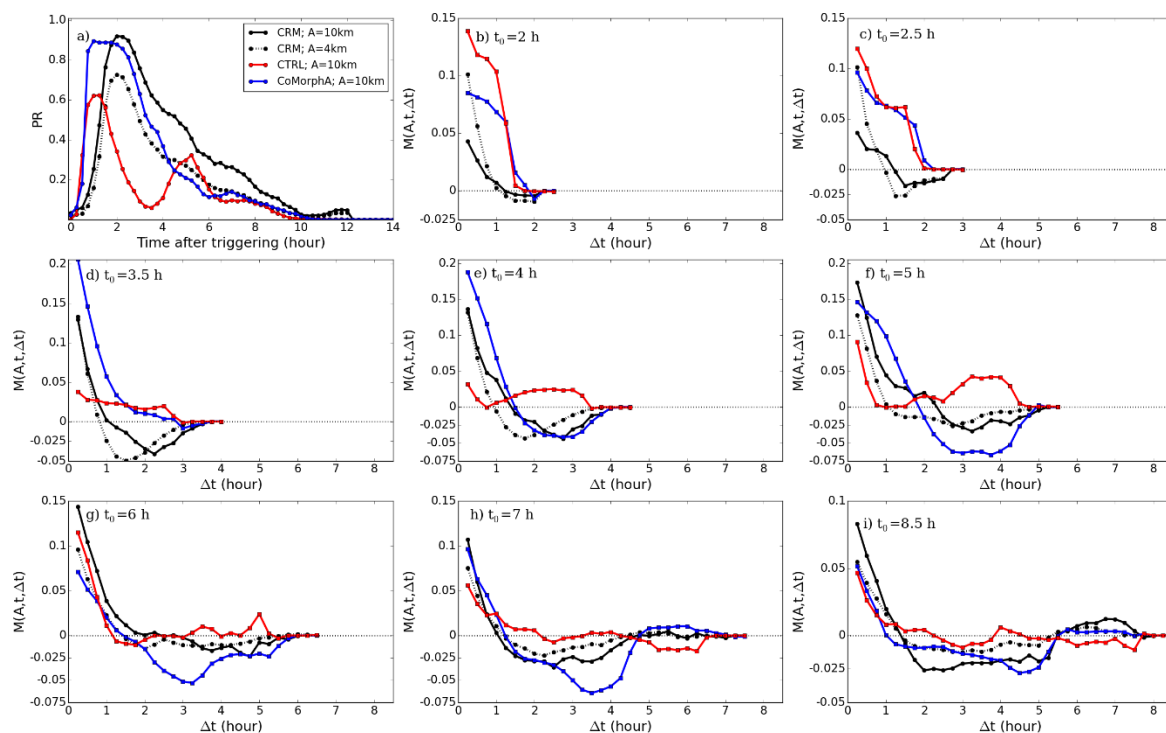
400 Using the setup from section 3.3.3 (Guichard et al., 2004), Daleu et al. (2020) introduced a
 401 memory function which could be separated into three phases; the first representing the

1
2
3 402 persistence of convection, the second representing the suppression of convection in areas
4 403 which had precipitation in the previous few hours and the third representing a secondary
5 404 enhancement of precipitation. This is calculated for each of the final 9 days of the simulation
6 405 as with the mean diurnal precipitation rate shown in Fig 5b.

11 406 The memory function, M , is defined in Daleu et al. (2020), and is based on the probability of
12 407 finding rain (mean precipitation greater than 0.1 mm hr^{-1}) at both time, t_0 , and at an earlier
13 408 time, $t_0 - \Delta t$, over a given area, A , compared to the expected probability assuming that these
14 409 two events occur independently of each other ($P^2[R(A, t_0, \Delta t)] = P[R(A, t_0)] \times P[R(A, t_0 -$
15 410 $\Delta t)]$):

$$M(A, t_0, \Delta t) = P[R(A, t_0) \cap R(A, t_0 - \Delta t)] - P^2[R(A, t_0, \Delta t)]. \quad (1)$$

21 412 A value of zero indicates that there is no memory in the system, while positive values
22 413 indicate an increased chance of raining at the later time, t_0 if it rained at the earlier time, $t_0 -$
23 414 Δt , and a negative value suggests that there is suppression of rainfall linked to the earlier
24 415 rainfall event. The threshold for Figure 6 shows the probability of finding rain ($P[R(A, t_0)]$)
25 416 and the memory function for a box of size $A = 10 \times 10 \text{ km}^2$ and $t_0 = 2, 2.5, 3.5, 4, 5, 6, 7,$
26 417 and 8.5 hours after the initial precipitation (triggering). The memory function is set to zero
27 418 beyond time lags (i.e., prior to triggering).



419

1
2
3 420 **Figure 6: Memory case. (a) Probability of finding rain ($P[R(A,t_0)]$) for $A=10\times 10\text{ km}^2$ in the deep**
4 **ARM case. The time axis is shifted relative to triggering time such that time 0 corresponds to**
5 **the time of triggering in all three simulations. Memory function ($M(A,t_0,dt)$) for $A=10\times 10\text{ km}^2$**
6 **and $t_0=$ (b) 2, (c) 2.5, (d) 3.5, (e) 4, (f) 5, (g) 6, (h) 7, (i) 8.5 hours after triggering. Results are the**
7 **ensemble mean obtained in the 200m CRM (black, solid), CTRL (red) and CoMorph-A (blue)**
8 **simulations. Results for $A=4\times 4\text{ km}^2$ are also shown for the CRM (black, dotted).**
9
10
11
12

13
14 426 The results using the UM CRM differ slightly from those in Daleu et al. (2020) which used
15 427 the Met Office NERC cloud model (MONC; Brown et al., 2015). The results using $A=4\times 4$
16 428 km^2 are shown for comparison with Figure 6 in the original paper. The UM CRM triggers
17 429 slightly later than MONC and the increase is more gradual over the initial 30 mins, but
18 430 rainfall remains higher for a longer time. The initial persistence of convection and subsequent
19 431 suppression (phase 2) is weaker in the CRM than MONC. The secondary enhancement
20 432 (phase 3) can only be seen after 5 hours for convection produced 8 hours after triggering and
21 433 is weaker than MONC. The difference between using different values of A ($A=4\times 4$ and
22 434 $A=10\times 10\text{ km}^2$) are consistent with results using MONC (Fig 5c in Daleu et al. 2020). Results
23 435 using $A=10\times 10\text{ km}^2$ for CRM, CTRL and CoMorph-A will now be compared to assess the
24 436 performance of CoMorph-A.
25
26
27
28
29
30
31
32

33
34 437 In the previous section we noted that CTRL triggers over an hour earlier than CoMorph-A
35 438 and the CRM. There are bigger differences in the probability of finding rain (Fig 6a) in the
36 439 two parameterized simulations than we saw in the rainfall rate in Fig 5 due to differences in
37 440 the number and spatial size of the events. Both CTRL and CoMorph-A show a higher
38 441 probability of finding rain over the first hour than the CRM, remaining lower for subsequent
39 442 times (Fig 6a). The probability of rain in CTRL decreases after the first 2 hours, reaching a
40 443 minimum 3—4 hours after triggering before increasing again. Neither CoMorph-A or the
41 444 CRM show this secondary peak. Over the first 2 hours after triggering (first phase) CTRL and
42 445 CoMorph-A have comparable memory with persistence of convection maintained for longer
43 446 than the CRM (Fig 6b). The suppression of convection (second phase) in MONC the CRM
44 447 starts within 1.5 hours for convection produced 2.5 hours after triggering (Fig 6c). For
45 448 CoMorph, there is an indication of suppression for convection produced before $t_0=3.5\text{ h}$ (Fig
46 449 6d) but this is weak, and only lasts 15 minutes. For convection produced from $t_0=4\text{ h}$ (Fig 6e),
47 450 the initial persistence of convection is followed by a suppression for a further 2.5 h in both
48 451 CoMorph-A and CRM with a maximum suppression of 4 h (for convection produced from
49 452 $t_0=7\text{ h}$; Fig 6h). This suppression of convection happens much later in CTRL and is only
50
51
52
53
54
55
56
57
58
59
60

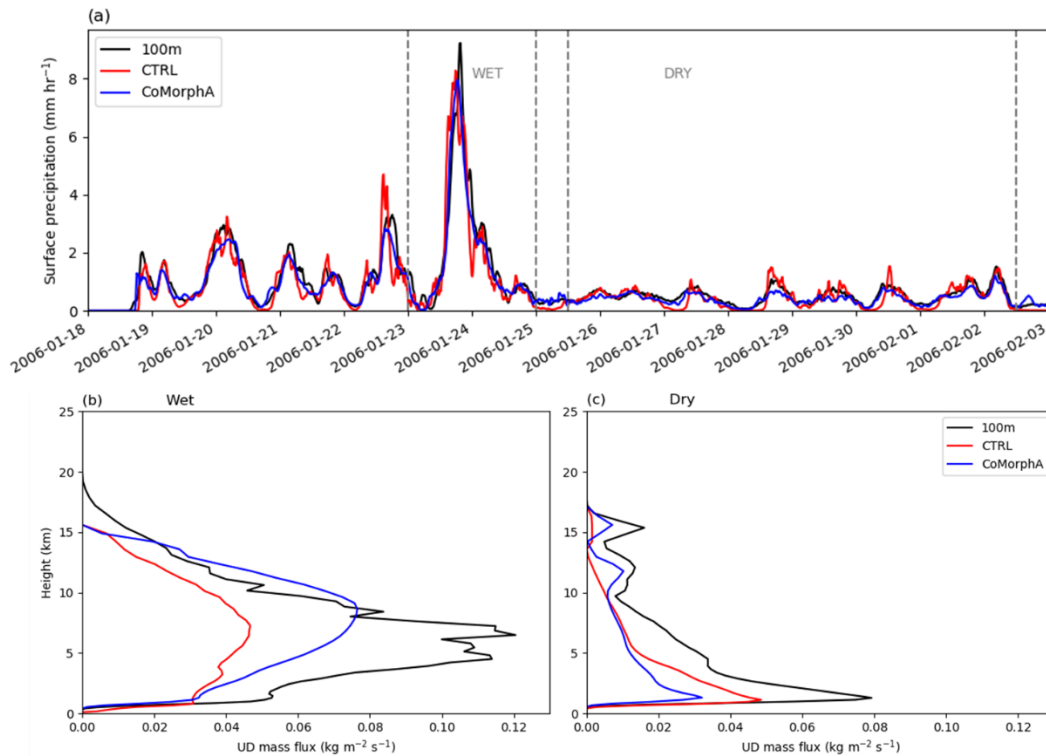
1
2
3 453 evident after 5 hours for convection produced over 7 hours after triggering (Figs 6ghi). The
4
5 454 secondary enhancement of convection (third phase) is weak but evident in the CRM for
6
7 455 convection produced over 8.5 hours after triggering (Figs 6i). This weak secondary
8
9 456 enhancement can also be seen in CoMorph-A for convection produced at $t=7$ h (Fig 6h) but is
10
11 457 not captured by CTRL. It is found that this secondary enhancement can be enhanced using
12
13 458 CoMorph-A but with a fixed low entrainment rate (not shown).

14
15 459 These results show that CoMorph-A has a more realistic relationship between earlier
16
17 460 precipitation than CTRL and although it is able to capture the secondary enhancement form
18
19 461 of memory, the timings and strength vary from the CRM. This was a multi-day case but
20
21 462 applying the same forcings each day to build up an ensemble. The next section evaluates a
22
23 463 multi-day case using time-varying forcings based on observations to show the performance of
24
25 464 CoMorph-A in simulating convective systems over a longer time period.

26 465 3.5. Multi-day tropical case

27
28
29 466 The multi-day analysis uses a well-documented case based on observations from the Tropical
30
31 467 Warm Pool–International Cloud Experiment (TWP-ICE; May et al. 2008) using a set-up
32
33 468 based on Fridlind et al. (2012). This involves a 16-day period during the Australian monsoon
34
35 469 featuring an active monsoon period followed by suppressed conditions and a monsoon break
36
37 470 (May et al. 2008). This case has interactive radiation, so provides evaluation of the influence
38
39 471 of cloud-radiative feedback on CoMorph but is highly constrained by the nudging to
40
41 472 observational data.

42
43 473 The CRM results compare well with other models (Petch et al. 2014). The peak precipitation
44
45 474 values differ slightly from observed as they did in the original comparison (Fridlind et al.
46
47 475 2012; Petch et al. 2014), particularly when there is only very light precipitation in the later
48
49 476 part of the period. CTRL shows more high-frequency variability than CoMorph-A.
50
51
52
53
54
55
56
57
58
59
60



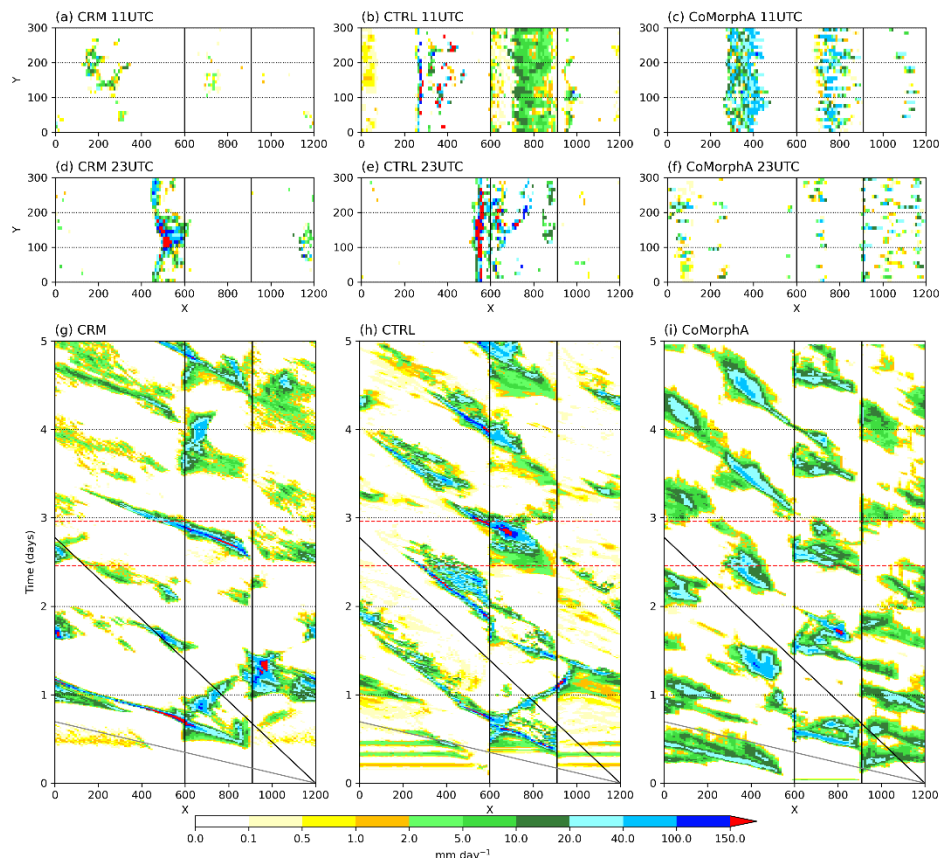
477

478 **Fig 7. TWP-ICE. (a) Timeseries of 15-minute precipitation rates [mm hr⁻¹] and mean updraught**
 479 **mass flux [kg m⁻² s⁻¹] during the (b) wet and (c) dry period of TWP-ICE from the 100 m CRM**
 480 **(black), CTRL (red) and CoMorph-A (blue) simulations. The wet and dry periods are shown**
 481 **by the grey dashed lines on (a).**

482 The mass flux profiles from the wet and dry periods are shown in Figure 7. The mass flux
 483 profiles from the wet period are very similar to those from the 90% EUROCS case (Fig 2d)
 484 with the parametrized runs peaking at higher altitude than the CRM. Like that case,
 485 CoMorph-A has a higher mass flux than CTRL ~~while it~~ while it ~~both are~~ both are lower than the CRM peak.
 486 Although, in this case both parameterised runs terminate 4 km lower than the CRM, again
 487 suggesting a need for the representation of overshoots in the parameterization. For the dry
 488 period all mass flux profiles show the expected bottom-heavy profile and terminate at the
 489 same altitude. The CRM has a higher mass flux throughout the profile than both
 490 parameterized runs. Compared to CTRL, CoMorph-A has a lower mass flux in the lower
 491 troposphere but higher in the upper troposphere. The CoMorph-A results from the dry period
 492 are very different from the 25% humidity case shown in Section 3.2 (Fig 2b) suggesting that
 493 under a different experimental setup CoMorph-A could be more sensitive to humidity than
 494 the earlier results implied.

495 All cases so far have assumed a homogenous surface. The following section details a new
 496 idealised case for evaluating the behaviour of convection when there is a strip of land (an
 497 island) in the domain and how this affects the propagation of convection under different wind
 498 regimes.

499 3.6. Inland propagation and nocturnal convection



500

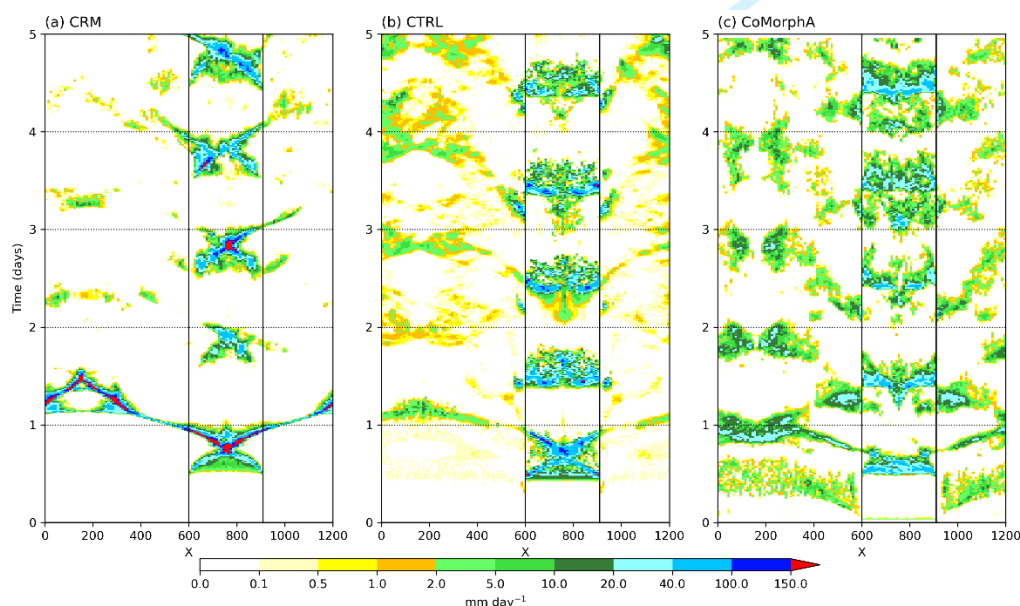
501 **Fig 8. Island case. Snapshots of precipitation [mm day⁻¹] at (a – c) 11 and (d-f) 23 UTC on**
 502 **day 3 of the island simulation with a 5 m s⁻¹ background wind (U=5) for (a, d) the CRM;**
 503 **regridded to 10 km, (b, e) CTRL and (c, f) CoMorph-A, for the idealised island case.**
 504 **Hovmöller of precipitation [mm day⁻¹] averaged over full y-domain from (g) CRM (250 m;**
 505 **regridded to 10 km), (h) CTRL and (i) CoMorph-A. The vertical black lines show the**
 506 **location of land (x = 600—90750 km). The diagonal black line shows the background wind**
 507 **(5 m s⁻¹) with the grey line showing 20 m s⁻¹. Red dashed lines show the times of the**
 508 **snapshots in (a–f).**

509 The Maritime Continent is difficult to represent accurately, with the initiation of convection
 510 by the convergence of sea-breeze circulations (Birch et al. 2015) and offshore gravity waves
 511 (Love et al. 2011) being vital for simulation of the region. An idealised island case has been

512 developed to analyse this behaviour and examine the ability of propagation of convection
 513 both on and off land. This new setup has an idealised island set at the equator, with
 514 interactive radiation and a real sandy land surface with plenty of moisture initially. It has
 515 been run with ($U=5 \text{ m s}^{-1}$; Fig 8) and without a background wind ($U=0 \text{ m s}^{-1}$; Fig 9). The
 516 case with the wind has a gravity wave propagating off the land initiating convection over the
 517 sea due to the heating profile of late afternoon convection over the land. The case with no
 518 wind illustrates the impact of land sea breezes.

519 With a background wind (Fig 8), snapshots of precipitation rate at 11am and 11pm show the
 520 location of precipitation in each simulation. At 11am on day 3 there is much more rain over
 521 land in the parameterized runs than the high-resolution CRM (Figs 8a—c), although there is
 522 a line of precipitation over the ocean in all three simulations. At 11pm (Figs 8d—f) there is
 523 a distinct line of precipitation associated with the gravity wave in the CRM. The CTRL has
 524 convection just off -land which isn't evident in CoMorph-A.

525 Propagation in the CRM (Fig 8g) is much quicker ($\sim 20 \text{ m s}^{-1}$) than the lower-resolution
 526 parametrized convection runs (Fig 8h,i) which propagate at a similar speed to the background
 527 wind (5 m s^{-1}), particularly over the ocean. CoMorph-A propagates at this higher speed over
 528 land but struggles to propagate off the land, unlike CTRL which is better at capturing this.
 529 CoMorph-A has widespread mid-intensity precipitation but not the very high intensities
 530 shown in CTRL.



531

1
2
3 **532 Fig 9. Island case. Hovmöller (averaged over full y-domain) of precipitation [mm day⁻¹] from (a)**
4 **533 CRM (250 m; regridded to 10km), (b) CTRL and (c) CoMorph-A from simulations of the**
5 **534 idealised island with no background wind (U=0).**
6
7
8

9 535 The case with no background wind (Fig 9a) shows precipitation over the island tending to
10 536 start close to the coasts, likely initiated by sea breezes, and gradually moving inland. Later in
11 537 the day the convection tends to become more widespread over the land. On some days
12 538 convection propagates for a small distance off land which is possible evidence of cold pools
13 539 and land-sea breezes. Both CTRL and CoMorph-A (Figs 9b,c) show no evidence of the
14 540 convection over land starting at the coasts, instead there is some evidence of convection in
15 541 the centre of the island starting far too early. This island setup shows some more work is
16 542 needed to correctly represent the interaction with sea breezes in CoMorph-A and will be a
17 543 useful testbed during future development of the scheme.
18
19
20
21
22
23
24

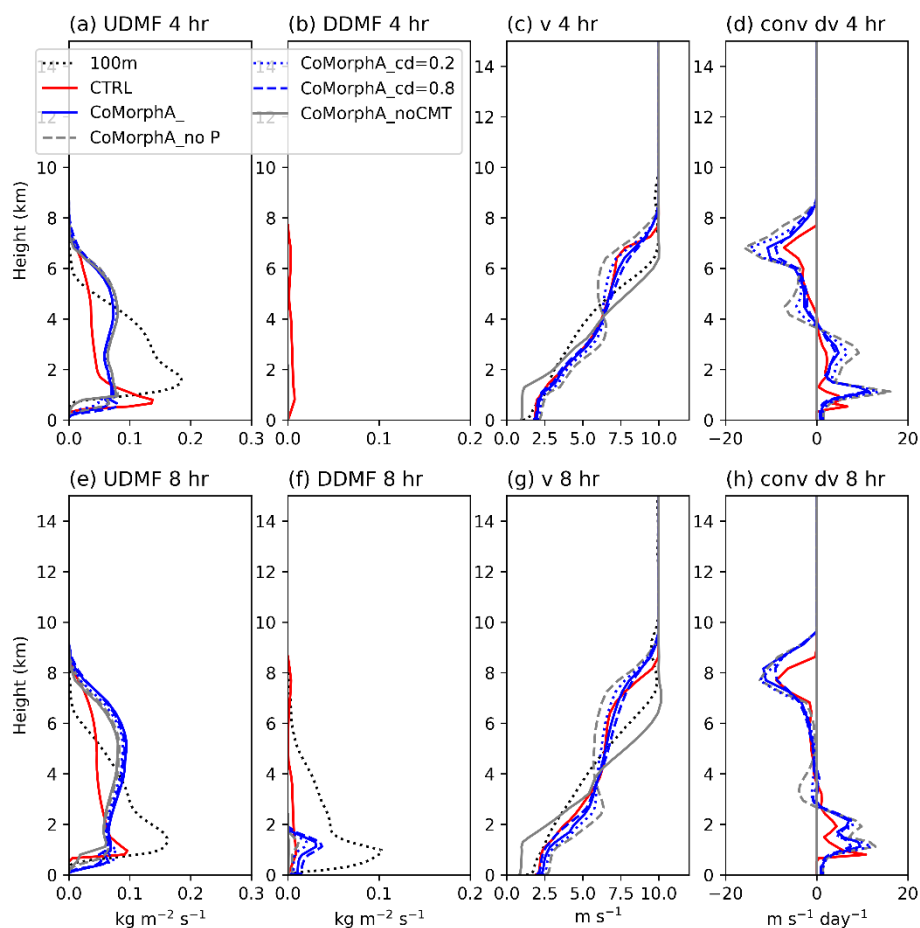
25 544 In the final case, we show the impact of different tunings on the representation of CMT and
26 545 the utility of idealised cases to inform tunings of the GCM.
27
28
29

30 546 3.7 Convective momentum transport

31
32

33 547 The transport of momentum vertically by convection (i.e. CMT) is an important process,
34 548 significantly affecting upper-level wind speeds in global models (e.g. Gregory et al. 1997),
35 549 and needs to be parametrized. The cold air outbreak case
36 550 from Kershaw & Gregory (1997) is used to test CoMorph's CMT behaviour. The CRM
37 551 profiles (black dotted, Fig 10) are similar to the results documented in the original paper (Figs
38 552 7,9 in Kershaw & Gregory 1997). The mass flux profiles (Fig 10a, b, e, f) differ between the
39 553 parametrized and CRM results with CoMorph-A having a secondary peak in updraught mass
40 554 flux at 5—6 km altitude compared with CTRL and CRM where there is a single peak just
41 555 above cloud base (Figs 10a, e). The CTRL downdraft mass flux remains fairly uniform with
42 556 height whereas both CoMorph-A and CRM show a peak at 1 km. Since the mass flux
43 557 profiles are different between the simulations, we do not expect to have the same wind
44 558 profile; however, by changing the CMT calculation we can see the effect on these profiles.
45 559 The shallower updraught mass flux profile in the CRM than the parametrized runs results in
46 560 the winds reaching the maximum value at lower altitude. Without the inclusion of CMT the
47 561 resulting winds are too weak at low levels and too strong above 2 km (grey solid line; Fig
48 562 10c, g). Originally the CMT was applied without a pressure gradient term to account for the

1
2
3 563 difference between in-cloud and environmental momentum, resulting in the overly strong
4 564 damping of the upper-level winds (grey dotted line; Fig 10c, g) which was also evident in
5 565 global simulations (not shown). Adding in a pressure gradient term with a quadratic drag law
6 566 leads to damping of the winds to an appropriate level, taking into consideration that the mass
7 567 flux profile does not compare perfectly with the CRM. The sensitivity to the value of the
8 568 drag coefficient in the pressure gradient term is also shown with a lower drag (dashed lines)
9 569 resulting in convection being more efficient at transporting momentum in the vertical (e.g.
10 570 Fig 8c,d,g,h). The magnitude of the convective increment to meridional winds are similar
11 571 between CTRL and CoMorph-A.



572

573 **Fig 10. CMT. Profiles at 4 hours of (a) updraught mass flux [$\text{kg m}^{-2} \text{s}^{-1}$], (b) downdraught**
574 **mass flux [$\text{kg m}^{-2} \text{s}^{-1}$], (c) meridional wind [m s^{-1}] and (d) the increment in meridional wind**
575 **due to convection [$\text{m s}^{-1} \text{day}^{-1}$] in the parameterized runs for the cold air outbreak case. (e-h)**
576 **as (a-d) but 8 hours into the run. Results shown for the 100 m CRM (black), CTRL (red)**

1
2
3 577 **and various configurations of CoMorph: CoMorph-A (blue, solid), CoMorph-A with no**
4 **CMT (grey), CoMorph-A but no pressure term in the CMT calculation (grey, dashed), drag**
5 **coefficient of 0.2 (blue, dotted) and 0.8 (blue, dashed).**
6
7

8
9 580 This final case has shown the impact of different formulations and tunings of the
10
11 581 parameterization on the results. The following section will bring all these cases together and
12
13 582 summarise the results.

14 15 583 4.Summary & Conclusions

16
17
18 584 CoMorph is a new convection scheme developed for the UM, a model which is used
19
20 585 extensively across the globe by various institutions. The CoMorph-A package has been
21
22 586 shown to perform well in a global configuration, with a reduction of biases under climate
23
24 587 configuration and improved NWP performance ([A. Lock, submitted work-et al. 2023](#)).
25
26 588 Although ultimately it is the GCM performance that determines if a scheme becomes
27
28 589 operational, throughout development the scheme has been tested using a 3D idealised UM
29
30 590 which uses the same science configuration as the full GCM but is substantially cheaper to
31
32 591 run. This has allowed us to understand in detail how the model behaves as a function of
33
34 592 regime. The present study has documented the performance of CoMorph-A in a selection of
35
36 593 idealised experiments, ranging from highly idealised with only high-resolution convection-
37
38 594 resolving data as a reference to those based on observational field campaigns with real data
39
40 595 and previous intercomparison studies to compare against. Although a number of these cases
41
42 596 were initially designed for SCM comparisons, the use of the 3D idealised model has several
43
44 597 advantages: Evaluation at higher resolutions with the same physics, dynamics and coupling
45
46 598 as used in the full GCM, comparison of the emergent organisation and spatial structures, and
47
48 599 allowing interaction with the winds leading to propagation of convection (Section 3.6). The
49
50 600 results are designed to serve as a baseline for others to compare against, and [for assessing](#)
51
52 601 [performance](#) as CoMorph evolves over the coming years.

53
54 602 CoMorph-A showed some organisation of convection when in RCE, consistent with the
55
56 603 majority of models compared in RCEMIP (Wing et al. 2020). The structures from the
57
58 604 sensitivity to humidity case showed the emergence of cellular behaviour that was observed in
59
60 605 the high-resolution reference. However, both parameterized runs produce too widespread
61
62 606 precipitation throughout the domain compared to the CRM. Profiles of updraught mass flux
63
64 607 have shown that the peak value is consistently greater in the high-resolution simulations than
65
66 608 the parameterised runs, although with lower associated precipitation rates. This may point to

1
2
3 609 a need for stronger downdraught representation in CoMorph in future. The sharper inversion
4 and low termination of updraught mass flux relative to the CRM also suggest the need for a
5 representation of overshoots.
6
7

8
9 612 All three diurnal cycle experiments (Section 3.3) show improvements in the timing of the
10 triggering and peak in precipitation over CTRL but still trigger too early relative to high
11 resolution simulations. This is consistent with the results from global simulations ([A. Lock,](#)
12 [et al. 2023, Zhu et al. 2023 submitted work](#)) where, although some regions such as [parts of](#)
13 Africa have a degradation in the diurnal cycle compared to the control, other regions are
14 improved but still precipitate too early in the day. The peak precipitation is too high across
15 the three cases, with the mass flux showing convection is too deep in most cases. Use of the
16 memory function (Section 3.4) shows CoMorph-A has a more realistic response to earlier
17 precipitation than CTRL. [A number of cases \(Figs 4,5,10\) show CoMorph has a more top-](#)
18 [heavy mass-flux profile than CTRL. This is likely due to convection triggering from multiple](#)
19 [different heights in the column as well as differences in the detrainment and entrainment](#)
20 [formulation.](#)
21
22
23
24
25
26
27
28
29
30

31 624 Overall, CoMorph-A is shown to perform competitively against the existing science
32 configuration. However, as might be expected with the development of a new convection
33 scheme there are still areas for improvement. In addition to the timing and amplitude of the
34 diurnal cycle of precipitation mentioned above, difficulties in simulating the propagation of
35 convection off land and representing sea breezes in CoMorph-A are made evident using the
36 idealised island case (Section 3.6). CoMorph-A is shown to have too little sensitivity to
37 humidity using the Derbyshire et al. (2004) experimental setup (Fig 2) with little variation in
38 the mass flux profiles. These results suggest the need to suppress convection at lower
39 humidities ([e.g Hiron et al. 2013](#)) and based on this [experiment](#) it is perhaps surprising that
40 CoMorph-A shows improvements in the representation of the MJO ([A. Lock, submitted work](#)
41 [et al. 2023](#)). However, the mass flux profiles do vary greatly between the wet and dry periods
42 of the TWP-ICE experiment (Fig 7) suggesting this sensitivity may be increased under a
43 different experimental setup. Using a SCM, Daleu et al. (2023) found the relationship
44 between precipitation and column relative humidity was well represented by CoMorph-A in
45 dry environments but breaks down above 70% relative humidity. This sensitivity and the
46 difference in results depending on the experiment needs to be investigated further using
47 additional tests.
48
49
50
51
52
53
54
55
56
57
58
59
60

641
642 Many of the convective-scale processes parameterised in CoMorph carry significant
643 uncertainties. In recognition of this, many of the formulae within the scheme are scaled by
644 dimensionless “tuning factors” which can be easily changed. CoMorph has around 30 of
645 these tuneable parameters, scaling the initial parcel perturbations, entrainment (and its
646 sensitivity to convective organisation), detrainment, various in-plume microphysical
647 processes, the area-fractions of convective cloud and precipitation passed to other parts of the
648 model, and other processes. In CoMorph A, many of these parameters have been tuned over
649 successive versions to ensure both model-stability and good global performance. Section 3.7
650 illustrates the need for a convection scheme to consider the sub-grid transport of momentum
651 by convection without which the upper-level winds are too strong. How the CMT is
652 parameterized, and the sensitivity to the drag coefficient, required careful consideration to
653 perform well in both global and idealised simulations. This is the only section where the
654 sensitivity of the results to parameters within CoMorph has been discussed. However, it is
655 worth noting that the CoMorph-A entrainment rate is variable depending on the previous
656 time-step precipitation rate, a development that was included based on global testing and is
657 found to improve the performance in climate simulations. Many of the idealised cases have
658 additionally been run with a fixed (high or low) entrainment rate. The higher entrainment
659 rate is found to be beneficial for some cases such as increasing the sensitivity to humidity and
660 the timing of triggering of precipitation in the diurnal cycle experiments, but the lower
661 entrainment is necessary for TWP-ICE and capturing the secondary enhancement of
662 convection in the convective memory (not shown). Global analysis suggests the tropical
663 mean temperature profiles are particularly sensitive to the parameters controlling
664 entrainment, detrainment and in-plume ice processes. Sub-tropical light rain (which exerts a
665 strong influence on climate sensitivity) is very sensitive to the in-parcel cloud-to-rain
666 autoconversion and precipitation fraction parameters. A more detailed analysis of the
667 sensitivity to a range of parameters may form the basis of future work.

668 There are several proposed improvements to CoMorph to help address the discussed
669 deficiencies-discussed. These include the representation of a second updraught type such that
670 both surface-driven and cold-pool forced convection are represented and allow the
671 proportion of cold-pool forced updraughts to grow more gradually as more deep clouds are
672 initiated. This, along with various additional scientific improvements, including the

1
2
3 673 representation of overshoots and formulation of downdraughts highlighted in this study, will
4
5 674 be included in a future release of CoMorph. At the time of writing, the next release of
6
7 675 CoMorph is undergoing extensive testing over a range of experiments, including the idealised
8
9 676 experiments discussed in the current study. Subsequently, the aim is to couple CoMorph with
10
11 677 the C-POOL prognostic cold-pool scheme (Rooney et al. 2022) and enhance the scale-aware
12
13 678 properties of the scheme for running at higher (< 10 km) resolutions.
14

15 679

17 680 *Acknowledgements*

18
19 681 SLL is funded through the Northern Australia Climate Program (NACP), funded by Meat and
20
21 682 Livestock Australia, the Queensland Government through the Drought and Climate
22
23 683 Adaptation Program, and the University of Southern Queensland. CD, RP and J-FG
24
25 684 gratefully acknowledge funding from NERC grant NE/N013743/1 as part of the ParaCon
26
27 685 programme (<https://www.metoffice.gov.uk/research/approach/collaboration/paracon>). The
28
29 686 authors thank two anonymous reviewers for their detailed and insightful comments that
30
31 687 helped to improve the manuscript.

32 688 *Author Contributions*

33
34
35 689 SLL: Formal analysis; data curation; methodology; investigation, software; visualization;
36
37 690 writing – original draft; writing – review and editing. AJS: Conceptualization; supervision;
38
39 691 writing – review and editing. MW: Software; writing – review and editing. RS: Data curation;
40
41 692 methodology; software; investigation, writing - review and editing. CLD: Formal analysis;
42
43 693 data curation; methodology; investigation, software; writing – review and editing. RSP:
44
45 694 Writing - review and editing. AL: Writing - review and editing. J-FG: Methodology; writing -
46
47 695 review and editing.

48 696 *Data Availability Statement*

49
50
51 697 The data generated from the model simulations used in this paper can be made available by
52
53 698 the lead author and Met Office co-authors.

54 55 699 **References**

56
57
58
59
60

- 1
2
3 700 Ahn, M.-S., Kim, D., Kang, D., Lee, J., Sperber, K. R., Gleckler, P. J., et al. (2020). MJO propagation
4 701 across the Maritime Continent: Are CMIP6 models better than CMIP5 models? *Geophysical Research*
5 702 *Letters*, 47, e2020GL087250. <https://doi.org/10.1029/2020GL087250>
- 6
7
8 703 Arakawa, A., and Schubert, W. H. (1974), Interaction of a cumulus cloud ensemble with the large-
9 704 scale environment, Part I. *J. Atm Sci*, 31.3, 674-701.
- 10
11
12 705 Birch, C. E., Roberts, M. J., Garcia-Carreras, L., Ackerley, D., Reeder, M. J., Lock, A. P. and
13 706 Schiemann, R. (2015) Seabreeze dynamics and convection initiation: the influence of convective
14 707 parameterization in weather and climate model biases. *Journal of Climate*, 28 (20). pp. 8093-8108.
15
16 708 ISSN 1520-0442 doi: <https://doi.org/10.1175/JCLI-D-14-00850.1>
- 17
18
19 709 Brown, A.R., Cederwall, R. T., Chlond, A., Duynkerke, P.G., Golaz, J.-C., Khairoutdinov, M.,
20 710 Lewellen, D. C., Lock, A. P., Macvean, M. K., Moeng, C.-H., Neggers, R.A.J., Siebesma, A. P. and
21 711 Stevens B. (2002) Large-eddy simulation of the diurnal cycle of shallow cumulus convection over
22 712 land. *Q.J.R. Meteorol. Soc.* 128, 1075-1093.
- 23
24
25 713 Brown, A., Milton, S., Cullen, M., Golding, B., Mitchell, J. and Shelly, A. (2012) Unified modeling
26 714 and prediction of weather and climate: a 25 year journey. *Bulletin of the American Meteorological*
27 715 *Society*, 93, 1865–1877. <https://doi.org/10.1175/BAMS-D-12-00018.1>
- 28
29
30 716 Brown, N., Weiland, M., Hill, A., Shipway, B., Maynard, C., Allen, T., & Rezný, M. (2015). A highly
31 717 scalable Met Office NERC Cloud model. In *Proceedings of the 3rd International Conference on*
32 718 *Exascale Applications and Software* (pp. 132– 137).
- 33
34
35 719 Bush, M., Boutle, I., Edwards, J., Finnenkoetter, A., Franklin, C., Hanley, K., Jayakumar, A., Lewis,
36 720 H., Lock, A., Mittermaier, M., Mohandas, S., North, R., Porson, A., Roux, B., Webster, S., and
37 721 Weeks, M. (2023) The second Met Office Unified Model–JULES Regional Atmosphere and Land
38 722 configuration, RAL2, *Geosci. Model Dev.*, 16, 1713–1734, [https://doi.org/10.5194/gmd-16-1713-](https://doi.org/10.5194/gmd-16-1713-2023)
39 723 [2023](https://doi.org/10.5194/gmd-16-1713-2023)
- 40
41
42 724 Chaboureau, J.-P., Guichard, F., Redelsperger, J.-L. and Lafore, J.-P. (2004), The role of stability
43 725 and moisture in the diurnal cycle of convection over land. *Q.J.R. Meteorol. Soc.*, 130: 3105-3117.
44 726 <https://doi.org/10.1256/qj.03.132>
- 45
46
47 727 Chen, S. S., Houze, R. A., Jr., and Mapes, B. E. (1996). Multiscale Variability of Deep Convection in
48 728 Relation to Large-Scale Circulation in TOGA COARE. *Journal of Atmospheric Sciences* 53, 10,
49 729 1380-1409, [https://doi.org/10.1175/1520-0469\(1996\)053<1380:MVODCI>2.0.CO;2](https://doi.org/10.1175/1520-0469(1996)053<1380:MVODCI>2.0.CO;2)
- 50
51
52
53
54
55
56
57
58
59
60

- 1
2
3 730 Christopoulos, C., & Schneider, T. (2021). Assessing biases and climate implications of the diurnal
4 731 precipitation cycle in climate models. *Geophysical Research Letters*, 48, e2021GL093017.
5
6 732 <https://doi.org/10.1029/2021GL093017>
7
8
9 733 Couvreux, F., Rio, C., Guichard, F., Lofthon, M., Canut, G., Bounoil, D. and Gounou, A. (2012)
10 734 Initiation of daytime local convection in a semi-arid region analysed with high resolution simulations
11 735 and AMMA observations. *Q.J.R. Meteorol. Soc.*, 138, 56-71.
12
13
14 736 Couvreux, F., Roehrig, R., Rio, C., Lefebvre, M.-P., Caian, M., Komori, T., Derbyshire, S., Guichard,
15 737 F., Favot, F., D'Andrea, F., Bechtold, P. and Gentine, P. (2015), Representation of daytime moist
16 738 convection over the semi-arid Tropics by parametrizations used in climate and meteorological models.
17 739 *Q.J.R. Meteorol. Soc.*, 141: 2220-2236. <https://doi.org/10.1002/qj.2517>
18
19
20
21
22 740 Daleu, C.L., Plant, R.S., Stirling, A.J. & Whittall, M.(2023) Evaluating the CoMorph-A
23 741 parametrization using idealized simulations of the two-way coupling between convection and large-
24 742 scale dynamics. *Quarterly Journal of the Royal Meteorological Society*, 1–23.
25 743 <https://doi.org/10.1002/qj.4547>
26
27
28
29 744 Daleu, C. L., Plant, R. S., Woolnough, S. J., Stirling A.J. and Harvey N.J. (2020) Memory Properties
30 745 in cloud-resolving simulations of the diurnal cycle of deep convection. *JAMES 12*
31 746 doi:10.1029/2019MS001897
32
33
34
35 747 Derbyshire, S.H., Beau, I., Bechtold, P., Grandpeix, J.-Y., Piriou, J.-M., Redelsperger, J.-L. and
36 748 Soares, P.M.M. (2004), Sensitivity of moist convection to environmental humidity. *Q.J.R. Meteorol.*
37 749 *Soc.*, 130: 3055-3079. doi:10.1256/qj.03.130
38
39
40
41 750 Fridlind, A.M., Ackerman, A.S., Chaboureau, J.-P., Fan, J., Grabowski, W.W., Hill, A.A., Jones,
42 751 T>R., Khaiyer, M.M, Liu, G., Minnis, P., Morrison, H., Nguyen, L., Park, S., Petch, J.C., Pinty, J.-P.,
43 752 Schumacher, C., Shipway, B.J., Varble, A.C., Wu, X., Xie, S. and Zhang, M. (2012) A comparison of
44 753 TWP-ICE observational data with cloud-resolving model results. *J. Geophys. Res.*
45 754 117, doi:10.1029/2011JD016595.
46
47
48
49
50 755 Gregory, D. and Guichard, F. (2002), Aspects of the parametrization of organized convection:
51 756 contrasting cloud-resolving model and single-column model realizations. *Q.J.R. Meteorol. Soc.*, 128:
52 757 625-646. <https://doi.org/10.1256/003590002321042126>
53
54
55
56 758 Gregory, D. and Rowntree, P. R. (1990) A mass-flux convection scheme with representation of cloud
57 759 ensemble characteristics and stability dependent closure. *Mon. Weather Rev.*, 118, 1483–1506.
58
59
60

- 1
2
3 760 Guichard, F., Petch, J.C., Redelsperger, J.-L., Bechtold, P., Chaboureau, J.-P., Cheinet, S.,
4 761 Grabowski, W., Grenier, H., Jones, C.G., Köhler, M., Piriou, J.-M., Tailleux, R. and Tomasini, M.
5 (2004), Modelling the diurnal cycle of deep precipitating convection over land with cloud-resolving
6 762 models and single-column models. *Q.J.R. Meteorol. Soc.*, 130: 3139-3172.
7
8 763 <https://doi.org/10.1256/qj.03.145>
9
10 764
11
12 765 [Hirons, L.C., Inness, P., Vitart, F. and Bechtold, P. \(2013\), Understanding advances in the simulation](#)
13 [of intraseasonal variability in the ECMWF model. Part II: The application of process-based](#)
14 766 [diagnostics. Q.J.R. Meteorol. Soc., 139: 1427-1444. https://doi.org/10.1002/qj.2059](#)
15 767
16
17
18 768 Kershaw, R. and Gregory, D. (1997) Parametrization of momentum transport by convection. I:
19 769 Theory and cloud modelling results. *Q.J.R. Meteorol. Soc.*, **123**, 1133-1151.
20
21
22 770 Kim, D., Kug, J., and Sobel, A.H. (2014): Propagating versus Nonpropagating Madden-Julian
23 771 Oscillation Events. *J. Climate*, **27**, 111–125, <https://doi.org/10.1175/JCLI-D-13-00084.1>.
24
25
26 772 Lenderink, G., Siebesma, A.P., Cheinet, S., Irons, S., Jones, C.G., Marquet, P., Müller, F., Olmeda,
27 773 D., Calvo, J., Sánchez, E. and Soares, P.M.M. (2004), The diurnal cycle of shallow cumulus clouds
28 774 over land: A single-column model intercomparison study. *Q.J.R. Meteorol. Soc.*, 130: 3339-3364.
29 775 <https://doi.org/10.1256/qj.03.122>
30
31
32
33 776 ~~Lock, A., Whitall, M., Stirling, A. J., Williams, K., Lavender, S. L., Morcrette, C., Matsubayashi, K.,~~
34 777 ~~Field, P. R., Martin, G., Willett, M., Heming, J. (2023), The performance of the CoMorph A~~
35 778 ~~convection scheme in global simulations with the Met Office Unified Model. Submitted to QJRMS.~~
36
37
38
39 779 Love, B.S., Matthews, A.J. and Lister, G.M.S. (2011), The diurnal cycle of precipitation over the
40 780 Maritime Continent in a high-resolution atmospheric model. *Q.J.R. Meteorol. Soc.*, 137: 934-947.
41 781 <https://doi.org/10.1002/qj.809>
42
43
44
45 782 May, P. T., J. H. Mather, G. Vaughan, and C. Jakob (2008), Characterizing oceanic convective cloud
46 783 systems—The Tropical Warm Pool International Cloud Experiment, *Bull. Am. Meteorol. Soc.*, 154,
47 784 153–155, doi:10.1175/BAMS-89-2-153.
48
49
50
51 785 McIntyre, W.A., Efstathiou, G.A. & Thuburn, J. (2022) A two-fluid single-column model of turbulent
52 786 shallow convection. Part III: Results and parameter sensitivity. *Q.J.R. Meteorol. Soc.*, 1–20.
53 787 <https://doi.org/10.1002/qj.4390>
54
55
56 788 Petch, J., Hill, A., Davies, L., Fridlind, A., Jakob, C., Lin, Y., Xie, S. and Zhu, P. (2014), Evaluation
57 789 of intercomparisons of four different types of model simulating TWP-ICE. *Q.J.R. Meteorol. Soc.*,
58 790 140: 826-837. <https://doi.org/10.1002/qj.2192>

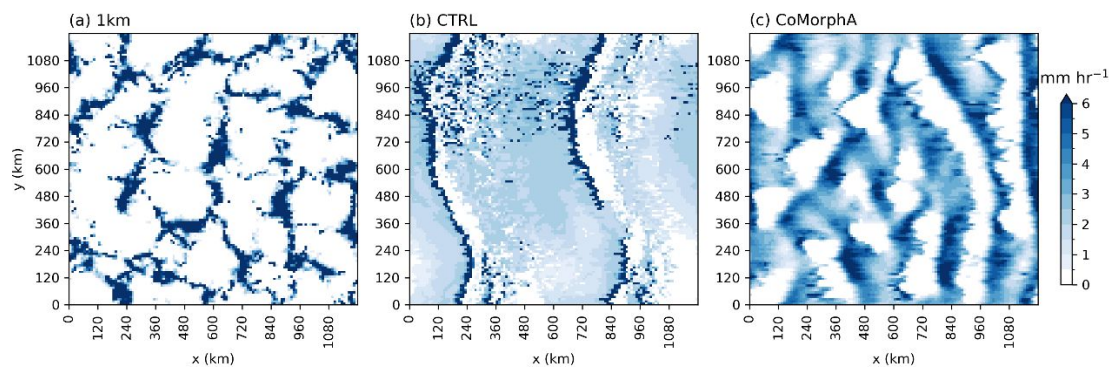
- 1
2
3 791 Roberts, N. M., (2001), Results from simulations of an organised convective event using the New
4 Dynamics at 12, 4 and 2 km resolution. *NWP Technical Report No. 344*. Joint Centre for Mesoscale
5 792 Meteorology, University of Reading, PO Box 243, Reading, Berkshire RG6 2BB, UK
6 793
7
8
9 794 Rooney, G.G., Stirling, A.J., Stratton, R.A., and Whitall, M.(2022) C-POOL: A scheme for modelling
10 795 convective cold pools in the Met Office Unified Model. *Q J R Meteorol Soc*, 962– 980.
11 796 <https://doi.org/10.1002/qj.4241>
12
13
14 797 Smith, R. N. B., (1990), A scheme for predicting layer clouds and their water content in a general
15 798 circulation model. *Quart. J. Roy. Meteor. Soc.*, 116, 435–460, doi:10.1002/qj.49711649210.
16
17
18 799 Tomassini, L., Parker, D.J., Stirling, A., Bain, C., Senior, C. and Milton, S. (2017), The interaction
20 800 between moist diabatic processes and the atmospheric circulation in African Easterly Wave
21 801 propagation. *Q.J.R. Meteorol. Soc.*, 143: 3207-3227. doi:[10.1002/qj.3173](https://doi.org/10.1002/qj.3173)
22
23
24 802 Walters, D., Baran, A. J., Boutle, I., Brooks, M., Earnshaw, P., Edwards, J., Furtado, K., Hill, P.,
25 803 Lock, A., Manners, J., Morcrette, C., Mulcahy, J., Sanchez, C., Smith, C., Stratton, R., Tennant, W.,
26 804 Tomassini, L., Van Weverberg, K., Vosper, S., Willett, M., Browse, J., Bushell, A., Carslaw, K.,
27 805 Dalvi, M., Essery, R., Gedney, N., Hardiman, S., Johnson, B., Johnson, C., Jones, A., Jones, C.,
28 806 Mann, G., Milton, S., Rumbold, H., Sellar, A., Ujiie, M., Whitall, M., Williams, K. and Zerroukat, M.
29 807 (2019) The Met Office Unified Model Global Atmosphere 7.0/7.1 and JULES Global Land 7.0
30 808 configurations. *Geoscientific Model Development*, 12 (5). pp. 1909-1963.
31 809 <https://doi.org/10.5194/gmd-12-1909-2019>
32
33
34 810 Whitall, M., Stirling, A., Lock, A., Lavender, S., Stratton, R., Matsubayashi, K. (2022) The CoMorph
35 811 convection scheme. UM Documentation Paper 043.
36
37
38 812 Willett, M. R., & Whitall, M. A. (2017). A simple prognostic based convective entrainment rate for
39 813 the unified model: Description and tests (technical report no. 617). Met Office.
40
41
42 814 Williams, K. D., Copsey, D., Blockley, E. W., Bodas-Salcedo, A., Calvert, D., Comer, R., ... Xavier,
43 815 P. K. (2017). The Met Office Global Coupled model 3.0 and 3.1 (GC3.0 and GC3.1) configurations.
44 816 *Journal of Advances in Modeling Earth Systems*, 10, 357–380.
45 817 <https://doi.org/10.1002/2017MS001115>
46
47
48 818 Wilson, D. R., Bushell, A. C., Kerr-Munslow, A. M., Price, J. D., and Morcrette, C. J. (2008) PC2: A
49 819 prognostic cloud fraction and condensation scheme. I: Scheme description, *Q. J. Roy. Meteorol. Soc.*,
50 820 134, 2093–2107, <https://doi.org/10.1002/qj.333>
51
52
53
54
55
56
57
58
59
60

- 1
2
3 821 Wing, A. A., Reed, K. A., Satoh, M., Stevens, B., Bony, S., and Ohno, T. (2018) Radiative–
4 822 convective equilibrium model intercomparison project, *Geosci. Model Dev.*, 11, 793–813,
5 823 <https://doi.org/10.5194/gmd-11-793-2018>
6
7
8
9 824 Wing, A. A., Stauffer, C. L., Becker, T., Reed, K. A., Ahn, M.-S., & Arnold, N. P., et al. (2020).
10 825 Clouds and convective self-aggregation in a multimodel ensemble of radiative-convective equilibrium
11 826 simulations. *Journal of Advances in Modeling Earth Systems*, 12, e2020MS002138.
12 827 <https://doi.org/10.1029/2020MS002138>
13
14
15
16 828 Yang, G. Y., & Slingo, J. (2001). The diurnal cycle in the tropics. *Monthly Weather Review*, 129,
17 829 784–801.
18
19
20 830 ~~Zhu, H., Hudson, D., Li, C., Shi, L., Young, G., Stirling, A., Whitall, M., Lock, A., Lavender, S.,~~
21 831 ~~Stratton, R. (2023) Impacts of the new UM convection scheme, CoMorph A, over the Indo-Pacific~~
22 832 ~~and Australian regions. Submitted to Journal of Southern Hemisphere Earth Systems Science.~~
23
24
25
26
27
28
29
30
31
32
33
34
35
36
37
38
39
40
41
42
43
44
45
46
47
48
49
50
51
52
53
54
55
56
57
58
59
60

The use of idealised experiments in testing a new convective parameterization: Performance of CoMorph-A

Sally L. Lavender*, Alison J. Stirling, Michael Whitall, Rachel Stratton, Chimene L. Daleu, Robert S. Plant, Adrian Lock, Jian-Feng Gu

This study documents and discusses the performance of a new convection scheme, CoMorph-A, in a range of idealised experiments using the Met Office Unified Model. These experiments range from highly idealised with only high-resolution convection-resolving data as “truth” to those based on observational field campaigns with real data and previous intercomparison studies to compare against. Results show what works well in this configuration, and what areas will require further work.



Snapshot of surface precipitation rate [mm hr⁻¹] on day 4 of the 90% case, 1200 km domain simulations from the (e) 1km CRM; regridded to same 10 km grid (f) CTRL and (g) CoMorph-A.